J/ψ level one trigger based on the Cellular Automaton method for CBM experiment.

Maciej Krauze

J/ψ level one trigger based on the Cellular Automaton method for CBM experiment.

A doctoral dissertation submitted to the Faculty of Mathematics, Physics and Chemistry of the University of Silesia

by

Maciej Krauze

Thesis Advisor
Prof. dr. hab. Wiktor Zipper

KATOWICE 2011

Abstract

The J/ψ meson event selection using Transition Radiation Detector information only was the main goal of this study. The developed procedures operate at low level (Level 1) of the data acquisition system of the Compressed Baryonic Matter experiment. In order to find a signature of the meson, the dedicated track reconstruction algorithm was created. As a signature of J/ψ presence, e^+e^- pair with transversal momentum $p_t > 1$ GeV/c of each particle and with invariant mass around 3.1 GeV/c^2 was chosen. The reconstruction algorithm is based on the Cellular Automaton idea, which is optimal for parallel processing of data. During the selection, events without interesting information are rejected, while events containing J/ψ decay signature are accepted. The algorithm reconstructs high-momentum ($p > 1$ GeV/c) particle trajectories from a single Au+Au central collision at 25 AGeV with the efficiency of 92.6% in a time of 0.24 s on a standard 3 GHz Pentium 4 processor. For minimum bias event at the same energy, the efficiency for high-momentum particles is 89.7% and the time per event is 0.05 s. The results showed that the signature-based event selection is able to reduce the number of background minimum bias events by a factor of 1000, passing 1 background event per 1000, and preserving 11.7% of J/ψ decay signal events. It offers a factor of 1000 more time for a next level analysis to perform additional on-line processing methods.

Streszczenie

Głównym tematem pracy jest selekcja zdarzeń zawierających mezon J/ψ przy użyciu Detektora Promieniowania Przejścia. Stworzone procedury działają na niskim poziomie (Poziom 1) systemu akwizycji danych eksperymentu Compressed Baryonic Matter. Na potrzeby poszukiwania sygnatury mezonu stworzono dedykowany algorytm rekonstrukcyjny. Jako sygnaturę wybrano parę e^+e^- z pędem poprzecznym każdej cząstki $p_t > 1$ GeV/c i o masie niezmienniczej w okolicach 3.1 GeV/c^2. Algorytm rekonstrukcyjny bazuje na idei Automatu Komórkowego, optymalnej dla równoległego przetwarzania danych. Podczas selekcji, zdarzenia pozbawione interesujących informacji są odrzucane a te zawierające sygnaturę rozpadu J/ψ są akceptowane. Algorytm rekonstruuje tory wysokopędowych ($p > 1$ GeV/c) cząstek z pojedynczego centralnego zderzenia Au+Au przy energii 25 GeV/nukleon z wydajnością 92.6% w czasie 0.24 s na standardowym, 3-gigahercowym procesorze klasy Pentium 4. Dla zderzeń peryferyjnych przy tej samej energii, wydajność dla wysokopędowych cząstek wynosi 89.7% a czas jednego zdarzenia to 0.05 s. Wyniki pokazują, że oparta na sygnaturach selekcja zdarzeń pozwala na redukcję ilości zdarzeń tła dla kolizji peryferyjnych o czynnik 1000, przepuszczając 1 zdarzenie tła na 1000 przy zachowaniu 11.7 % zdarzeń z sygnałem z rozpadu J/ψ . Oferuje 1000 razy więcej czasu dla systemów analizy wyższego rzędu na przeprowadzenie dodatkowych operacji w trybie on-line.

Contents

1 Introduction **1**
- 1.1 Motivation . . . 1
- 1.2 Key observables . . . 2
- 1.3 Heavy-ion collisions . . . 3
- 1.4 History of J/ψ discovery . . . 3

2 Theory overview **7**
- 2.1 Phases of water . . . 7
- 2.2 Phases of nuclear matter . . . 8
- 2.3 Ultra-relativistic Quantum Molecular Dynamics . . . 10

3 Overview of the CBM detector **11**
- 3.1 Diamond Pixel Detector . . . 13
- 3.2 Superconductiong Dipole Magnet . . . 13
- 3.3 Micro-Vertex Detector . . . 14
- 3.4 Silicon Tracking System . . . 14
- 3.5 Ring Imaging Cherenkov Detector 17
- 3.6 Transition Radiation Detector . . . 19
- 3.7 Resistive Plate Chambers . . . 20
- 3.8 Electromagnetic Calorimeter 21
- 3.9 Muon Chamber . . . 21
- 3.10 Projectile Spectator Detector (PSD) . . . 22
- 3.11 Data Acquisition System . . . 22
- 3.12 Detector Summary . . . 22

4 The event selection algorithm **25**
- 4.1 Introduction . . . 25
- 4.2 General assumptions . . . 27
- 4.3 Investigation: step by step . . . 28
  - 4.3.1 First step: selection without particle identification . . . 28
  - 4.3.2 Second step: usage of the Rejection Factor of the TRD 32
  - 4.3.3 Third step: usage of Geant3 libraries . . . 33
  - 4.3.4 Fourth step, including real tracking algorithm . . . 43
  - 4.3.5 Fifth step, using Geant3 libraries and realistic tracking . . . 45
    - 4.3.5.1 Track Purity . . . 46

5 Cellular Automaton Tracking Algorithm 55
5.1 Tracking algorithm 55
5.1.1 Introduction to Cellular Automaton 55
5.1.2 Tracking algorithm overview 57
5.1.3 Data structure 60
5.1.4 Segment creation part 61
5.1.5 Friends finding procedure 63
5.1.6 Tagging 64
5.1.6.1 Initial state. before the tagging procedure starts 65
5.1.6.2 Zero-assignment state 65
5.1.6.3 Tagging state 65
5.1.6.4 Final state 67
5.1.7 Creating track candidates 68
5.1.7.1 Calculation of χ^2-like value 69
5.1.7.2 Collecting the track candidates 69
5.1.8 Results and performance 71
5.1.9 Possible improvement using CUDA 74
5.1.10 Tracking Algorithm Summary 75

6 Summary and conclusions 77

A Overview of the Kalman Filter method 79

B Transition radiation effect 83
B.1 Additional mechanisms for energy loss of charged particles 83
B.2 Energy loss of a particle in a TRD detector 85

C The parameters used in the Track Finding procedure 87

D Multicore Processors 89

E Generation of events with UrQMD and Pluto 91
E.1 UrQMD central collisions 91
E.2 UrQMD minimum bias collisions 92
E.3 Pluto source 92

Acknowledgements 95

Bibliography 97

Chapter 1

Introduction

1.1 Motivation

The main motivation of this study was the physical program of the Compressed Baryonic Mater (CBM) experiment. The experiment. which will be held in Darmstadt. Germany operates in moderate energy region and high nuclear matter densities. That state of matter exists inside the neutron stars as well as in the core of supernova. Such form of matter is created in a collision of two heavy ions. accelerated to ultra relativistic speed. The baryon density and the temperature of the created fireball depend on the beam energy. This implies that by varying the beam energy. different phases of nuclear matter can be produced. within a certain limits (Fig. 1.1 on the following page).

The hadronic state exists in the region of low hadron density and relatively high temperature up to high density and low temperature (up to 170 MeV at baryon density zero). The phase transition occurs when the hadrons melt and new phase of matter is created from their consistuents. These consistuents. i.e. quarks and gluons. form the so called quark-gluon plasma. The process when quarks are liberated from the hadrons is called "deconfinement". When deconfinement phase transition begins. the matter is about 130 times hotter than the interior of the sun. Such conditions existed in the early universe. a few microseconds after the Big Bang. We are able to reproduce such state in heavy ion collision at ultra-relativistic energies at modern accelerators like SPS (CERN). RHIC (Brookhaven) or LHC (CERN) and. in the near future. at SIS300 at FAIR.

At the other hand. in highly compressed cold matter (as it may exist in the interior of neutron stars) the baryons also lose their entity and dissolve into gluons and quarks.

At present the critical density at which this transition begins is unknown. and it regards the entire high-density area of the phase diagram. At very high densities and low temperatures. the new phase is expected to appear. as the quarks correlate and form a color superconductor [2].

It is predicted that at some point. the deconfinement/chiral phase transition loses its character [3]. This point is called the "critical point" and its possible location lays within the reach of the new GSI facility. The scientific goal of CBM experiment is to explore the QCD phase diagram in the region of higher baryonic densities. The research program is complementary to the experiments carried out at BNL and CERN scientific facilities.

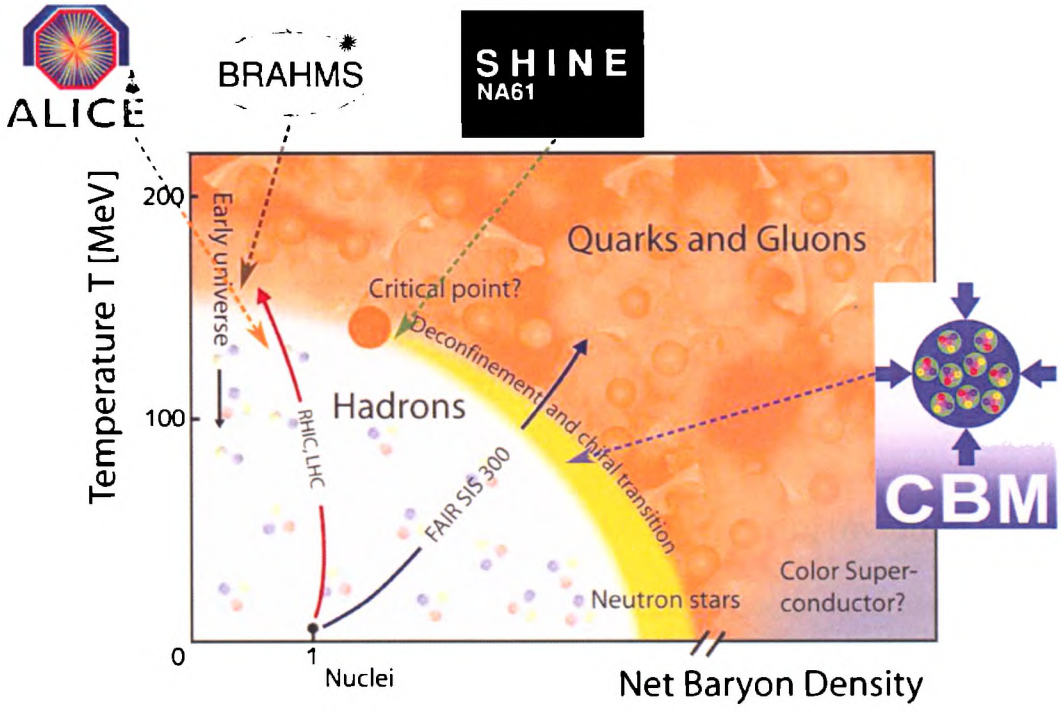

Figure 1.1. Schematic phase diagram of strongly interacting matter. The presence of a predicted *critical point* is shown here. The net baryon density is the density of baryons minus the density of antibaryons. Modified from [1]

1.2 Key observables

The fundamental properties of Quantum Chromo Dynamics (QCD) such as breaking chiral symmetry and confinement can be explored in heavy-ion collisions by using rare particles as probes in the strong interacting matter. The theoretical quantitative explanation of these effects still does not exist. Hence it is a motivation and a challenge for further investigations. An experiment offering the opportunity to observe the modification of hadron properties in a dense and hot nuclear matter is essential for study of deconfined matter consisting of quarks and gluons.

There is still much to be explored in the region of highest baryon densities and moderate temperatures of the QCD phase diagram (see Fig. 1.1). The planned SIS300 accelerator is capable of experiments with baryon densities up to 3 times the density of the nuclei during nuclear collisions in the beam energy between 10 and 40 AGeV, while the present SIS18 facility may serve as an injector. The CBM Experiment aims at the areas of study which were pioneered at the AGS in Brookhaven [4], such as [5, 6]:

- in-medium modifications of hadrons in dense matter,
- indications of the deconfinement phase transition at high baryon densities,
- the critical point providing direct evidence for a phase boundary,
- exotic states of matter such as condensates of strange particles.

In particular. the research program is focused on the investigation of [7–11]:

- short-lived light vector mesons (e.g. the ρ-meson) which decay into electron-positron pairs. These penetrating probes carry undistorted information from the dense fireball.
- strange particles. in particular baryons. so called multistrange hyperons (A. Ξ. Ω).
- mesons containing charm or anti-charm.
- collective flow of all observed particles.
- event-by-event fluctuations.

1.3 Heavy-ion collisions

When two heavy ions of relativistic velocities collide. a reaction that produces various types of elementary and complex particles can be observed. If the fireball has also been constricted. we deal with moderatelly hot. highly compressed nuclear matter. Such a state of matter can be created and investigated in modern accelerators. such as the one being built in the FAIR (Facility for Antiproton and Ion Research) in Darmstadt. It also exsists in so far unexplored phases in an interior of a neutron stars and in a core of type II supernova explosions. Modern theoretical models derived from the equation of state of ultra-dense nuclear matter (like relativistic mean-field model [12] or density dependent relativistic Brueckner-Hartree-Fock model [13]) predict structure of a neutron star as shown in Fig. 1.3 on the following page. At present. none of these phases of subatomic matter can be ruled out by an experiment. Future research may provide additional data on structure of neutron stars. as well as the information on nuclear equation-of-state at high baryon densities. on the in-medium properties of hadrons and on location of the deconfinement phase transition.

In the CBM experiment. J/ψ meson is one of the essential particles in the quark-gluon plasma study. The detection. selection and identification of the meson are also key goal of this study.

The modern high energy experiments are focused on detecting rare particles. which can be used as probes in the nuclear matter created during the collision. Such particles have very low multiplicities. therefore the experiment must be performed at high beam intensity. Since the interaction rate is high. the complete detector data cannot be stored and the sophisticated data selection algorithm must be used. The algorithm combined with computational farm is capable of selecting the potentially interesting data among the other. reducing the background event rate. After the pre-selection stage. the data rate is adequate to be stored for further off-line analysis.

1.4 History of J/ψ discovery

The J/ψ particle was first encountered in two independent experimental groups. one at the Stanford Linear Accelerator Center (SLAC) led by Burton Richter and another at

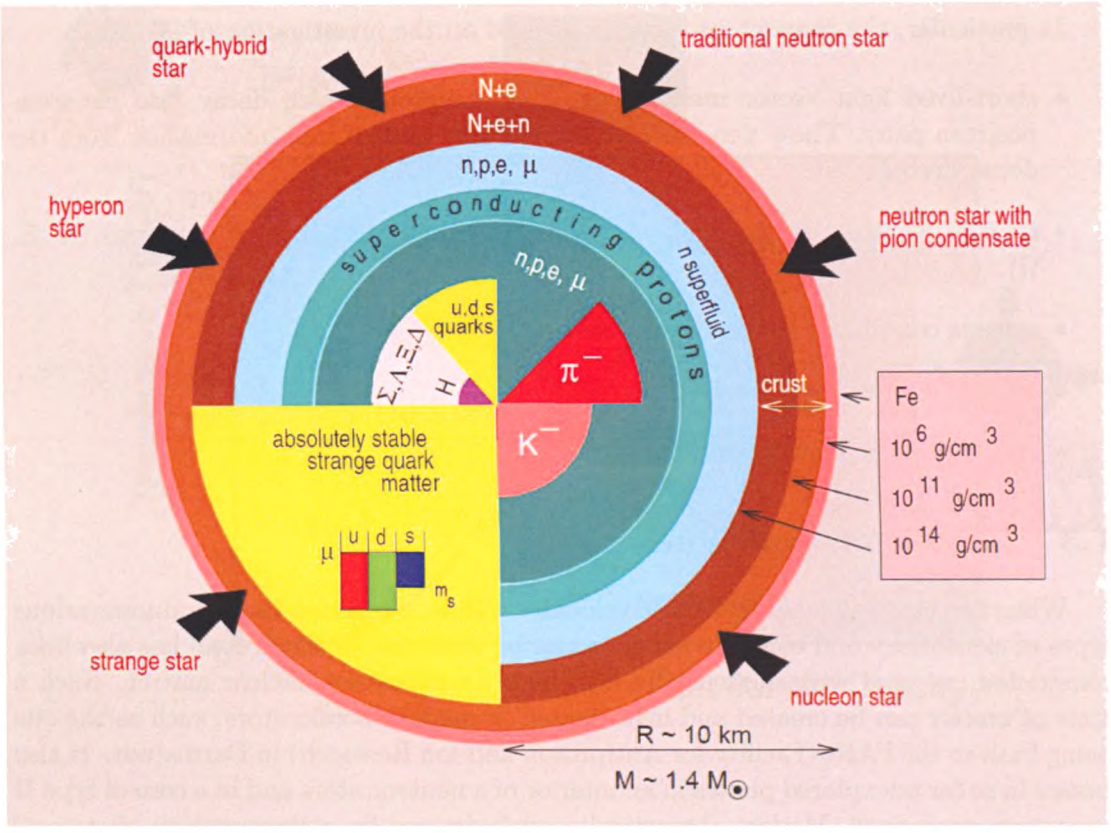

Figure 1.2. The interior of a neutron star. Neutron stars are space objects that contain matter in one of the densest form found in the Universe. The matter in the core regions of a star is highly compressed, exceeding the density of ordinary atomic nuclei, even by the order of magniture. The compression provides the environment for numerous subatomic particle processes, that are likely to compete with each other. These are, among others, generation of hyperons and baryon resonances (Σ, Λ, Ξ, Δ), quark (u, d, s) deconfinement, formation of boson condensates (Π^-, K^-, H-matter). The quark matter in neutron stars, strange stars, or strange dwarfs ought to be in a color superconducting state. Picture adopted from [14].

the Brookhaven National Laboratory headed by Samuel Ting. The Ting's experiment used high-intensity proton beams accelerated by the Alternating Gradient Synchrotron (AGS). which bombarded stationary beryllium target with protons to produce showers of particles. The analysis of collected data revealed a strong peak in electron and positron production at an energy of 3.1 GeV. This brought the suspection that a new particle has been produced. Meanwhile. the other experiment was being carried out on the newly built accelerator SPEAR. Burton Richter had no specific agenda in mind. outside of an interest in the structure of strongly interacting particles. when he started his new research. What he found in November of 1974. however. was a new particle that was about three times the size of a proton and with an approximately 5 000 times greater lifespan than naturally expected.

The discovery has been made in almost the same time. and the scientists realized that they found the same particle. One of the teams proposed to name it J. while the other stuck to the name ψ. The discovery was announced on November 11. 1974 and

the name J/ψ has been agreed.

The successful detection of previously unknown particle earned in 1976 the Nobel Prize in Physics for Richter and Ting. It also helped to confirm the existence of the charmed quark, which was predicted by, previously ignored, theoretical works.

The J/ψ is a meson which appear in high-energy collisions of elementary particles or heavy ions. This subatomic particle is neutrally flavored, and consists of a charm quark and a charm antiquark. Mesons that are formed by a bound state of a charm quark and a charm antiquark are generally known as "charmonium".

The J/ψ and its discovery shed new light on quarks and their interactions. It provided support for the theory that there existed a fourth quark, called the charmed quark, in addition to those predicted by early quark models (i.e., the up, down, and strange quarks).

Chapter 2

Theory overview

The investigation of the recent years conclude that the nuclear matter. at various pressures and temperatures. as well as plain water have much in common as far as their properties in different states are concerned. Certain analogies can be pointed. which are the basis for the following study.

2.1 Phases of water

The most commonly known substance throughout the Earth is water. It exists as ice. steam or liquid. At the temperatures below 0°C and atmospheric pressure. equal to 101.325 kPa (760 mmHg. standard atmosphere) water appears as ice. Between 0°C and 100°C we have liquid. As one adds more energy to water. i.e. by heating. above 100°C water evaporates creating the gas called steam.

However. when water reaches either its melting or boiling points. further heating does not effect in an immediate rise of temperature. Instead. the latent heats of fusion (which is equal 80 kcal/kg) or vaporisation (540 kcal/kg) need to be overcome. If water. when boiling. receives more heat. more of the fluid water turns into steam. The temperature of boiling water stays at 100°C even if further ammount of energy is added. The gas and liquid coexist as long as there is still liquid water left. There is no further rise of temperature until all the liquid is converted to steam. Such type of transition between two phases with a latent heat and phase coexistence is called "first order phase transition" [15].

As the pressure is being raised. the boiling temperature of water increases up to the critical point at a pressure 22.1 MPa (which is 218 times the atmospheric pressure) and to the temperature of 374°C. At this point the phases coexist no more and the phase transition becomes continuous or "second order". The diagram which shows the phases of water depending on pressure and temperature is shown in the Fig. 2.1 on the next page.

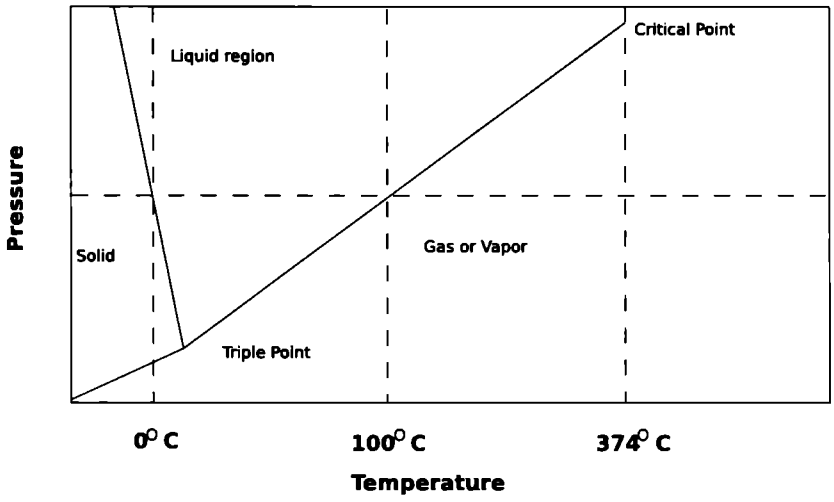

Figure 2.1. This is water phase diagram. The triple point, at which three phases coexist, is situated at low temperature and pressure. The critical point is located at high temprature and pressure.

This phase diagram shows that with the increase of pressure, ice can become water. The diagram shows the state of H_2O and its dependency to temperature and pressure. It can be used to predict the state of water, as it is described by the mathematical relations. These relations are called the "equation of state" of water.

2.2 Phases of nuclear matter

As water and its relation to pressure and temperature belongs to the macroscopic world, there is the analogy in the microscopic one, namely the state of a nucleus depends on temperature and on density of the nucleons.

The question is: what is the equation of state of nuclear matter?

In their normal states of lowest energy, nuclei expose liquid-like characteristics and have the density of 0.7 nucleons/fm^2.

In the laboratory environment, the only known method to heat the nuclei to higher temperatures is to collide them with other nuclei. This technique allows to achieve the energy region of hundreds of MeV. As 1 MeV is an equivalent of $1.2{\cdot}10^{10}$ K, the temperature possible to reach is more than 200 million times the temperature at the surface of the Sun (~5500 K).

When the nuclei are heated to a temperature of a few MeV, the nuclear "liquid" starts to evaporate. From the general form of the interactions between nucleons, we know that, like water, the nuclear liquid also has a latent heat of vaporisation. Furthermore, the nuclei should also undergo a first-order phase transition. The coexistence of the liquid and gas forms is expected to cease at a critical point, the critical point of nuclear matter. One of major goals of heavy ion research institutes is to find out whether these theoretical predictions are correct. The experiments are aimed at determination of the temperature and density at which the critical point of nuclear matter is located.

There are some major experimental challenges that need to be faced when exploring the nuclear equation of state. The hot and dense conditions can be fulfilled during the heavy ion collisions. There is very short time scale (of about 10^{-21} s) when the nuclear

matter meets some certain demands. Furthermore, the matter almost immediately cools down and expands, making the conditions unsuitable for research. There is also no direct way to measure the state variables (such as temperature, pressure and density). They can be determined using one of the above indirect measurements:

- the ratio of isotopes
- the population of excited nuclear states
- the shapes of the energy spectra from nuclear collision remnants
- the production of particles such as pions.

One must remember that during the heavy ion collision, thermal equilibrium cannot be established during very short time scales. Another difficulty is the number of particles. Usually, when studying the properties of water, each sample contains enormous numbers of molecules, while nuclear collision provides up to a couple of hundreds only. This makes it hard to find the evidence of commencing phase transition.

The modern science has at its disposal the resources to measure the thermodynamics state variables during heavy ion collisions. The thermal equilibrium can be established for the moments of order of 10^{-21} seconds, allowing to find the signs of phase coexistence. There are also experiments being built that have the potential to pin down the critical point of the nuclear liquid-vapor phase diagram [16]. Essential information on the nuclear equation of state are revealed by the size of fragments produced when nuclear matter is near its critical point, as confirmed by recent experiments on nuclear breakup.

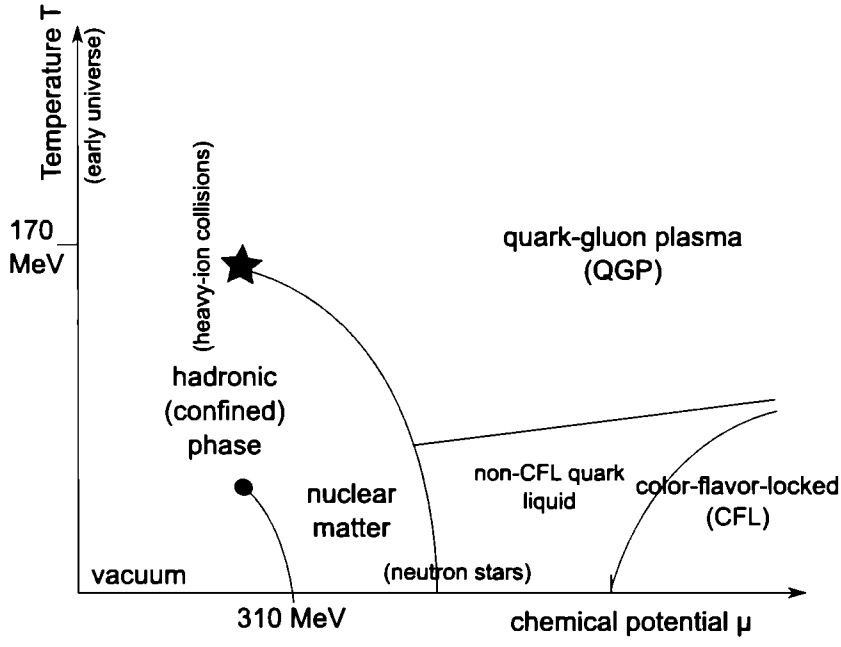

Figure 2.2. The nuclear matter phase diagram. The critical point is expected to be at a temperature 170 MeV and at baryon density higher than in the ordinary atomic nuclei. The area is within the reach of modern particle accelerators. Redrawn from [15]

The figure 2.2 shows that phase transition between the nuclear liquid and a gas of

nucleons may occur, as well as that the nucleons may undergo a phase transition at higher temperatures.

In extremely dense gas of hadrons, the boundaries of nucleons overlap and its consistuents, i.e. quarks, can move freely across the entire nuclear volume. This state is called quark-gluon plasma in analogy with atomic plasma, where electrons are no longer restricted to atoms. The theorists expect the phase transition from hadrons to quark-gluon plasma to be of first order, with a phase coexistence region present [17].

A region, which appears at the greater hadron densities and low temperatures, belongs to space object called neutron stars. When a massive star undergoes a supernova explosion, a core of iron nuclei remains. All remnants are held together by the gravity, while the short-range nuclear repulsive force is not strong enough to separate the nuclei. When the core of a star collapses, the nuclei fall apart, transforming into unbound protons and neutrons. By inverse beta decays, the former is converted into the latter, resulting in a tremendous collections of neutrons. The typical size of a neutron star is a few kilometers in diameter, which is enough to produce matter densities above the average nuclear matter density (i.e. up to 7 kg/m^3 [18]).

2.3 Ultra-relativistic Quantum Molecular Dynamics

The Ultra-relativistic Quantum Molecular Dynamics (UrQMD [19]) model has been proposed to evaluate the reactions during the collisions of hadron-hadron, hadron-nucleus and heavy ion. It uses a microscopic many-body approach to simulate multiple interactions of in-going and newly produced particles, the excitation and fragmentation of colour strings and the formation and decay of hadronic resonances. The model can produce particles created during the collision of Au+Au ions at the energy 25 GeV per nucleon in the laboratory frame, and its results are consistent with the experimental data [20]. It has been successfully applied to heavy-ion reactions at the Bevalac, SIS, AGS and SPS accelerator facilities, spanning incident beam energies from 0.5 GeV per nucleon (at the Bevalac and SIS facilities) up to 200 GeV per nucleon (at the SPS facility). Therefore the output of this model is a good representation of a real reaction with such parameters. Main goals in the application of the UrQMD model are to gain an understanding about the following physical phenomena within a single transport model:

- creation of dense hadronic matter at high temperatures,
- properties of nuclear matter, Delta & Resonance matter,
- creation of mesonic matter and of anti-matter,
- creation and transport of rare particles in hadronic matter,
- creation, modification and destruction of strangeness in matter,
- Emission of electromagnetic probes.

A drawback of the used model is a lack of generation of short-lived particles, like mesons. It is assumed at the end of calculation time that all mesons decay and only hadron particles remain.

Chapter 3

Overview of the CBM detector

CBM Experiment is a part of Facility of Antiproton and Ion Research (FAIR) project being built at the suburbs of Darmstadt. Germany. The schematic overview of FAIR is shown in Fig. 3 on the next page. The new SIS100 synchrotron will provide up to U^{238} beams at 2.7 AGeV at the intensity $4 \cdot 10^{13}/s$. After installation of SIS300. beams of U^{238} ions at 34 AGeV with the intensity of $2 \cdot 10^{10}/s$ will be possible.

In CBM. it is planned to measure high-penetrating probes of the nuclear matter. such as rare mesons. which emerge when two compressed heavy ions collide. In order to stand a chance to detect such particles. one has to built a sophisticated detector system. At present. throughout computer simulations show that the optimal setup is as follows:

- Diamond Pixel Detector
- **S**uperconducting **D**ipole **M**agnet (SDM)
- **S**ilicon **T**racking **S**ystem (STS)
- **M**icro-**V**ertex **D**etector (MVD)
- **R**ing **I**maging **Ch**erenkov detector (RICH)
- **T**ransition **R**adiation **D**etector (TRD)
- **R**esistive **P**lates **C**ounter (RPC a.k.a TOF)
- **E**lectromagnetic **Cal**orimeter (ECAL)
- **Spec**lectromagnetic **Cal**orimeter (ECAL)
- **MU**on **CH**amber (MUCH)

The CBM dielectron setup is shown in Fig. 3 on the following page. Many of the signatures aimed with the CBM experiment are based on rare processes. Also. the detector data flow from such setup is very high when measuring with interaction rates of 10 MHz for A-A collisions and up to 100 MHz for p-p and p-A collisions. This requires a powerful data acquisition and on-line analysis systems to maintain adequate sensitivity. The most demanding matter is production of open and hidden charm characterized by low cross sections. therefore highest beam intensities must be used for that purpose. Below are described individual detector units and the data acquisition system.

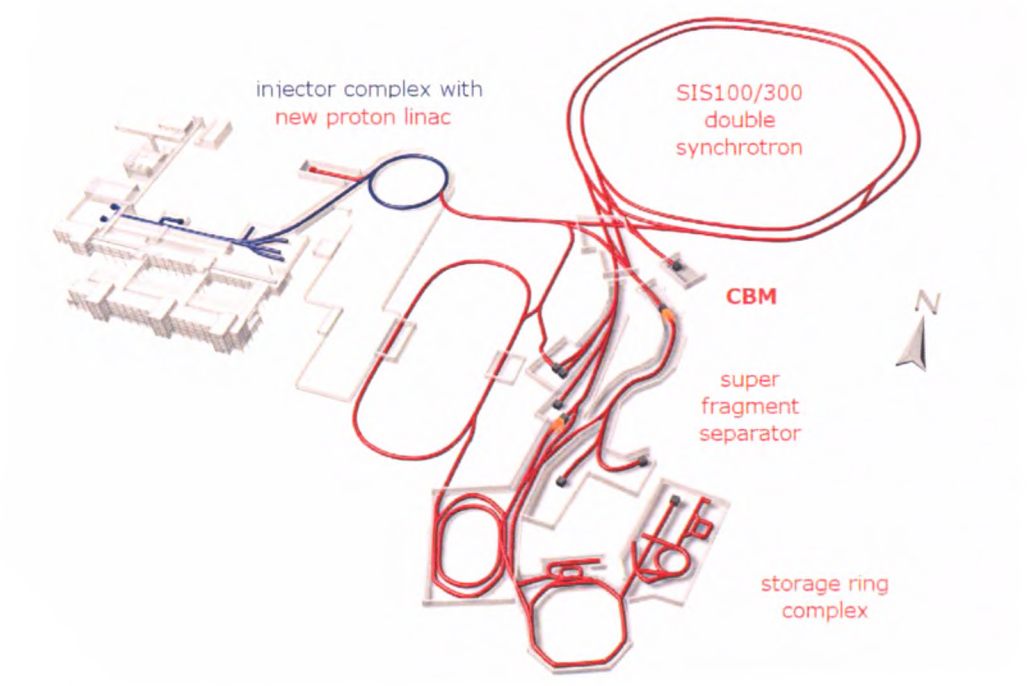

Figure 3.1. FAIR project overview. The existing facilities are marked with blue while the red ones are under construction. Picture adopted from [21].

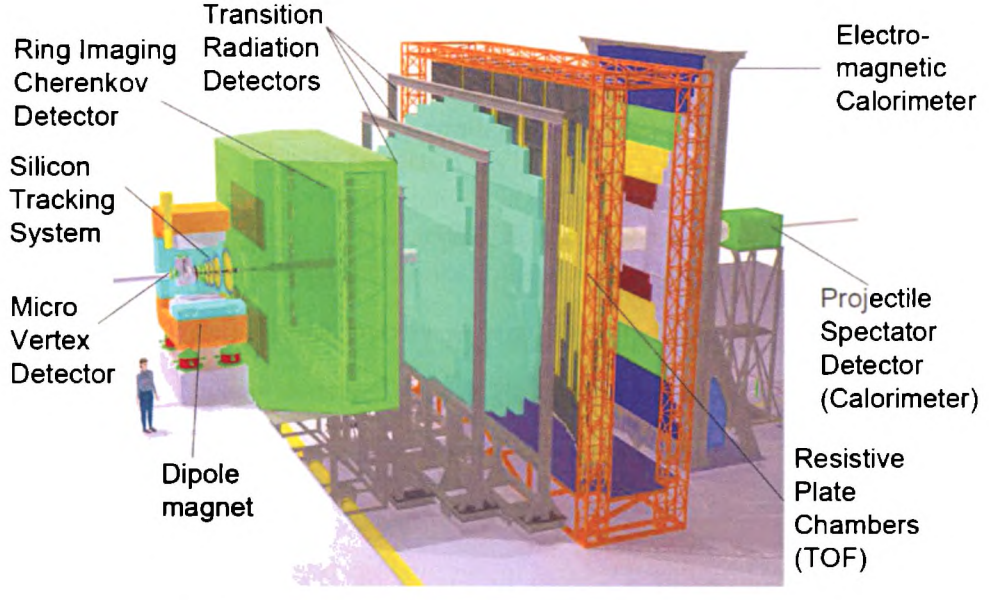

Figure 3.2. The CBM dielectron setup. Picture adopted from [21].

The full setup will be available along with the SIS300 particle accelerator, allowing for 40 AGeV Au+Au collisions of high intensity beams. This configuration will offer J/ψ measurement capabilities at sufficient effciency per day. Prior to SIS300, the setup will operate using SIS100 beams, and the particle identification will be done using RICH

and RPC subsystems only. Also, the research program will cover different goals, vector mesons among others. The TRD will not be included into SIS100-driven setup, giving the additional time for development of this sophisticated detector.

For the purpose of charmonium and light vector mesons measurements, muon option is proposed. The setup will consist of STS. TRD and RPC detectors along with special MUCH subsystem. The setup overview is shown in Fig. 3. For further information see 3.9 on page 21.

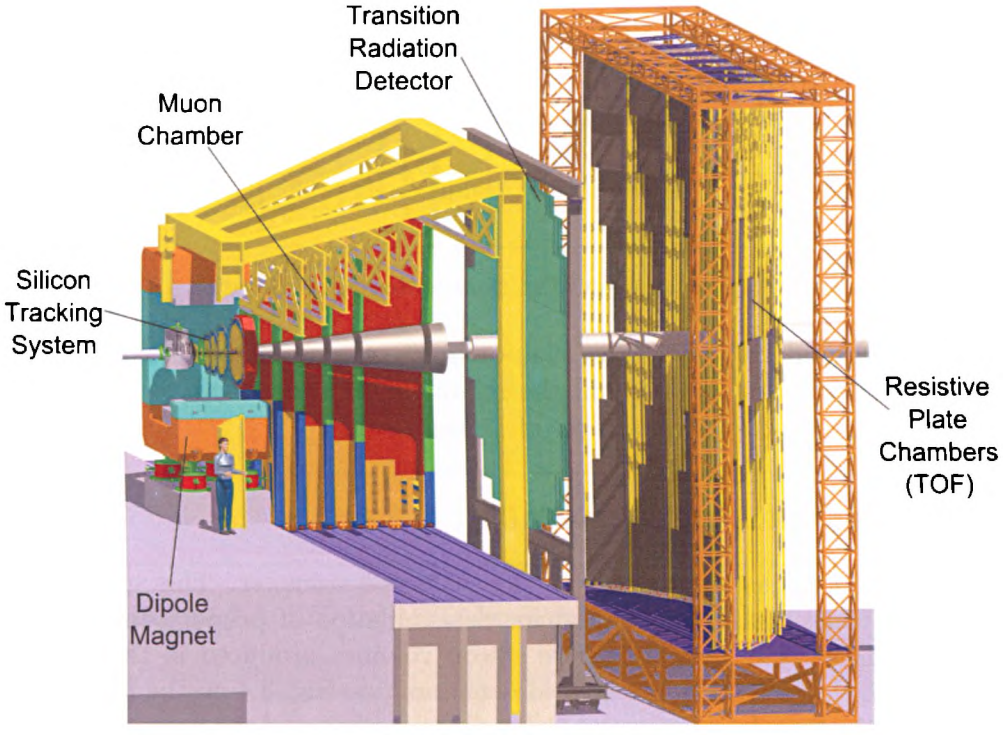

Figure 3.3. The CBM muon setup. Picture adopted from [21].

3.1 Diamond Pixel Detector

The radiation-hard Diamond Pixel Detector serves as a START signal for the Time Of Flight system. STOP signal is generated by RPC detector.

3.2 Superconductiong Dipole Magnet

The dipole magnet is used for bending the particle trajectories, which is essential for accurate momentum determination. The magnet serves also as a deflecting force, which removes the delta electrons. Inside, there are the MVD and STS systems, which require the apropriate gap to fit into. The bending force will be of order 1T which allows to achieve by the STS the momentum resolution of the order of 1%.

3.3 Micro-Vertex Detector

MVD detector consists of two layers of MAPS (Monolythic Architecture Pixel Sensors) situated closest to the target. The most probable locations are shown in Tab. 3.1(z = 0 corresponds to the target center). Detector stations operate inside a vacuum vessel. MVD is meant to distinguish particle decay vertices from the event vertex, and it is optimized for very good precision. This task requires a detector with high position resolution, very low material budget, high radiation tolerance and a fast self-triggered readout.

Z positions of the MVD stations	
Station No.	**Z position [cm]**
1.	5
2.	10
Alternatively/Additionaly	
3.	20

Table 3.1. Placement of stations within MVD detector.

MAPS will be used with a pixel size of 40×40 μm^2, offering spatial resolution of 3 μm. The thickness of 100 μm would fulfill the requirements concerning vertex resolution needed to measure the displaced vertices of D mesons [22].

3.4 Silicon Tracking System

The STS is the mainstream device in the CBM spectrometer. This subdetector is responsible for track measurements and for determination of primary and secondary vertices. It consists of 5 layers of active silicon volumes produced in three different technologies: Pixel, Microstrip and Hybrid detectors (see Fig. 3.4 on the facing page).

The STS is the first detector in the direction donwstream of the beam axis, capable of registering tracks of all charged particles created in the target. It resides in the geometrical center of the magnetic field which is essential for momentum reconstruction of the particles. The maximum value of the field, B_{max}=1.5 T, provides the perpendicular momentum kick of $p \approx 0.3$ GeV/c over the full extension of the tracking station [22]. That makes possible to achieve the three basic goals:

- track reconstruction of all charged particles with momenta above 0.1 GeV/c, with momentum resolution better than 1% at 1 GeV/c (read above)
- primary and secondary vertex reconstruction allowing for studies open charm production
- V_0 vector meson track recognition for reconstruction of weak decays

The STS-MVD combined detector consists of 8 stations placed inside a magnetic dipole field which provides the bending power required for momentum determination with an accuracy of about $\Delta p/p = 1\%$.

The proposed STS positions are shown in Tab. 3.2 on the next page. Although this layout gives the highest tracking efficiency, other options are still under consideration.

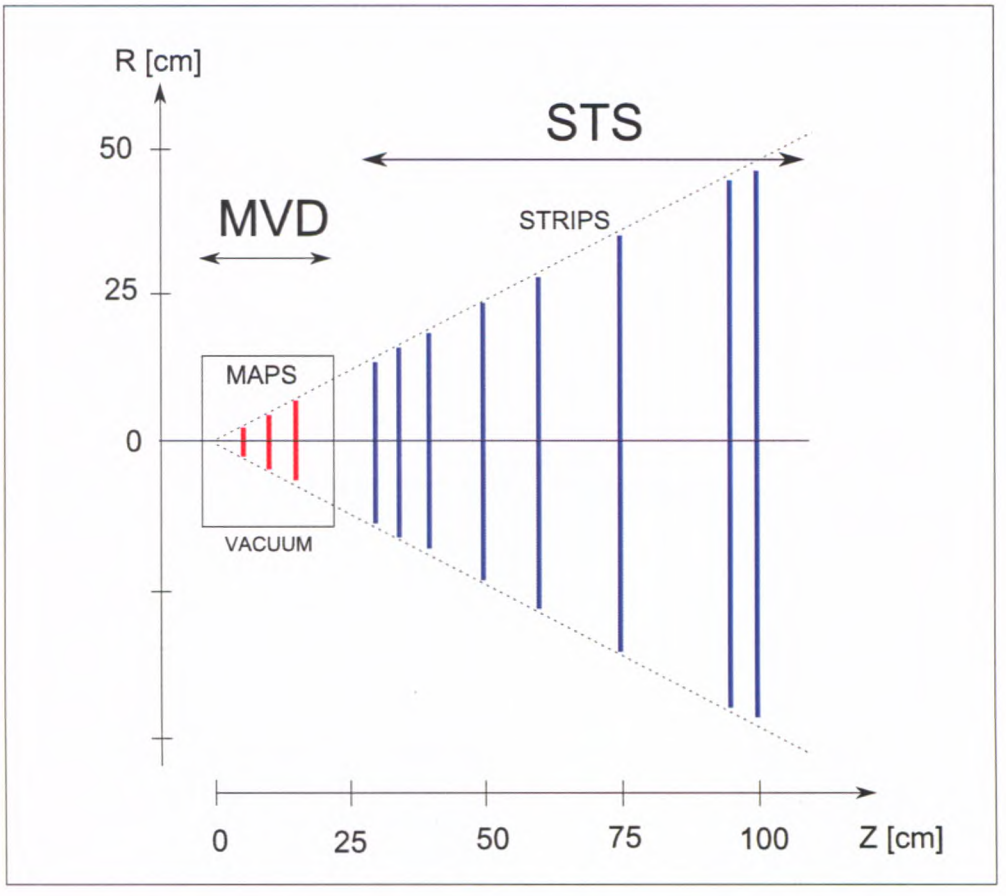

Figure 3.4. STS and MVD detectors layout. Modified from [23]

Z positions of the STS stations	
Station No.	**Z position [cm]**
1.	30
2.	35
3.	40
4.	50
5.	60
6.	75
7.	95
8.	100

Table 3.2. Placement of stations within STS detector.

Track information is needed for all charged particles, under conditions of high event rate. going up to 10 milion reactions per second (10 MHz). The STS-MVD stations are situated inside the magnet, and each provides two-dimensional information about a given particle crossing the station. Also. the first MVD layers are contained inside the vacuum vessel of the beamline. The construction provides the necessary amount of geometrical information. allowing to reach the desired track reconstruction efficiency. As STS detector is situated entirely within the magnetic field. therefore the trajectories

of crossing charged particles are bent. In order to reconstruct particle tracks. sophisticated tracking must be incorporated. It bases on the Cellular Automaton approach. and uses Kalman Filter method for track fit [23, 24]. The efficiency of the tracking in STS can be observed in Fig. 3.6 on the facing page. Detailed description about tracking in detector is presented in Chapter 5.

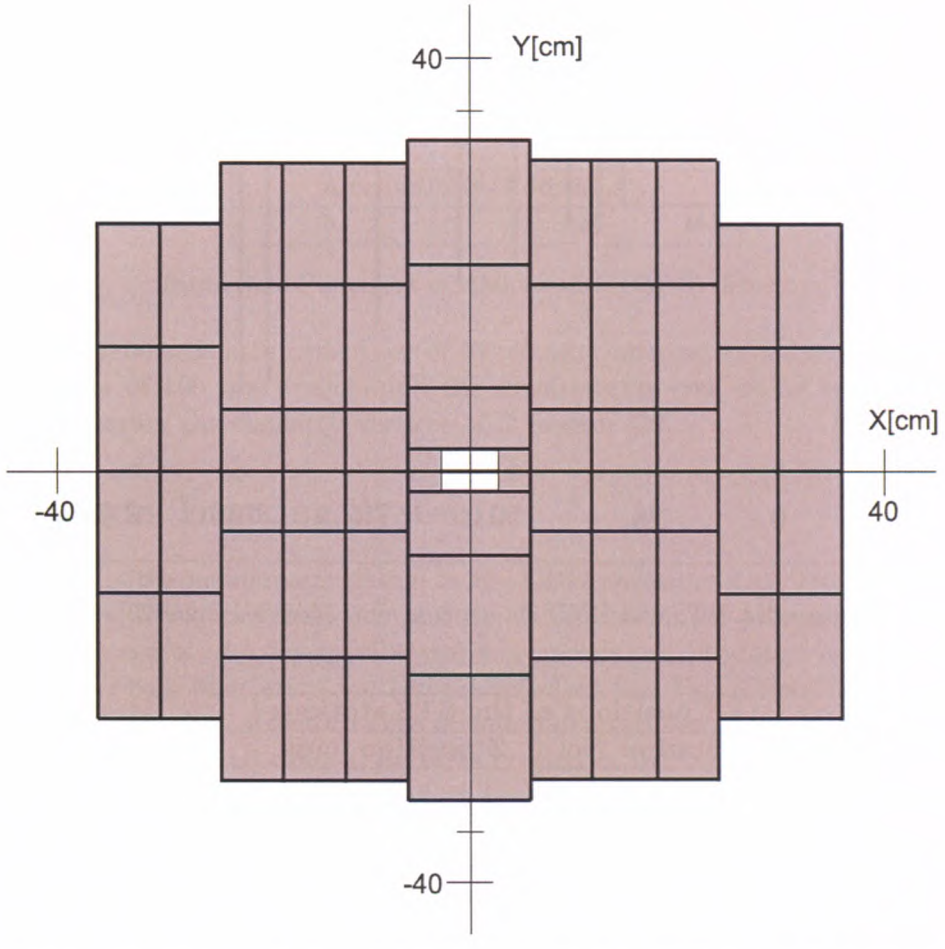

Figure 3.5. Section of an example STS station (situated at Z = 50 cm). The sensors are arranged in vertical modules of horizontal sizes of 6 cm which correspond to the rectangular regions in the picture. The readout electronics are placed in the outer rims, outside the sensitive area.

The stations have ladder structure (see Fig. 3.5) and are built of double-sided silicon micro strip sensors, 300 μm thick. The read-out electronics is placed at the perimeter of the STS to achieve low-mass detector with 60 μm strip pitch. These are connected to front-end boards with thin capton micro-cables. which aquire signals from individual sectors [22].

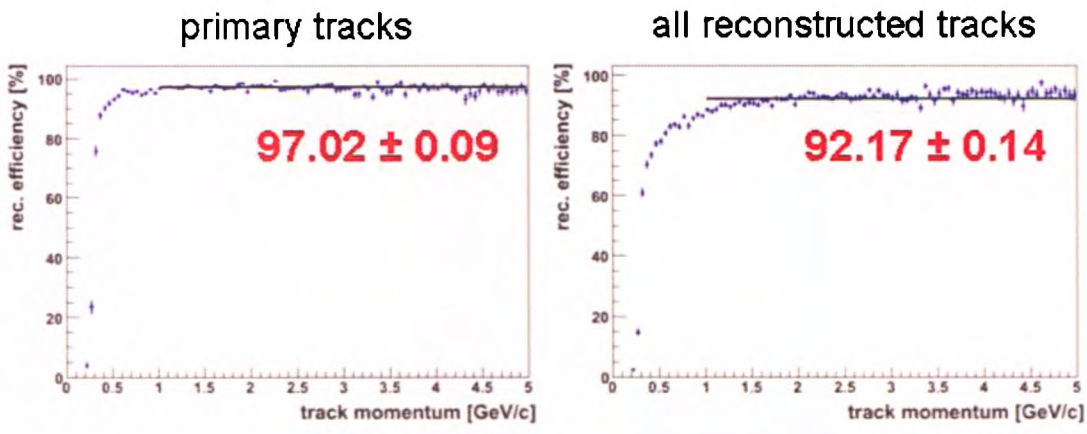

Figure 3.6. Tracking efficiency in STS for particles coming from the target (left part), and for all particles (right) [25].

3.5 Ring Imaging Cherenkov Detector

The RICH detector has been introduced into setup to provide the means to distinguish electrons from pions coming out of last STS station. The layout of the detector is shown in Fig. 3.5 on the following page.

The principle of this detector is based on registering the Cherenkov radiation: a kind of electromagnetic radiation that is emitted when a charged particle (such as electron) passes through an insulator at a constant speed greater than the speed of a light in that medium. In a typical RICH detector, a cone of Cherenkov radiation is produced when a particle traverses a suitable gaseous medium called radiator. The photons from the light cone are collected by a spherical mirror and focused onto the photon detector placed at the focal plane. The result is a circle with a radius independent on the emission point along the particle track [26]. The example is shown in Fig. 3.5 on the next page.

The momentum range covered by RICH is suitable for identifying electrons from low-mass vector meson decays, as well as these coming from decays of charmonium. The required pion suppression is a factor 100-1000 for RICH alone, which, combined with other detectors, such as TRD mentioned below, will lead to an overall efficiency of 10^4 (see Fig. 3.9). The other purpose of this detector is separation of fast kaons, which requires simultaneous lepton identification in a restricted momentum range (< 5 GeV/c).

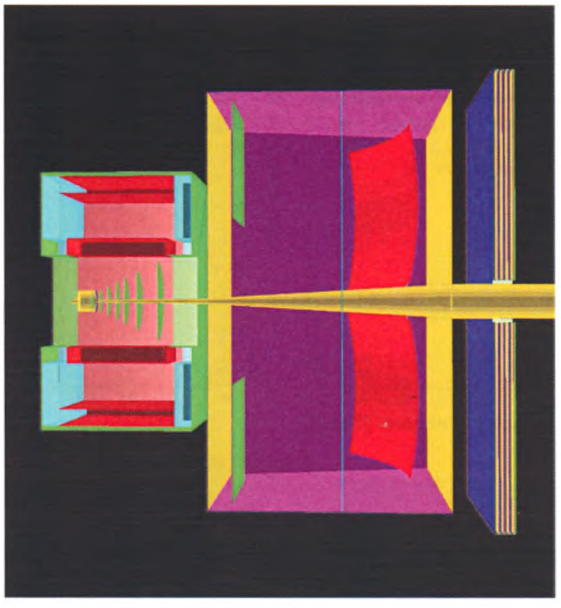

Figure 3.7. The schematic layout of RICH detector. Photodetector plane is marked green: glass mirror is presented in red. Light blue planes to the right perpendicular to the beam axis are the first TRD station. Adopted from [27].

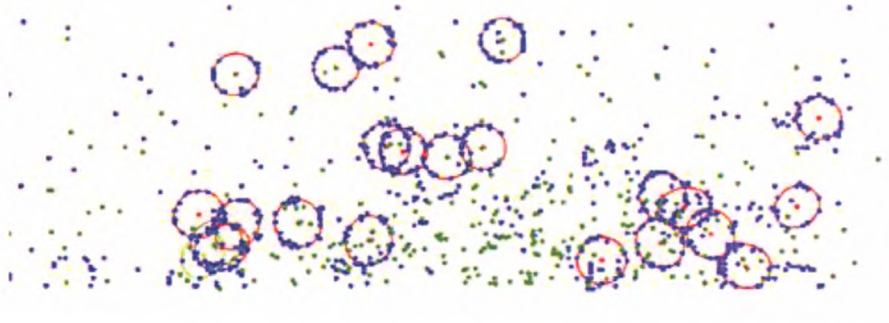

Figure 3.8. An example of rings collected in RICH. Each ring consists of about 20 photoelectrons and has approximately 6 cm in diameter. Adopted from [27].

Cherenkov detector will be positioned behind the magnet (with silicon tracking system inside) and in front of the first transition radiation detector station, covering 25° of the geometrical acceptance. The detector is composed of a vessel (6-7 m width, 5 m height, 3 m depth) filled with radiator gas (N_2 with admixture of CO_2 for suppression of fluorescent light, if needed), the mirror (made of glass or carbon substrate with Al+MgF_2 coating) of a surface about 5-6 m x 4 m, and a photon detector with an array of about 100 000 channels (granularity 6 mm x 6 mm) with photon efficiency of 20%.

The detector array, situated on the focal plane, registers UV photons reflected by the mirror. Photons coming from the light cone emitted by a single particle form a shape of a ring if detected by a photodetector. If there are more than 10 hits per ring detected, a sophisticated ring recognition method can be applied (Elastic Net approach [28]). The method is fast (10 ms per one Au+Au event at 25 AGeV on Core2Duo machine [1]).

efficient (reconstructs 90% of all rings) and suitable for applying in the experiment.

The readout is assumed using data from two arrays of photodetectors shielded by a yoke of the magnet. 3.2 m x 1.4 m each. The number of channels differs from 140 000 to 214 000. depending of a type of the photodetector used. The current design assumes over 20 points per ring with N_2 radiator.

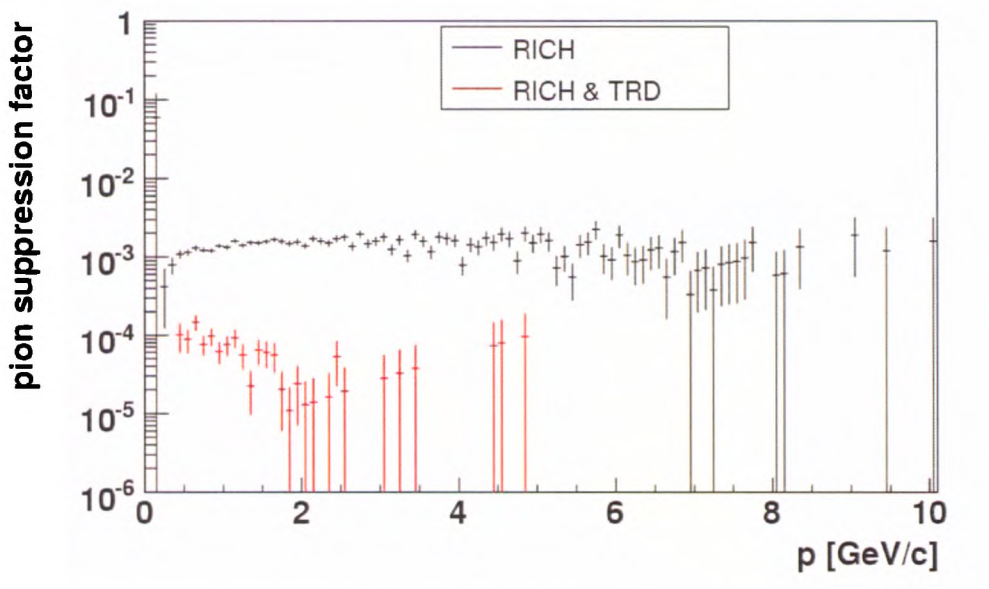

Figure 3.9. Pion suppression factor= $\frac{\pi \ identified \ as \ e}{\pi \ in \ RICH \ and \ TRD}$. Picture adopted from [29].

3.6 Transition Radiation Detector

Transition Radiation Detectors are being used in high energy physics to improve the identification of electrons with respect to pions for momenta above 1 GeV/c. The TRD will allow to study various aspects of dielectron decays. among them production of quarkonium state (J/ψ and Ψ'). as well as the production of open charm.

TRD is the only CBM detector subsystem which allows both to perform particle identification and to determine particle momentum. It consists of three stations. four sensitive layers each. giving 12 layers in total (see Tab. 3.3). Such number of measuring planes is enough to achieve good tracking efficiency (about 90% or more).

Z positions of the TRD stations	
Station No.	**Z position [m]**
1.	5.00
2.	7.25
3.	9.50

Table 3.3. Placement of stations within TRD.

A single layer of TRD consists of radiator. which produces the TR as electrons and positrons pass through. and a gas detector. which allows to measure the energy deposited by particles and TR quanta. The latter contains a Drift Chamber (DC) and

an amplification region. The gas mixture is based on Xenon in order to maximize the absorption of TR. As a radiator, mylar and polypropylene could be used.

The identification is performed employing the Transition Radiation effect: Transition Radiation (TR) is produced when a relativistic object traverses through inhomogenius medium, especially the boundary between materials with different dielectric constants ϵ. Particle identification works for at least 1.5 GeV/c electrons and positrons (i.e. for $\gamma > 1000$), which are essential for reconstruction of J/ψ meson decays. In such momentum region, only electrons and positrons have a chance to produce TR, thus offering the possibility to separate them from charged pions or protons.

The electron efficiency of 90% can be reached, as well as the pion suppresion factor of 100 and more for high-momentum particles (of 2 GeV/c or more). There are several pion identification techniques available, which offer even more effiective results. They will be presented later in this work.

The high interaction rate (of the order 10^9 Hz) requires the detector readout to be very fast, as large multiplicities and high counting rates are expected in CBM detector setup, especially in the inner part of the detector layer (which is less than 30% of the active TRD area). The central part of the TRD, covering forward emission angles will be exposed to counting rates of up to 100 kHz/cm^2 for 10 MHz Au+Au collisions at 25 AGeV. In order to minimize the space charge effect, the gas volume must be sufficiently thin. On the other hand, certain pion suppression must be achieved. Moreover, the TRD tracking feature will be used for all charged particles, achieving position resolution 300-500 μm[1], for x and y (z is assumed to be parallel to the beamline). Prototype gas detectors based on MWPC and GEM technology have been built and tested with particle rates of up to 400 kHz/cm^2 without deterioration of their performance. [21]

Each TRD layer covers an area of about 30 m^2. With pad sizes between 1 cm^2 and 25 cm^2, the total number of channels per layer amounts to about 35 000. The occupancy is assumed to be 5%.

The major technical challenge is to develop highly granular and fast gaseous detectors which can stand the high-rate environment of CBM in particular for the inner part of the detector planes covering forward emission angles.

3.7 Resistive Plate Chambers

The RPC detector serves as a *STOP* signal for Time Of Flight (TOF) system. The *START* signal is generated by a Diamond Pixel Detector situated upstream the target. Although the RPC is relatively old technology (dating back to 1981 [30]), it was shown only in year 2000 that it is possible to use RPCs for precise time of flight measurement at normal conditions of pressure and temperature with inexpensive materials [31]. In such way it has been incorporated in several working or planned experiments like Alice [32], FOPI [33], HADES [34], HARP [35], STAR [36]. The main function of RPC detector is identification of hadrons by time of flight. It can be used to eliminate most charged pions and to separate kaons from electrons.

[1]The resolution for the more precise coordinate; the other coordinate is determined with accuracy 3-30 mm.

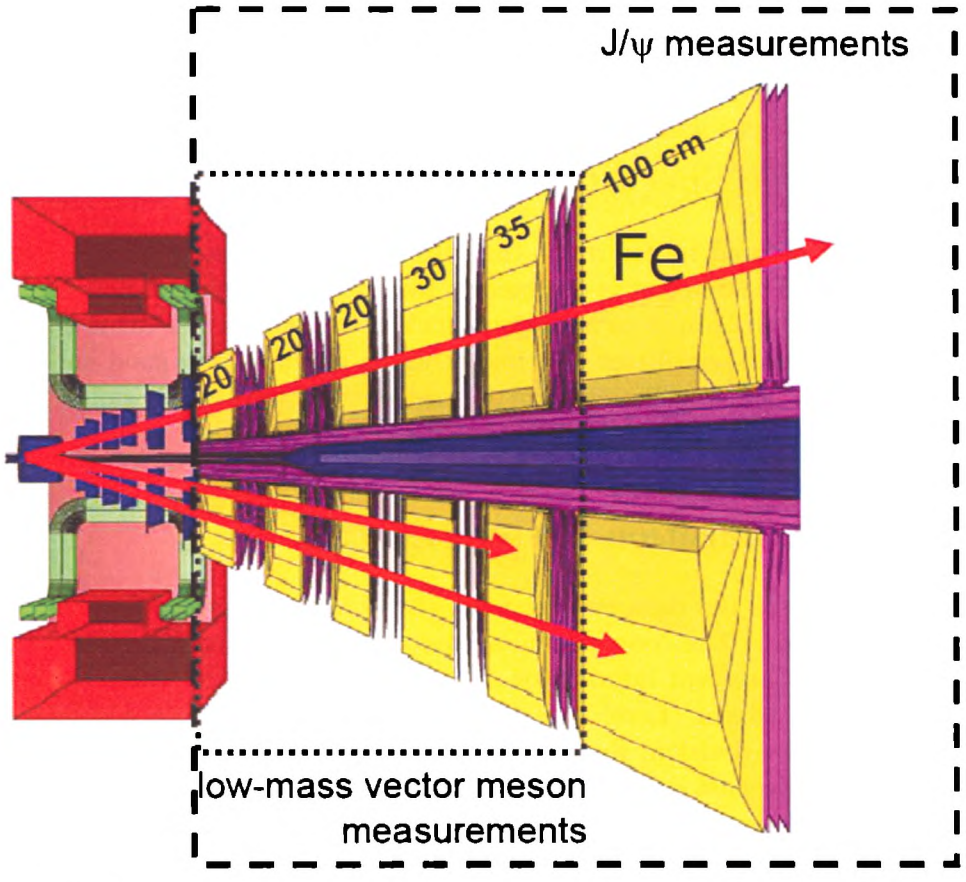

Figure 3.10. Muon setup for CBM experiment. Dipole magnet is marked with red, STS is blue and iron absorbers are presented in yellow. Violet plates perpendicular to the beam axis are gaseous detectors.) [37]

3.8 Electromagnetic Calorimeter

ECAL will measure direct photons and neutral mesons (π^0, η) decaying into photons. A "shaslik" type calorimeter as installed in the HERA-B [38]. PHENIX [39] and LHCb [40] experiments will be used. The detector will be composed of modules which consist of 140 layers of 1 mm lead and 1 mm scintillator, with cell sizes od 3×3 cm^2, 6×6 cm^2 and 12×12 cm^2. The shashlik modules can be arranged either as a wall or in a tower geometry with variable distance from the target.

3.9 Muon Chamber

The muon chamber is an alternative approach to the dielectron measurement - see Fig. 3.10. The possibility of detecting light vector mesons and charmonium via dimuon decay is under study. The MUCH setup is dedicated for muon measurements, therefore 6 massive iron absorber plates interleave STS detectors which serve as tracking and momentum determination subsystem. In such approach the RICH and the two first TRD stations are removed. Only the last TRD station is left to identify the incoming

particles. In addition, several layers of gaseous detectors based on Gas Electron Multipliers (GEM) technology and straw tubes are incorporated, residing between the iron absorbers. ECAL is removed from the setup, as it is unusable for muons.

3.10 Projectile Spectator Detector (PSD)

The PSD will be used to determine the collision centrality and the orientation of the reaction plane. The detector is designed to measure the number of non-interacting nucleons from a projectile nucleus in nucleus-nucleus collision. The PSD is a full compensating modular lead-scintillator calorimeter which provides very good and uniform energy resolution. The scintillation light is read out via wavelength shifting (WLS) fibers by Multi-Avalanche Photo-Diodes (MAPD).

3.11 Data Acquisition System

In order to handle the data coming from the detectors, new dedicated data acquisition is developed. The conventional system design involving triggered front-end electronics requires the event information to be kept for a limited time. During that time, the first level trigger (Level 1 or L1) makes the decision from a subset of the data. After a positive decision, the data are transported to higher level processing or mass storage unit. Because complex algorithms are involved in making decisions, such system does not correspond to CBM goals. Also, the computational effort needed for a decision varies from event to event in high beam intensity measurements.

The CBM data processing system incorporates self-triggered front-end electronics, where each particle hit is autonomously detected and the measured hit parameters are stored with precise timestamps in large buffer pools. The event is built by evaluation of the time correlation of hits. Further selection of interesting event is performed by processing data resources stored in buffers. The access to buffers is provided via a high speed network fabric. The essential performance is limited by the total computational power rather than the decision latency. Also, as there are no dedicated data paths, all detectors may contribute to event selection decisions at all levels, offering the flexibility in different operation modes.

In the above approach there is no physical trigger which forces the data acquisition system to read a selected event and transport it to further processing or storage. Therefore, the term "trigger" is inadequate and the "event selection" is used instead. The selection is done in several layers of processing resources, corresponding to the trigger level hierarchy in conventional systems.

3.12 Detector Summary

The CBM detector setup allows to measure multiplicities, phase-space distributions and flow of protons, pions, kaons, hyperons, hadronic resonances, light vector mesons, charmonium and open charm including their correlations and event-by-event fluctuations in heavy-ion collisions. The measurement will require extremely fast and radiation hard detector (and electronic) components, making the slow detectors like

Time-Projection Chambers (TPC) inadequate. Moreover, the experiment has to provide lepton identifcation, high-resolution secondary vertex determination and a high speed trigger and data acquisition system. The CBM detector system will have the capability to measure both electrons and muons. This approach combines the advantages of both methods, and guarantees reliable results as in the end both data sets should agree to each other in spite of the very different background sources.

Chapter 4

The event selection algorithm

4.1 Introduction

In the CBM Experiment heavy ions will collide in energy range from 15 to 45 GeV per nucleon at high density of nuclear matter. The scientific program of the project is to search for a phase transition from hadronic matter to the quark-gluon plasma. and also to look for a critical point in highly interacting matter. as predicted by the quantum chromodynamics (QCD).

One of the probes which carry information about the presence of phase transition is the J/ψ meson. The most probable J/ψ decay mode is into e^+e^- pair. with the 6% probability. In order to register electron-positron pair and to reconstruct its trajectories. sophisticated tracking detector must be applied. In CBM project there are two such detectors: STS and TRD. each of different properties and certain advantages.
Although STS offers very good resolution and momentum determination. alone it is unable to identify the particle. Thus it cannot be used alone for event selection. The STS can be used to determine the particle charge precisely although for complete and robust tracking and particle information it has to be combined with other detectors (RICH. TRD and RPC). Is such case. tracking procedures must be finished in STS and TRD independently. then matching tracks from these two sets must be merged together. Next. rings obtained from RICH are assigned to merged tracks and then the tracks are prolonged into RPC. which provides further hadron identification by time of flight.
This requires some complicated global tracking routines to be incorporated. which may not be suitable for Level 1[1] event selection. as they need much computational power. They are time consuming. and a large amount of data has to be processed in short time. Such setup may be more suitable for higher level analysis. when time used for calculation and reconstruction is less important.
On the other hand. TRD offers reconstruction of particle trajectory as well as gives a possibility to identify electrons and allows to distinguish them from charged hadrons. The additional feature is momentum estimation capability. which provides moderate momentum resolution. Therefore. TRD combines the advantages of more advanced setups. and the amount of data needed to be transferred and processed is relatively low compared to the STS-based concepts. This standalone Level 1 TRD event selection is

[1] L1 - the first level of on-line data processing, see the chapter CBM Detector

the main focus of the following study.
If detection data from the TRD alone can be used to eliminate events which do not contain electron/positron pair from J/ψ decay (J/ψ signature), higher level online analysis would benefit from that. For example, if Level 1 algorithm can reduce the background (no J/ψ signature) by 90%, which leaves about 10% of irrelevant data, the Level 2 subsystem has 10 times less data to process. Therefore it has the time frame to process each event extended by a factor of 10. This allows either more complicated procedures to be performed online, making the offline analysis easier, or the Level 2 hardware can be simplified without degrading the performance.
The expected beam intensity in Au + Au collision at the energy 25 GeV per nucleon is 10^9/s. Therefore, there are approx. 15 J/ψ particles produced every second (J/ψ multiplicity for minimum bias collisions is $5{\cdot}10^{-6}$ [22]). After taking into account the decay probability in e^+e^- channel (which is 5.93±0.10%, see in Tab. 4.1) and the angular acceptance of a detector setup (21%), the total J/ψ detecting rate is about 0.17/s. Thus finding the procedures which will be able to filter the background events is crucial. The main demand for the algorithm is to be not only quick but also extremely efficient.

Property	Value
Mass	3096.87±0.04 GeV/c^2
e^+e^- decay	(5.93±0.10)%
$\mu^+\mu^-$ decay	(5.88±0.10)%
mean lifetime	10^{-20}s

Table 4.1. Selected properties of the J/ψ particle [21, 41].

In order to conduct either online or offline physical analysis of the data, one must have particle trajectories in TRD fully reconstructed. Tracks are also needed for identification. A track in TRD consists of 12 hits, each registered in individual sensitive layer. When there are any mismatched hits, the probability for particle (whether it is electron or pion) identification via Transition Radiation (TR) decreases. If a reconstructed track has one hit mismatched, there may be insufficient amount of energy deposited by TR quanta to properly identify the particle, so high track finding efficiency is crucial at this point. Good tracking is also essential for correct momentum determination, which needs precise trajectory information in order to calculate the point coordinates where a particle left the magnetic field. Then, knowing the spatial distribution of the B_y field constant, the particle curvature can be determined, resulting in the initial momentum estimation. Another area which require tracking is an invariant mass calculation. As we are looking for a trace of the J/$\psi \rightarrow e^+e^-$ decay, the invariant mass is calculated with two identified particles of unlike charge. Therefore it is necessary to determine the charge of a given particle prior to any combinatorial mass calculation. The charge is calculated from the direction of bent of particle track in the magnetic field, which accuracy strongly depends on the quality of reconstructed trajectory in TRD.

Energy			
Value	**15 GeV**	**25 GeV**	**35 GeV**
Multiplicity	$2{\cdot}10^{-6}$	$1.92{\cdot}10^{-5}$	$5.45{\cdot}10^{-5}$
Efficiency ($p_t > 1.2$ GeV/c)	12%	13%	10%
S/B ($p_t > 1.2$ GeV/c)	7	12	12

Table 4.2. Multiplicities, efficiences and signal-to-background ratios for the J/ψ meson in the dielectron decay channel for central Au+Au collisions at 15, 25 and 35 AGeV. The presented efficiences include geometrical acceptance, reconstruction and particle identification efficiencies. The Signal to Background (S/B) ratio is determined in a 2σ region around the peak [21]. The transversal momentum threshold was put on 1.2 GeV/c (described further in the chapter).

4.2 General assumptions

Because the J/ψ particle is very rare (see Tab. 4.3 on the next page for maximum multiplicities). it is almost impossible to gather and then store all the information received from detector system during J/ψ measurement with maximum available beam intensity. Thus. the algorithm which rejects as many background events as possible. and at the same time preserves interesting data is required. This is a challenge for a sophisticated pre-analysis system. the so called *level one trigger* (L1 trigger). In a classic approach. *a trigger* operates on *single particles*. storing a portion of detector data only if a given coincidence conditions have been met. It filters interesting data from a bulk of background. for instance if we measure positron annihilation in matter. we look for γ quanta travelling each in the opposite direction. If two detectors (e.g. CsI detectors) register a particle at the same time. such coincidence will be enough to increase the counter of detected annihilations by one. Any other non-coincidental signals produced by detectors are discarded.
In our case. the algorithm processes the *whole event* at a time. *An event* we call the amount of data generated by detectors in response to a single act of collision: a target particle hit by a projectile particle. The primary particles created during the collision and all the secondary particles created by primary ones. leave some signals in the detector array. Then the signals are digitized and stored in a buffer. This is the moment when *event selection algorithm* is launched and the selected data is being processed. In the final scenario. only the information from TRD alone is required for such purpose. There is no need to use computing power for data from other detectors. If the J/ψ signature is found. i.e. invariant mass calculation gives a result of around the J/ψ mass. the entire data part from the buffer will be *accepted*. e.g. transferred to a higher level analysis or directly to mass storage unit. In the opposite case. contents of the buffer are discarded (rejected). buffer cleared and then prepared for the next incoming data event. Therefore. the algorithm rejects uninteresting events while preserving the J/ψ decay signal. Thus the principal feature of the algorithm is to remove background events. This is the main difference between a classical trigger and the event selection method: *trigger* operates on simple criteria to make decisions while *event selection* works with a whole event at the time. The trigger gathers data. while the event selection discards background events by complex algorithms.

Myltiplicities of J/ψ meson		
Beam energy [AGeV]	**J/ψ multiplicity produced in minimum bias collisions**	**J/ψ yield detected per week**
10	$5{\cdot}10^{-8}$	$1.8{\cdot}10^{3}$
15	$6{\cdot}10^{-7}$	$2.2{\cdot}10^{4}$
20	$2{\cdot}10^{-6}$	$7{\cdot}10^{4}$
25	$5{\cdot}10^{-6}$	$1.8{\cdot}10^{5}$
30	$1.0{\cdot}10^{-5}$	$3.6{\cdot}10^{5}$
35	$1.5{\cdot}10^{-5}$	$5.4{\cdot}10^{5}$

Table 4.3. Multiplicities of the J/ψ meson and yield per week of signal generated during the measurement at 5 MHz interaction rate. Minimum bias collision is a collision of impact parameter $b = 0 \div 100$ fm. The total amount of events produced in the experiment is about $3{\cdot}10^{12}$ per week, which correspond to 110 TB of collected data [22].

The primary goal of algorithm is to search for a signature in the data being processed and to reject whole events that do not contain it. In this study, a signature is some special value of an invariant mass, calculated for two particles of unlike charge. The invariant mass of the J/ψ meson is 3.096 GeV/c^2, thus the algorithm "looks" for a signature in a region around that value. The width of the region depends on the quality of momentum determination by a tracking procedure. In the TRD standalone scenario, the mass window is between 2.5 GeV/c^2 and 3.5 GeV/c^2 for an average momentum resolution $\Delta p/p = 14\%$ as the calculations show.
At this point, after the particle identification and directly before the combinatorial loop we *assume* every remaining particle to be an electron or positron, depending on reconstructed charge. Some of these particles are in fact misidentified charged pions or protons, and they contribute to the high regions of invariant mass spectrum when pairs of unlike charge are created.
Finding a high invariant mass value means that the event potentially contains the full information about the J/ψ decay, i.e. both particles from the decay have been registered by the detectors. If there is only one J/ψ decay particle within detector acceptance, it may be combined with other opposite charged particle forming false signature.

The matter of tracking was very important at every step of the above studies. For example, reconstructing particle trajectories is necessary to perform particle identification in TRD. The energy deposition in the detector layers along the particle's path must be determined in order to reject hadrons. The reconstructed tracks are fundamental for every part of the event selection, thus the tracking routine and its progression will be discussed in the following sections.

4.3 Investigation: step by step

4.3.1 First step: selection without particle identification

In this section the step by step event filter development is presented. As the lifetime of the J/ψ meson is 10^{-20} s, the mean range $c\tau = 3{\cdot}10^{-12}$ m. It means the J/ψ is created and decays into e^+e^- within the target. Therefore any particle that is created further from the target cannot be a part of our meson's decay signal and should be

eliminated before combinatorial part of the procedures. Because the invariant mass of J/ψ is equal 3.1 GeV/c^2 thus the electrons and positrons from J/ψ decay have to have a transversal momentum above 1 GeV/c. Therefore only particles with such high momentum are in the center of interest of current research. Finally, the most important particles are high energetic ones, with a transversal momentum p_t above 1 GeV/c (see Fig. 4.1).

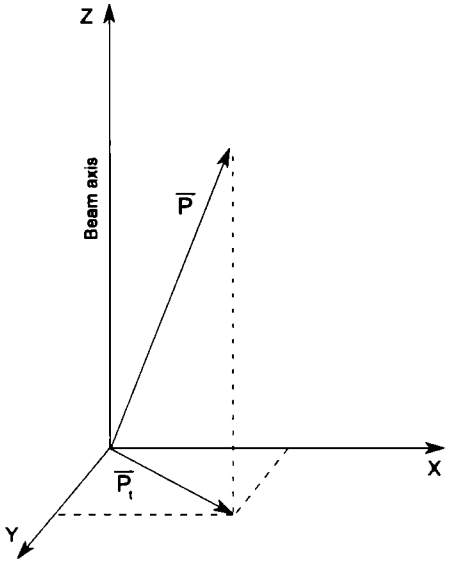

Figure 4.1. The components of the transversal momentum vector (p_t) in CBM coordinate system.

If the filter is not restrictive enough, it will find a potential J/ψ signature in most events, making the data selection useless. On the other hand, if the applied conditions are too strict, the data bulk will be significantly reduced, together with the true J/ψ signal. In presented work the first step was background study. The first quastion was: is it feasible to reduce background events with reconstructed tracks and momenta but without any particle identification?

The Ultra-relativistic Quantum Molecular Dynamics (UrQMD [19]) model was used to simulate the reactions during Au+Au ions collisions. The data from UrQMD was treated as a background due to lack of J/ψ in it because UrQMD outputs only stable particles. Such data allows to test algorithm on a basic level. At this point the assumption about ideal tracking was made. It means that the exact and complex information about the particle trajectories, momenta and energies were available. Each particle track consists of 12 hits registered in each detector layer, and all 12 hits belong to the true track. The initial momentum vector of every particle is provided by UrQMD and charge and type of paticle are known.

After analysing the data from such 10 000 Au+Au collisions, the average yields for the main particles are shown in Tab. 4.4 on the next page:

Particle	Particles/event
π^+	34
π^-	37
p	16

Table 4.4. The average number of particles per event for Au+Au reaction 25 AGeV generated by UrQMD model.

These results show that there is sufficient number of positive and negative particles to perform combinatorics in every event - see Tab. 4.4. The transversal momentum threshold is applied to every particle, filtering out most secondary electrons and lower-energy pions. The 1 GeV/c is a standard value in the J/ψ studies, preserving most of the signal, while considerable amount of background particles are removed (such criterion was applied in Fig. 4.2 on the next page; the data sample was built by mixing UrQMD background with e^+e^- from J/ψ decay generated with Pluto [42][2]).

When J/ψ particle decays, it leaves an electron and positron that move at a certain angle to the beam axis. At low angle the probability that e^+e^- came from J/ψ decay is minute. It also corresponds to low p_t value. Typical example of a particle with high energy but low p_t is a proton, travelling with a considerable velocity but at a low angle with relation to the beam axis. Such particle should be removed. True J/ψ decay products have both: high velocity and high transversal momentum. About 85% of J/ψ decay products are preserved after the 1 GeV/c transversal momentum cut.

Energy	Background (1000 events)			J/ψ (20 000 events)		
	No cut	1 GeV/c	1.2 GeV/c	No cut	1 GeV/c	1.2 GeV/c
15 AGeV	$5.70{\cdot}10^5$	2.42%	1.07%	$2{\cdot}10^4$	74.23%	59.50%
25 AGeV	$6.50{\cdot}10^5$	2.56%	1.12%	$2{\cdot}10^4$	74.19%	59.50%
35 AGeV	$7.13{\cdot}10^5$	2.63%	1.17%	$2{\cdot}10^4$	74.20%	59.49%

Table 4.5. The results of p_t cut on pure signal and background data samples. The threshold value is 0 (no cut), 1 GeV/c and 1.2 GeV/c. The ideal tracking and momentum values are used here. The numbers in the "No cut" column correspond to the total number of detectable particles in the data sample.

In presented background study each particle was treated as electron or positron, with respect to its charge. As the majority of delta electrons are removed by a p_t cut, and most of low momentum particles are rid of as shown in Tab. 4.5.

The momentum criterion is the first filter applied. The transversal momentum (p_t) of each particle has to be greater than a certain arbitrary value (here: 1 GeV/c). The value comes from the momentum distribution of particles from the studied meson's decay (as explained above - see in Fig. 4.2 on the next page). All the particles that survived the momentum filter are sorted according to the charge: all positive an negative particles are gathered in corresponding buffers. Then the buffers are combined in accordance to

[2]Pluto is a Monte Carlo simulation tool for hadronic physics originally created for HADES collaboration. It consists of a collection of C++ classes and allows to generate decaying particles like J/ψ meson.

the following schema: to every positive particle is assigned a negative one (the Cartesian product of two buffers is created) and for every such pair the invariant mass is calculated. It is assumed that every pair consists of an electron and positron. Thus calculated invariant mass of two particles of unlike charge is placed on an invariant mass spectrum. If the value is higher than an arbitrary chosen 2.5 GeV/c^2, the event is accepted. The value 2.5 GeV/c^2 is roughly the lower limit of the range of 0.5 GeV/c^2 around the J/ψ mass (Fig. 4.3 on the following page). The invariant mass filter corresponds to a second criterion.

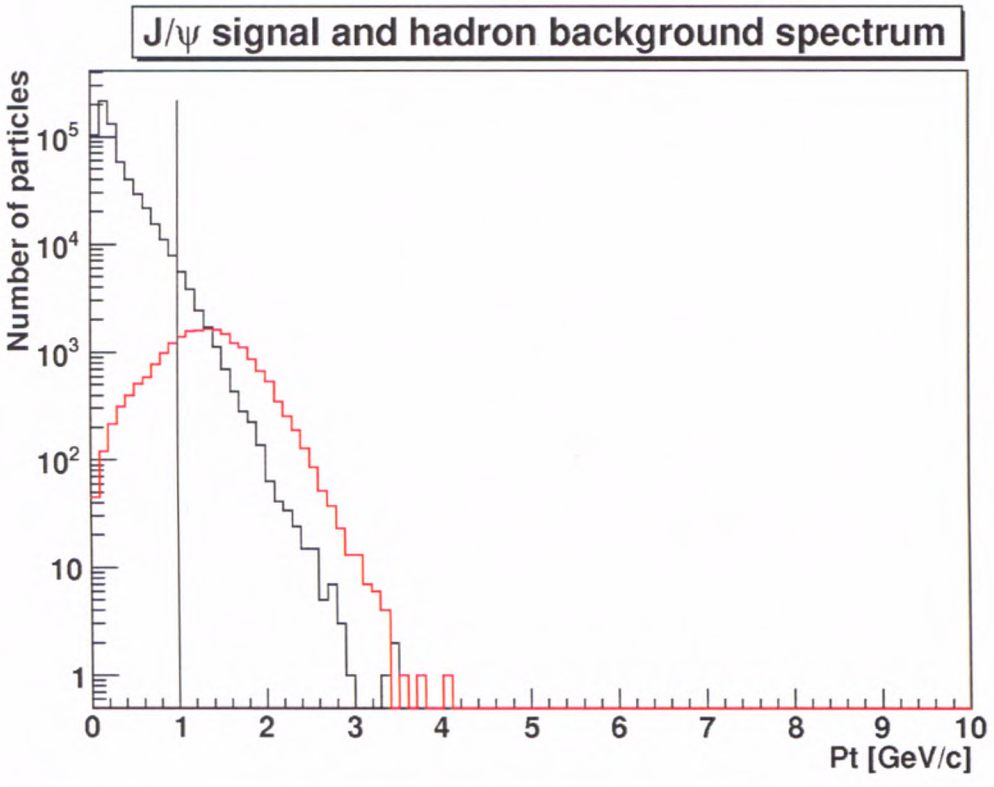

Figure 4.2. The comparison of transversal momenta of signal and background particles. The p_t of electrons and positrons from J/ψ decay are marked with red line. The black line shows the transversal momentum of background particles. The vertical line denotes the 1 GeV/c threshold. The ratio between signal and background is not to be scaled, as the purpose of the picture is to show the fraction of particles rejected by the cut. The beam energy is 25 AGeV and the background is composed of minimum bias events.

The results reveal that the above criterions are not enough - the algorithm finds a *signature* in every event, and that makes this particular approach insufficient.

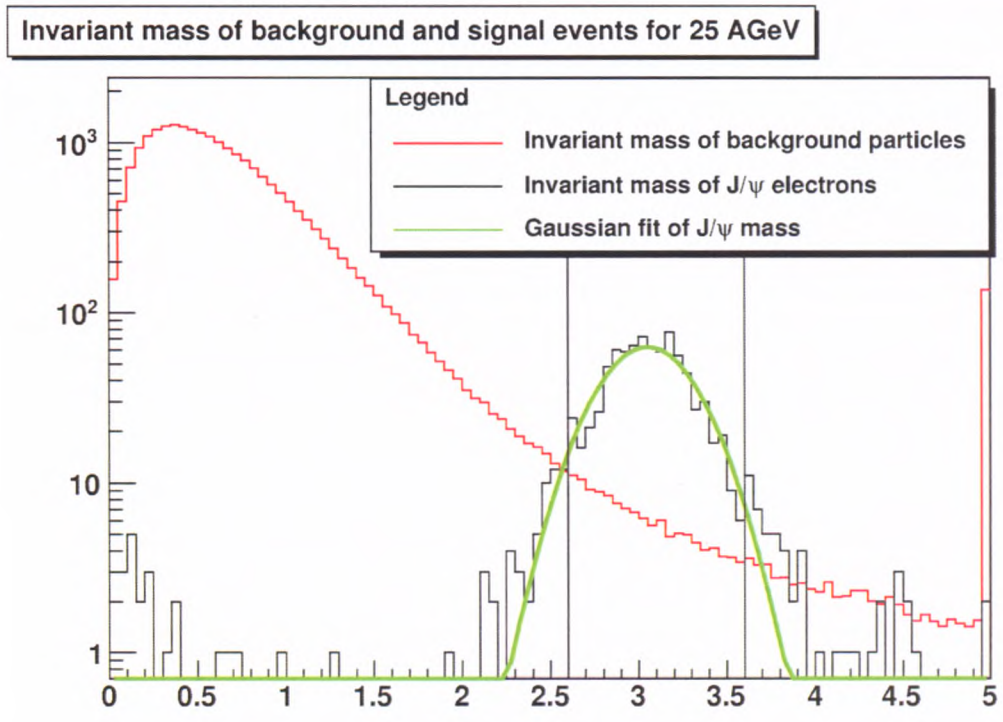

Figure 4.3. The invariant mass calculated for background events (peripheral collisions (minimum bias data) at 25 GeV/c) in comparison to $J/\psi \rightarrow e^+e^-$ decays at the same energy. Both data samples calculated independently. The samples are drawn in different scale. The invariant mass was calculated using reconstructed tracks and reconstructed momentum. The method offers the mass resolution of 26%.

4.3.2 Second step: usage of the Rejection Factor of the TRD

The main feature of the Transition Radiation Detector is ability to distinguish electrons/positrons from other charged particles. Incorporation of this intrinsic feature allowed to improve previous scenario. This is realized with the use of a *transition effect.* which appears when a relativistic charged particle crosses the boundary between two materials of a different dielectric constants. If particle possesses high enough velocity it emits an electromagnetic quantum. The high energy electron and positron are the most probable particles which are able to emit such radiation. Pions and other heavier particles (hadrons and muons) created in investigated reaction in CBM are not fast enough to create transition radiation. Thus if we consider an electron and a pion of a momentum 1 GeV/c each. only the electron emits electromagnetic radiation because it possesses a higher. relativistic speed.

The quanta are generated in a part of a detector called *radiator.* which consists of a large number (a couple of hundred) of foil layers of two different types. The foil is usually made of organic materials. polypropylene or mylar. and each type of foil is followed by another type. The drift chamber is situated next to the radiator looking downstream the beam axis. Any charged particle travelling through the chambers looses a part of its energy. which corresponds to a charge pulse collected by anodes. If the particle is high-energy electron or positron. the TR photon is also created. The photon traverses

the chamber and deposits an amount of energy into the gas contained within. This corresponds to the additional pulse peak on the readout. Analysing the energy loss of a particle in all gas chambers along the trajectory, allows to determinate the type of particle registered. More detailed description of the TR effect is written in the Appendix B on page 83.

By employing the TRD it is possible to distinguish the signal particles (high-energy electron/positron) from the background pions or protons. Particles from interesting J/ψ decay type are high-energy e^+e^- pair, which are characterized by relativistic velocity. Other particles, contributing to the high invariant mass region that cannot induce transition radiation can be identified and rejected at this point. It means that a particle is discarded and removed from further analysis if there is no TR detected in any sensitive layer of TRD detector. The *hadron Rejection Factor* (RF) can be defined as a ratio of a number of identified hadrons to a number of all detected hadrons in a given event. The realistic value of the RF is 95-99% for momenta above 1 GeV/c [43]. At this point, there is no algorithm available to analyse the energy loss of a particle. Therefore a statistical assumption has been made instead. Every hadron is identified in 98% of cases, and a pseudo-random number generator has been applied to randomly reject 98 hadron out of 100. At this stage of simulation, work still is performed only with hadrons generated by UrQMD without presence of e^+e^- from J/ψ decay (so called "true signal").
The filter criteria are applied in the following order:

1. Transversal momentum p_t cut.
2. Hadron rejection factor RF.
3. Invariant mass window M_{inv}.

In the ideal case up to 999 per 1000 minimum bias events can be suppressed. In most of events, there are no pairs contributing to the higher mass area, as they are identified and removed. The result for central events is worse due to a higher amount of high-energy particles. Filtering out 99.9% of peripheral events in ideal case is a promising result. One must keep in mind that moving from ideal to realistic scenario the result will be at least a couple of times worse due to lower precision and the uncertainties of apparatus.

4.3.3 Third step: usage of Geant3 libraries

The step towards more ralistic analysis was to use the Geant3 [44] which is a toolkit for the simulation of the passage of particles through matter developed in CERN (European Organization for Nuclear Research). It allows to introduce the geometry of the detector as well as the material which the detector consists of. Geant uses experimental cross sections for physical processes during the passage of particles through matter. The toolkit is characterised by following features:

- the geometry of the system,
- the materials involved.

- the fundamental particles of interest,
- the generation of primary events,
- the tracking of particles through materials and electromagnetic fields,
- the physics processes governing particle interactions,
- the response of sensitive detector components,
- the generation of events,
- the storage of events and tracks,
- the visualization of the detector and particle trajectories, and
- the capture and analysis of simulation data at different levels of detail and refinement.

With a use of the library one can transfer the full detector concept into software data, with the addition of the magnet yoke, beam pipe and target (see Fig. 4.4 on the facing page). The proportions of the detectors are maintained and each volume has detailed information on material implemented. The magnetic field has been mapped in order to transfer it into a digital representation using TOSCA software by Vector Fields Software [45][3]. The package, called CBMRoot [46][4], has made it possible to simulate the interaction between the charged particles and the material of the detector. FairRoot/CBMRoot is a framework fully based on the ROOT system [47]. It allows to create simulated data and perform analysis with the same framework. Moreover, Geant3 and Geant4[5] transport engines are supported but the created data do not depend on a particular Monte Carlo engine. The users can construct their detectors and analysis tasks in a simple way. Some general functionality, like track visualization, is also supported.

The FairRoot combined with Geant3 engine simulates the delta electrons and other secondary particles, created during the collision with the materials of the setup and distorts particle trajectories due to multiple scattering inside matter (see Fig. 4.5 on page 36). The information on energy loss inside an active volume is also provided.

[3]At present, the TOSCA toolkit exists as a module for a greater simulation package OPERA by Cobham Technical Services.

[4]Which is now a part of a more general package called FairRoot. FairRoot is a base for a set of experiment-related subprojects, like PandaRoot, R3B, CBMRoot etc. Each subproject has the detector geometry implemented along with other related information.

[5]A next generation of Geant3 engine, rewritten from scratch in C++ programming language in CERN.

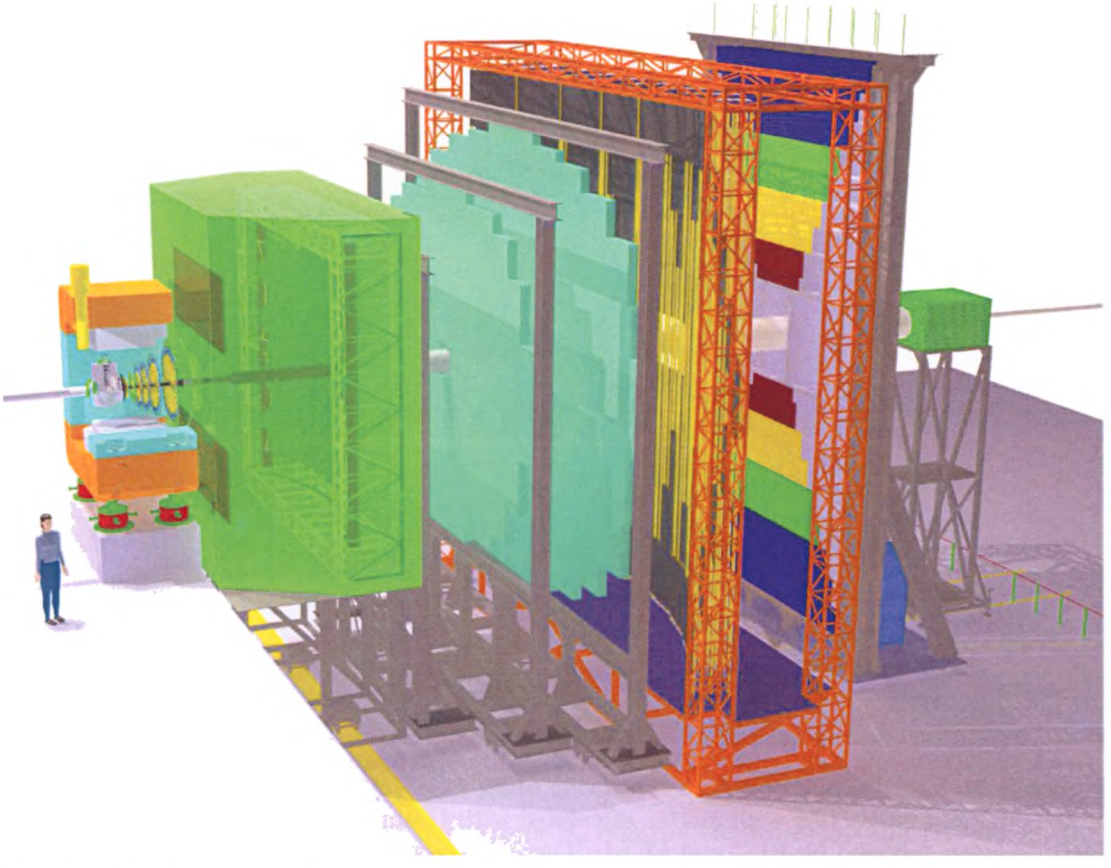

Figure 4.4. The visualisation of detector geometry implemented in Geant3. The depicted setup is optimized for dielectron measurements.

The output from CBMRoot contains information about collisions with target and detector materials, beam pipe and dipole magnet. It also provides realistic detector response. In current CBM configuration, there are 12 TRD layers implemented. They are grouped in 3 TRD stations by 4 layers each. When an electron crosses all the stations, 12 spatial coordinates with known Z coordinate and (X,Y) pair laying within a detector plane are created. One set of spatial coordinates from one TRD layer is called *a point*. A set of 12 points belonging to single real trajectory is called *a track* in TRD (see in Fig. 4.6 on the following page).

At this point, the ideal track reconstruction was applied. Geant3 package provides all the necessary data for this purpose. There are no mismatched points (i.e. belonging to other track) in the reconstructed trace and also a set of variables are known: type, charge, energy and momentum of every particle.

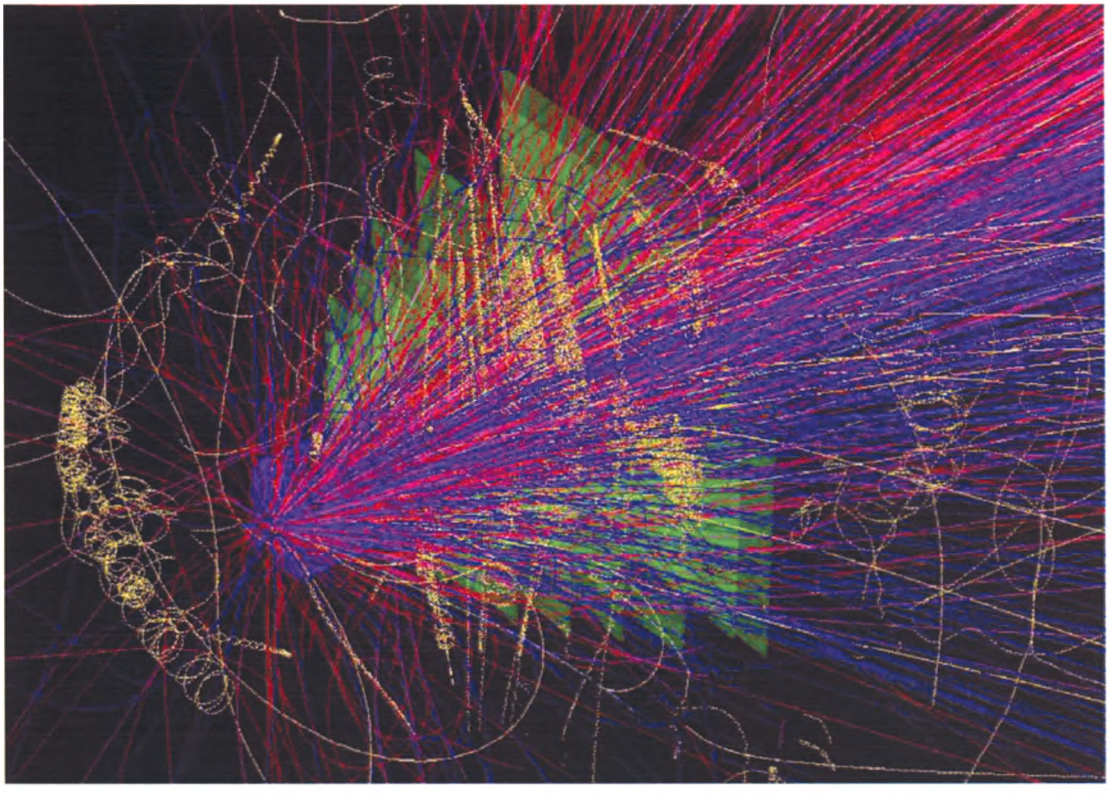

Figure 4.5. Visualization of a typical collision of 25 AGeV Au+Au. Hadrons are generated by UrQMD and interaction with matter calculated with Geant3. The first 3 green stations are TRD detector, followed by RPC and ECAL. There are more than 700 hits in each TRD layer detected in such event. Picture adopted from [48].

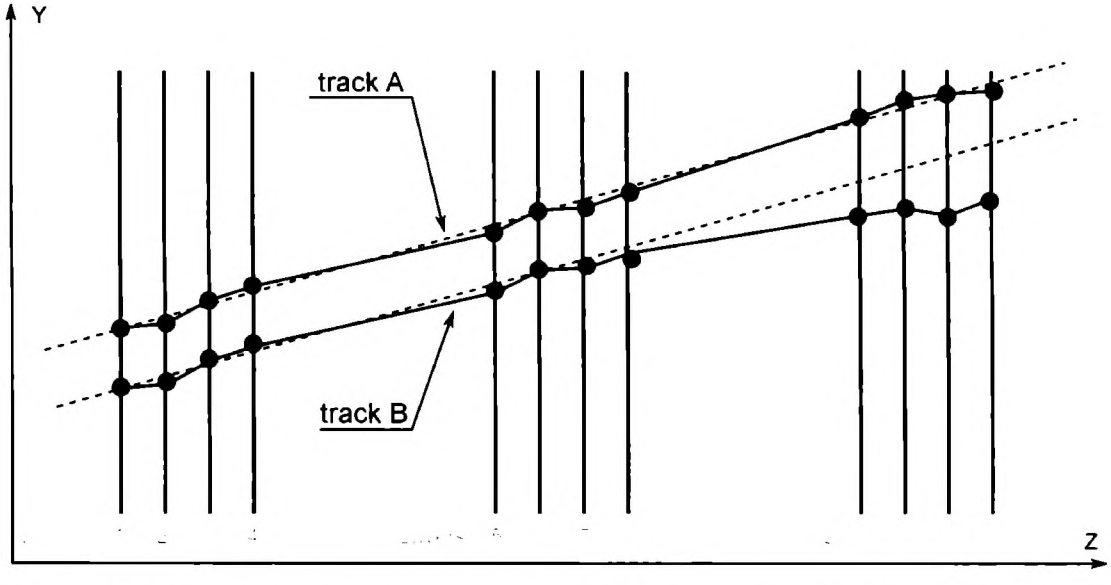

Figure 4.6. The example of two tracks in TRD detector. A single track consists of 12 hits (denoted with black dots). The multiple scattering process affects every charged particle.

The crucial improvement over the previous step is taking into account the electrons emitted from material when collisions with ionising particles occur. The e^+e^- pairs created in interaction with material are taken into account. in addition to hadrons from UrQMD. Geant provides realistic particle multiplicities. particle energies and momenta in all interaction points along the flight path and allows to determine the "mother" and "daughter" relations between simulated particles. The Geant-simulated data is sometimes called (M)onte-(C)arlo (MC) data. the name originating from one of numerical methods used inside the package[6].
The whole detector setup of the CBM experiment was modelled in Geant 3. Any ionising particle that crosses the sensitive volume of TRD is traced. and its track parameters can be obtained for any interaction point. After particle traversed through the single TRD station. various particle parameters for all four layers of the station are available (e.g. direction distortion. momenta. energies and energy loss. Fig. 4.7 on the next page)
.
The results were promising: using the above conditions. at most 98% of unwanted events can be rejected. One must however keep in mind that the ideal track reconstruction is still used.

A reliable simulation library (Geant) allows the further background studies to be performed. Every collision event. generated by UrQMD was processed by the libraries. giving output containing interaction data.

In order to remove particle trajectories that do not come from the target area one can reconstruct the track in TRD and then extrapolate the track to the $Z = 0$ plane. As the magnetic field of the magnet has strong B_y component while B_x and B_z vanish. the particle trajectory is bent in the XZ plane (see Fig. 4.3.3 on the following page). Therefore the particle flights along a straight line on the YZ plane and the two-dimensional straight line can be calculated to obtain its Y component at $Z = 0$.

As in experiment there is no exact way to distinguish secondary particles from primary ones. one has to assume that all registered by TRD particles are the primary ones. Then. so called non-bending plane cut is applied. removing products of more distant decays. If a track is extrapolated to the target plane with a straight line (i.e. back-tracked) and is projected to the two-dimensional midplane (YZ). then the Y position at $Z = 0$ is considered. If a particle originates from the target (i.e. is a primary particle). the Y value in the target plane is small. The secondary particles have displaced vertex. as their decay points of their mother particles has been located somewhere downstream from the target. The illustration of the method is shown in Fig. 4.10 on page 40. The radius of the area around the target for accepting primary particles was arbitrary chosen to be 5 cm.

[6]"Monte Carlo methods (or Monte Carlo experiments) are a class of computational algorithms that rely on repeated random sampling to compute their results. Monte Carlo methods are often used in simulating physical and mathematical systems. Because of their reliance on repeated computation of random or pseudo-random numbers, these methods are most suited to calculation by a computer and tend to be used when it is unfeasible or impossible to compute an exact result with a deterministic algorithm." [49]

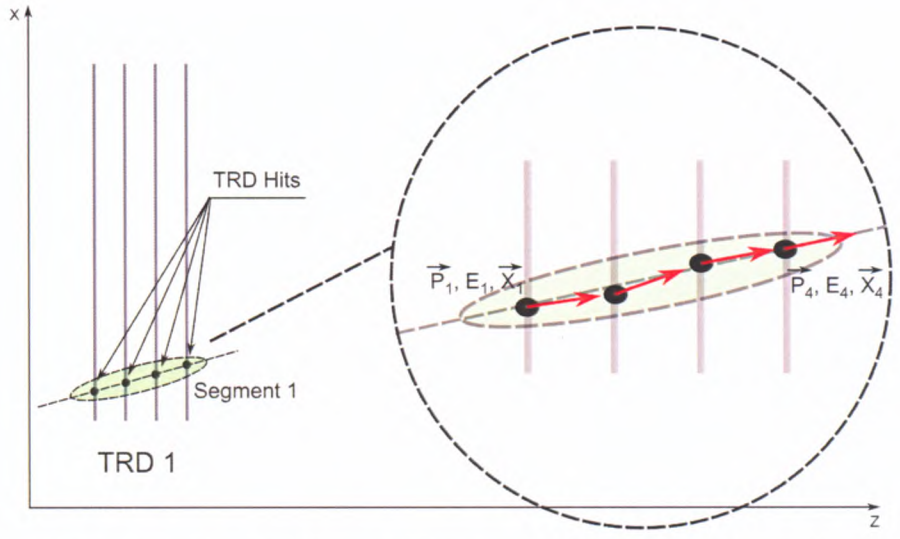

Figure 4.7. One set of points from a single TRD station. Geant provides coordinates from four individual layers, as well as momenta, energies and energy loss on each layer. The information is provided *exactly*, i.e. with maximum precision available in Geant. P, E and X designate momentum vector, energy and spatial position of a particle that has been registered in a given point.

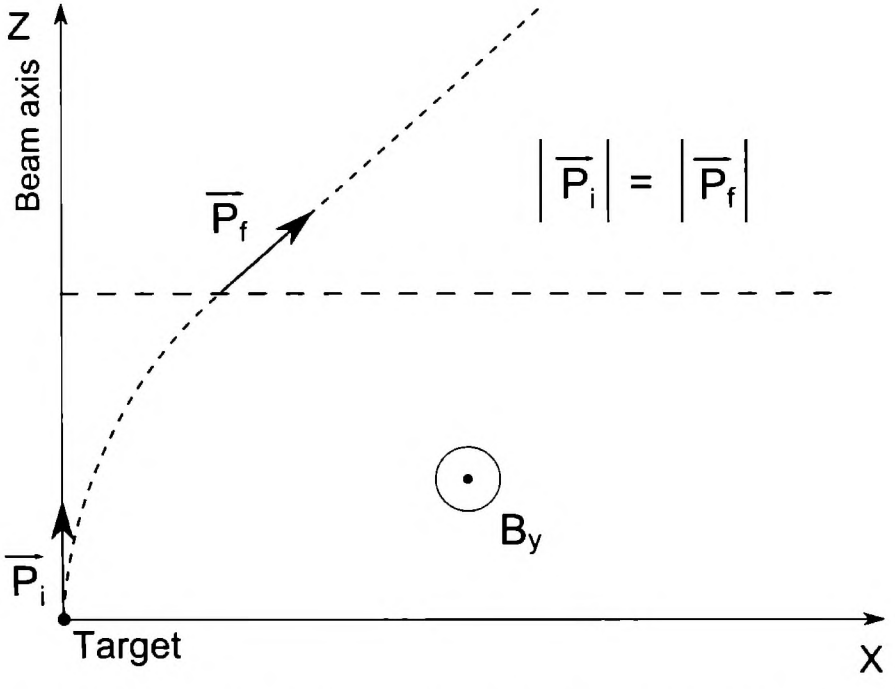

Figure 4.8. The bending plane. The consistuent of a magneting field B_y causes the particle trajectories to bend in XZ midplane by the Lorentz force. At the point where the field induction vanishes, the particle can move along a straight line. The bending does not change the total particle momentum value.

The precision of the method depends on the precision of track reconstruction. The multiple scattering process can affect the linearity of a track in such way that the al-

gorithm is unable to achieve good precision in backtracking trajectory to the target. The multiple scattering is strictly related to the material crossed by traversing particle. Linearity of the tracks is mostly distorted by bulky RICH detector and TRD.
As more accurate methods are time-consuming, the straight line backtrack has been chosen at this point. Non-bending plane cut allows to reject 60.0% of secondaries, preserving 99.1% of primary ones, reducing the number of tracks that survive to the final combinatorial phase (calculated for the energy 25 AGeV).

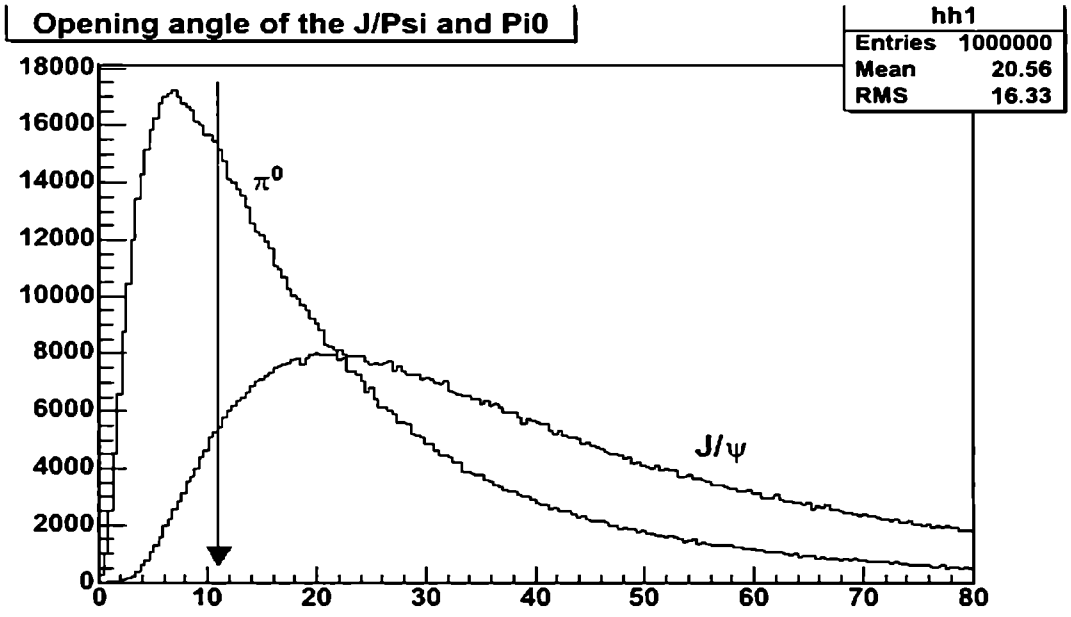

Figure 4.9. The opening angle distribution of products of two decays: π^0 and J/ψ into e^+e^- for 25 AGeV generated by the Pluto code [42]. Proposed angular cut at 11deg removes the major fraction of background particles (represented by electrons and positrons from π^0 decay and estimated at the level of 2/3) while preserving most of the signal. The J/ψ signal loss is at the level of 15%. The used data sample contains 1 milion of J/ψ $\rightarrow e^+e^-$ decays.

Similar to the above method is bending-plane cut (see in Fig. 4.11 on page 41). The trajectories in the XZ midplane are affected by B_y component of the magnetic field B. Any charged particle is deflected in the direction of positive or negative values of the X axis, depending on its electric charge. If a particle leaves the target with high momentum, its trajectory is bent by a couple of degrees, while for low momentum particles the influence of magnetic field is significant, and may result in ejecting the particle out of the detector acceptance. Upon registering the particle by TRD detectors, its trajectory can be backtracked in the XZ midplane to a point at Z= 1 meter. This is a place where the magnetic field vanishes and it is assumed that the field does not impact the trajectories from here downstream. If a particle is registered on the positive X axis side, and the extrapolation points to the negative values of the X axis, the particle is assumed to be a low-momentum one, and its track is strongly bent by a magnetic field. If both: extrapolated and measured X coordinates are of the same sign, either positive or negative, the particle is assumed to be a high-momentum one, since the magnetic

field distorts its trajectory's linearity only slightly, such particles are accepted. The described situation takes also place when a particle is a secondary, i.e. it has its vertex outside the target. It is unlikely that such particle survives the XZ cut. The primary one, especially with higher energy, is accepted by filter. The method removes 43.0% of the background particles, passing 87.6% of the signal particles.

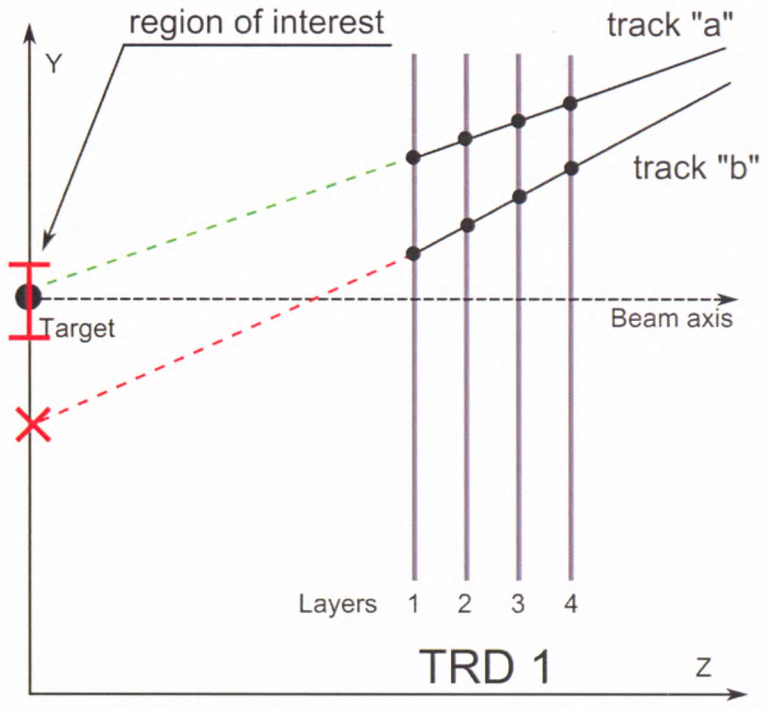

Figure 4.10. The idea of the non-bending plane cut. The green line denotes the primary particle coming from the target. The particle is registered by 12 TRD layers, and then the track is extrapolated upstream to the target plane. The red line symbolizes the secondary particle created during the decay of a mother particle in some distance from the target.

One must notice that the above cut is in some way a momentum cut, removing low energy particles without any momentum determination.

The above filters are suitable to reject particles that either are likely to be secondary particles or particles of unwanted properties. Combined, the cuts remove 74% of background particles, preserving 97% of signal (at 25 AGeV). Another issue taken in this step is an opening angle. Since the objective is to find two particles coming from a single decay, one can study the opening angle between particles taken into combinatorics. J/ψ particle possesses high momentum, so the momentum is also transferred to daughter particles. The angle between two particles being products of a single decay coming from the same decaying particle is called an opening angle, and can be used to discard less probable combinations of particles. The angle has been studied for true J/ψ meson decays, and the angle is shown in Fig. 4.9 on the previous page. In addition, the angle of background particles, i.e. π^0 decayed into e^+e^- is shown for comparison. Thus the most probable opening angle is between 10 and 50 degrees and in such range particle

pairs are sought.

After passing all the filtering thresholds, the remaining bunch of single particles are combined into pairs of unlike charge. For each pair, the invariant mass M_{inv} is calculated in a process of looking for a signature.

To calculate the invariant mass, two goals must be accomplished:

- the momentum of a particle must be approximated,
- the charge of a particle must be determined.

If there is no charge determination, the particles have to be combined on an each-to-each basis.

Calculating the invariant mass, all particles are treated as electrons, i.e. the rest mass is assumed to be equal 511 keV. For true electrons this approach is correct, but misidentified pions are source of errors, giving diminished values of M_{inv}. This degrades the efficiency of a trigger, as lepton-pion pairs appear as a signature-like signal in the proximity of 3.1 GeV J/ψ mass.

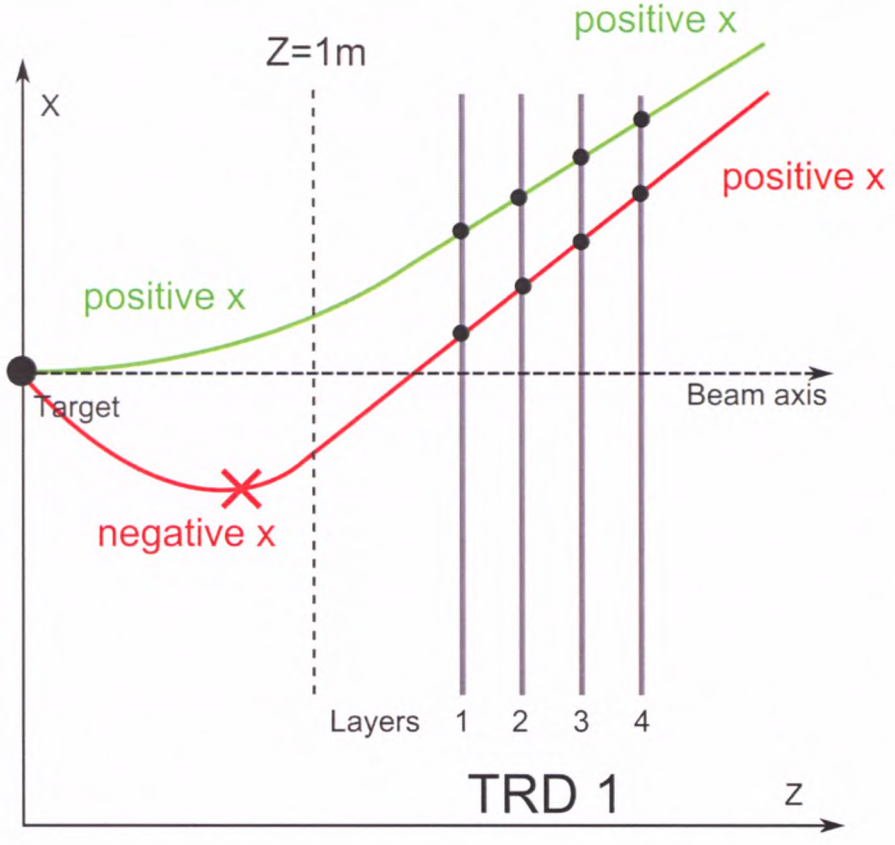

Figure 4.11. The idea of the bending plane cut (described in the paragraph).

The momentum approximation method is based on the simulation data calculated once for a given energy. The field integral is used as a magnetic field constant and the

field is assumed to be uniform. The method allows to achieve relative precision of 11.4% as shown in Fig. 4.12

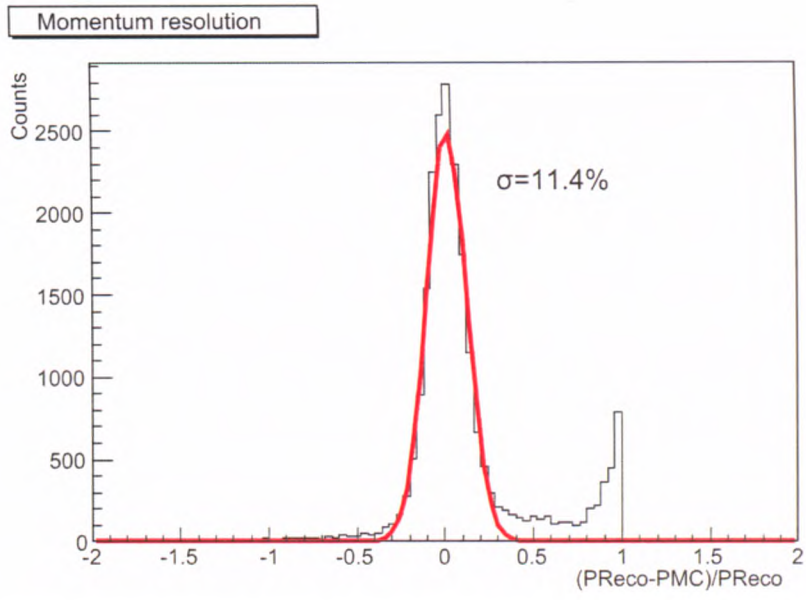

Figure 4.12. The resolution of momentum reconstruction of the method described below. Momenta calculated for the Au+Au 25 AGeV data sample. The PReco is reconstructed momentum and PMC is ideal momentum taken from Monte Carlo simulation. The results were fitted with Gaussian curve. The standard deviation σ is equal to 0.114. The peak visible to the right of the main peak comes from the secondary particles, i.e. those which do not origin from the target area. The method assumes that the particle traversed the magnetic field on its way to TRD, therefore the momentum value reconstructed for secondaries has considerable errors.

The inverse momentum of a particle is approximated using the following formula [22]:

$$\frac{q}{p} = \frac{[x - (z - z_{target})t_x]\sqrt{1 + t_x^2}}{(z_{magnet} - z_{target})\sqrt{1 + t_x^2 + t_x^2}\int dlB_y}) \tag{4.1}$$

where z_{target} and z_{magnet} denote the z coordinates of the target midplane ($z = 0$) and the center of a magnet ($z = 0.5$ m) respectively and q is charge of a particle. The slopes defined as follows: $t_x = p_x/p_z$ and $t_y = p_y/p_z$ are calculated at the z position of the first TRD layer from reconstructed track. The average field integral $\int dlB_y$ is obtained by simulation of electrons from J/ψ decay using framework with Geant3 [22]. Numerous electrons have been transported through the detector setup using the framework. and each time all the coefficients like momentum and angles were known from the Monte-Carlo data. This allowed for the average field integral to be calculated.
In this case, ideal track finding is assumed and a track between first and last TRD layer is approximated with a straight line. Since B_x and B_z components of the magnetic field are vanishing, the slope components of the magnetic field are vanishing, the slope t_y^i (the index "i" stands for "initial") can be approximated by t_y^f ("f" stands for "final") measured in TRD. On the other hand, in bending plane. t_x^f differs from t_x^i by the

deflection angle Θ. which corresponds to a bending force which impacts the particle when it traverses the magnetic field.
The initial and final slopes are correlated and the dependence is linear within a small p_z range. for instance $p_z \in <1.3$ GeV/c. 1.4 GeV/c $>$ (see [22]). The deflection angle can be parameterized as $\delta p = 0.304/p_z$ GeV/c in a range 0.5 GeV/c $< p_z <$ 1.5 GeV/c. Using this parameterization. t_x^i can be calculated from the measured t_x^f with the accuracy of about 5% Having t_x^i reconstructed and assuming t_y^i is constant during the magnetic field passage. one have the following set of values: (x,y,z,t_x^f,t_y^f) and the value of initial momentum p. allowing to calculate the initial momentum vector p_i. Finally. with the full momentum vector. and assuming all the particles are either electrons or positrons. one can calculate the invariant mass of a pair of particles.
As the total invariant mass resolution for J/ψ $\rightarrow e^+e^-$ products is equal 26% - see Fig. 4.3 on page 32. the mass region has to be broaden. The mass event signature was decided to be between 2 and 4 GeV/c^2. so if any particle pair appears inside the region of interest. the whole event is accepted.

4.3.4 Fourth step, including real tracking algorithm

In order to come closer to realistic situation. one needs to have realistic track reconstruction scenario. For the trigger purpose it needs neither to be very precise nor versatile procedure. The most iportant thing is to be able to reconstruct tracks of particles of momentum above 1 GeV/c. In the mentioned area one can find particles from the J/ψ meson decay.
There are a few possible ways to achieve that:

- Track Following - using the Kalman Filter and forward propagation to predict the particle next movement section. The multiple scattering process is taken into account here.
- Hough Transform - transforming points in a plane to axes. and analysing their points of intersection.
- Cellular Automaton - based on the "game life" algorithm. Fully parallel and feasible to be implemented on multicore processors (such as nVidia Tesla which host up to 512 cores (in 2011) in a single unit). The algorithm analyses geometrical points. standing them together and generating segments. Then. segments are connected. creating tracks.

Among the above algorithms. the Cellular Automaton (CA) was selected. Its implementation has been conducted in the following steps:

- Test of the algorithm
  Each of the three TRD detector stations consists of four sensitive layers. therefore a single particle that crossess all of them leaves at most 12 registered hits. They can be represented as 5 segments. each of these consisting of two points. Each point has its spatial coordinates (i.e. $[x,y,z]$ ideally determined); a segment consist of the leftmost and rightmost points in each station. In a case of in-between segments. last point from one station and first point from the next station stand one segment. So. we have 3 segments in stations plus 2 segments in between

stations. While selecting the points for segments, geometric cuts are applied. This removes combinations that are unlike to exist in the reality. Proposed scenario allows to reconstruct 95% of particle trajectories of momentum greater than 1 GeV/c and 25% of the low-momentum ones. The wrong reconstructed tracks are on the level of 5%.

- The detector resolution
  Each layer has the intrinsinc property of measuring accuratelly one of the two variables: either X or Y. The layers are situated in such a way, that all even stations measure X and all odd stations measure Y precisely (or in the opposite). Two points from neighbouring stations are joined, creating a *space point*. Each space point has accuratelly determined X and Y coordinates. Two space points are used to create a segment, and, like in the previous case, long tracks are built with 5 segments (see in Fig. 4.3.4 on the facing page). The additional geometric cuts help to speed up the process. The procedure has been divided into two parts. The first one uses very restrictive conditions, i.e. cut values, therefore it reconstructs most of high-momentum tracks. Each reconstructed track is removed from available data (i.e. all hits belonging to a track are market as "used", what prevents them from being used again). When the first part is over, the softer cuts are applied, allowing to process particles with lower momentum. This improves the efficiency in low-momentum region from 25% to 89%, while almost 97% of high-energy tracks are recognized. The percentage of errors are as low as 5%.

- Moving to 3-segment model
  From 5-segment scheme we moved towards 3-segment one. That shortened the time needed for event processing. Instead of using segments in-between stations, the straight propagation formula was used. Also, each track is checked for its linearity (the function measures the deviation of points from a straight-line track; the smaller it is, the better; it will be called χ^2). Only the best tracks in the terms of χ^2 are selected. The efficiency is 97.3% (90.1%) for high (low) momentum particles, and 5.2% of ghosts.

- Removing Monte-Carlo information
  This is the extended 3-segment scenario, with all MC information removed, so it is considered as a realistic case. The efficiency drop-down is a result of more combinatorics when the segments are being created. Also, the finite detector resolution has an impact on the phase of creating space point, thus on all further stages of algorithm excution. The efficiency is 92.5% for high momentum particles (87.7% for low momentum particles), and ghosts at the level of 10.2% for 25 GeV data sample.

The presented algorithm works efficiently for particle momenta above 1 GeV, reconstructing with 90% efficiency within three loops. The usage of the algorithm, along with other described filters (momentum cut, hadron separation, reconstructed mass window), allows to achieve rejection factors 333, 500 and 1000 for the energies 15, 25 and 35 GeV respectively. Details concerning tracking and event selection are covered in the Section 5 on page 55.

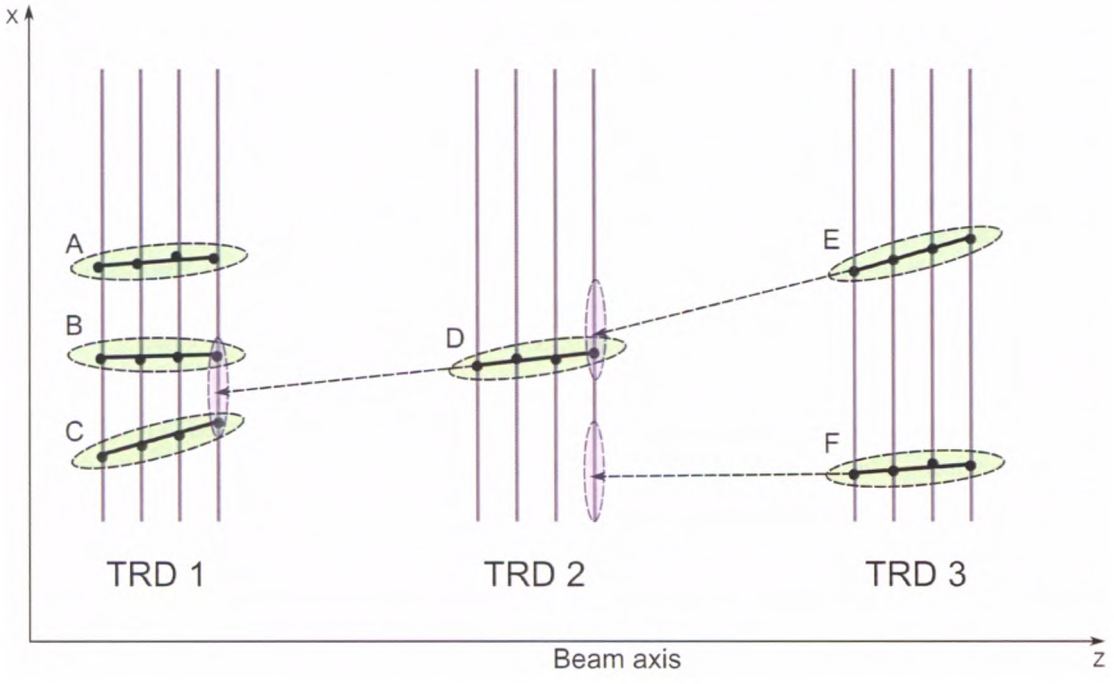

Figure 4.13. Finding neighbours for each segment. The procedure starts from segments in the rightmost TRD station (TRD 3 or Station 3). For each segment, the straight line is propagated to the previous station, and neighbouring segments are collected within a certain area around the extrapolated point, i.e. the segments which have the last hit inside the region. Each segment found within the area is stored as a potential track consistuent for further processing.

4.3.5 Fifth step, using Geant3 libraries and realistic tracking

With no real tracking incorporated one cannot obtain realistic results using ideal tracking routines. At this point, ideal tracking means that all detector hits belonging to one particle are assigned to the track number, and a logical "track" structure is created inside the analysis software. The structure contains all 12 hit indices, as well as the parameters (x, y, z, t_x, t_y) at first and last measurement taken by the detector (called first and last track parameters). So far, the information was extended by ideal momentum vector and energy, all taken from Monte-Carlo simulations.

From this point forward the realistic CA trajectory finding method is used, i.e. only limited information about the simulation conditions is available, closely related with experimental conditions. Also the data set is restricted to TRD detector data, as for the event selection scenario other data are unavailable.
In addition to the complete information about particles interacting with TRD material, the estimation of the detector response can be obtained. The single TRD detector layer consist of a few dozen of long and narrow chambers. Within the given layer all chambers are oriented in the same way, either vertically or horizontally. The orientation is organized in even-odd style. It means that two even layers have the same chamber orientation (the same is for the odd ones). The direct implication is impossibility to get both horizontal (X) and vertical (Y) coordinates with good precision. If the set of TRD chambers give one coordinate (for example X) with good accuracy, the other (Y) is measured with poor precision. For the next station the situation is opposite.

Moreover, position precision determination differs at the various parts of a TRD layer i.e. the size of a chamber is different at different radii (smaller at small radii). Around the beam axis, measurements are performed with maximum precision. For X (more precise) and Y (less precise) coordinate the error is 300 μm and 2.7 mm respectively. When the distance to the beam line grows, the precision of Y coordinate is getting worse. The precision differs also from station to station. The layers located in station situated further from target have larger area than station placed closer target. The same situation is found for chamber. It results in degradation of spatial resolution. In other words, the accuracy depends on the angle between particle track and beam axis and for all TRD stations it is shown in Tab. 4.6.

In order to simulate such precision dependencies, the exact TRD interaction points were smeared by usage of gaussian function. The smear were performed with various sigma precision. The lower sigma parameter corresponds the more accurate measurement.
The table of smearing parameters is shown below:

Station no.	σ_x[μm]	σ_x[μm]						
		$\Theta \leq 50$	50÷100	100÷200	200÷300	300÷400	400÷500	$\Theta < 500$
1	300	2700	3700	15000	27600	33000	33000	33000
2	400	6300	8300	33000	33000	33000	33000	33000
3	500	10300	33000	33000	33000	33000	33000	33000

Table 4.6. TRD detector position uncertainities σ_x and σ_y are show here. In this case, the precise coordinate is denoted x while the other one is represented by y. The precision of the y coordinate depends on the angle Θ, which is the smaller for measurements points situated further from the beam axis. Θ is given in miliRadians.

Summarized conditions are gathered in Tab. 4.7 on page 48. Having only TRD spatial hit coordinates and roughly mapped magnetic field is insufficient to perform signature search inside the simulation framework. At the very moment, the fast and accurate enough track reconstruction algorithm is needed in order to perform any particle identification, momentum reconstruction or invariant mass calculation.

4.3.5.1 Track Purity

The fraction of correct hits to the total number of hits in a single track is called track purity. This is one of the key factors, corresponding to the quality of track finding. During reconstruction, it may happen that some hits in the track are mismatched, and the output track consists of correctly assigned hits plus some wrong ones. If the number of correct hits is lower or equal to 70% of total number of hits, the track is considered wrong one and is called a ghost track. For 12 hits track model, in 3 stations of 4 layers scenario, the threshold number of correct hits is 9, thus there should be no more than 3 wrong hits in the tracks to consider it is properly reconstructed.

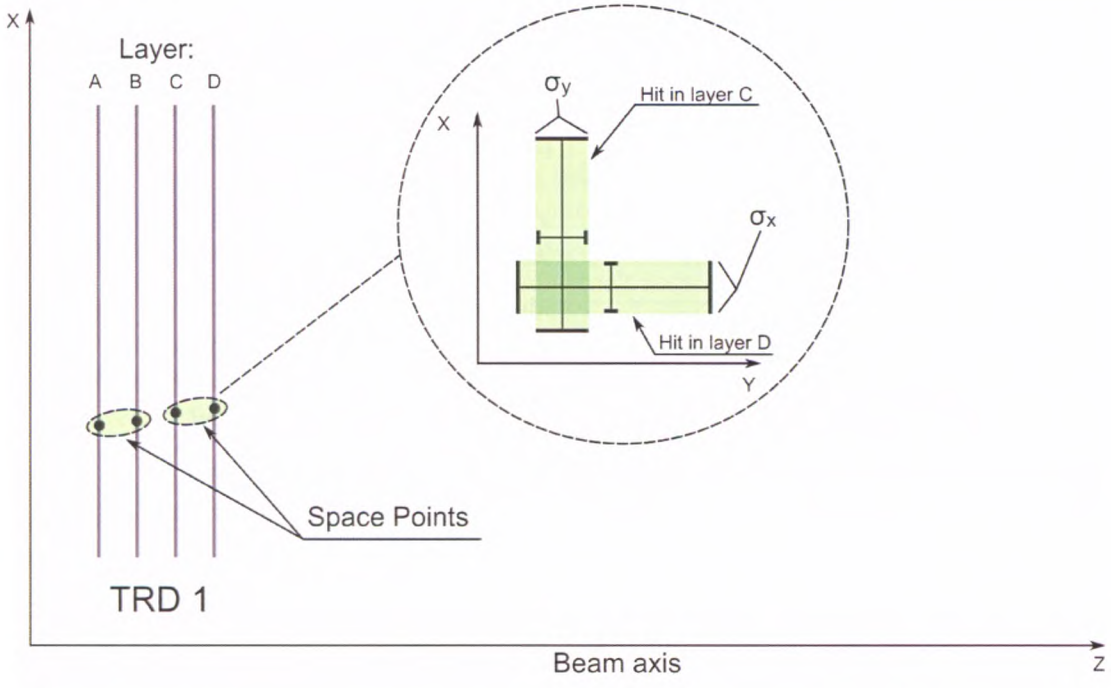

Figure 4.14. Schematic picture of Space Point creation. Two even-odd TRD Hits are picked if there is an intersection of their position uncerntainities, i.e. when $\sigma_x^1 \times \sigma_y^1$ area intersects the $\sigma_x^2 \times \sigma_y^2$ one. Overlaping hits are then selected and a Space Point structure is created. The structure has the (x, y) coordinates measured with good accuracy, and the z positions are known.

Also, there can be a real track reconstructed twice. Two output tracks may differ by some (mismatched) hits, but the majority (over 70%) of hits are common between them. This type of tracks is called clone tracks. For two tracks that share majority of hits, we have one reconstructed track and one clone track.
The particles created during collision can be divided into several categories with respect to their momentum and their place of creation. If a particle comes from interior of the target and then is registered by TRD detector, it is called primary. A typical example of such particle is proton struck out of the target by the beam projectile. On the other hand, the particle created in the vertex outside the target in the downstream direction is called secondary. As an example one might consider a delta electron created inside the material budget of RICH detector.
Considering the particle momentum, one can divide all particles into two groups: of momentum below 1 GeV/c (slow) and all others (fast). If a particle leaves hits in all TRD layers, it is called a reference track.

The above categories with addition of clones and ghosts serve as a basic critterion to classify the reconstructed trajectories and get a basic idea on the quality of track finding (see in Tab. 4.8 on page 49)

Piece of information provided in experiment	Piece of information available in simulation
(x, y, z) spatial hit coordinates smeared with the actual detector resolution, separately for each detector layer	spatial hit coordinates with maximum precision; ideal energy value
trajectory slopes (t_x, t_y) taken from reconstructed track; some mismatched hits present	ideal trajectory slopes, always calculated from 100% correct hit assignment
momentum reconstructed with the use of magnetic field mapping and analytic formula	ideal momentum, i.e. given with maximum precision provided by simulation engine; precise data on magnetic field at every point inside magnet
tracks fitted with Kalman Filter method to minimize the multiple scattering impact and to overcome limited detector resolution	high energy particles travel along nearly straight line (multiple scattering deviation still present!)
charge of a particle reconstructed by analysing the curvature of particle trace inside the magnetic field	particle charge
the number of reconstructed tracks known, as well as the total number of hits in each TRD layer; no information about the total number of particles created within target area and further	precise information about every particle track, including the secondaries and delta electrons created in the beampipe and detector material budget
some percentage of charged pions (below 5%, depending on their momenta) misidentified and incorrectly taken as electrons	particles identification
all tracks reconstructed in the TRD are assumed to be traces of primary particles, as there is no reliable way to distinguish secondaries other than mentioned in the previous sections	exact information on origin of a particle, including the information on the mother particle

Table 4.7. The information available in the realistic experimental environment.

In order to assess the performance of the tracking algorithm one must apply matching routines, which compare a simulated track (known from MC simulations) with the reconstructed one. This is realized in two steps: for a reconstructed track, one must first determine the particle that created each constituent hit in the track, and then identify which particle owns the most hits in the reconstructed track. After that, the real trajectory of the particle is connected to the reconstructed one, and, if the particle is neither a ghost nor a clone, one can say that this particle's trajectory has been reconstructed properly.

Name	Description
Primary	Particle created inside the target volume
Secondary	Particle created outside the target volume, i.e. having secondary vertex
Reference	12 hits in TRD
Fast	With momentum $\geq$ 1 GeV/c
Slow	With momentum $<$ 1 GeV/c
Ghost	Less than 70% correct hits (less than 9 correct hits)
Clone	The same track reconstructed twice
Efficiency	Ratio of reconstructed TRD-detectable tracks to all tracks in TRD

Table 4.8. The information available in the realistic experimental environment.

The ratio of reconstructed tracks to all detectable tracks within a given group is called reconstruction efficiency.
The realistic tracking in TRD using Cellular Automaton algorithm gives results suitable for reference particles. which trajectories are reconstructed with efficiency of 90% or more. therefore if both branches from the J/ψ decay are within the TRD acceptance. the overall probability (with respect to tracking efficiency) for finding the signature is 81% or more.
On the other hand. the efficiency for low energy particles. especially secondaries. is poor, as the algorithm is optimized for higher momenta. In consequence. roughly one fourth of slow particles are found. removing the remaining part from further processing.
A typical output from the quality assessment routine performed after the tracking part is shown in Listing 4.1:

Listing 4.1. Accumulated 100 central events at 15, 25 and 35 AGeV.

```
Accumulated 1000 events:
        Reconstructed TRDTracks :      51
  Eff. of primary reference all :   76.1%   35995
  Eff. of primary reference fast :  89.4%   35654
  Eff. of primary reference slow :   4.6%     341
-------------------------------------------------
    Eff. of extra reference all :   39.1%   12335
    Eff. of extra reference fast :  71.9%    8994
    Eff. of extra reference slow :  17.6%    3341
-------------------------------------------------
     Eff. of all reference all :    61.3%   48330
     Eff. of all reference fast :   85.2%   44648
     Eff. of all reference slow :   13.9%    3682
-------------------------------------------------
                  Ghost level :      4.7%    2435
                  Clone level :      0.0%       0
-------------------------------------------------
   Primary fast clone level :        0.0%       0
   Primary slow clone level :        0.0%       0
-------------------------------------------------
   Extra fast clone level           0.0%       0
   Extra slow clone level           0.0%       0
```

```
All fast clone level :      0.0%      0
All slow clone level :      0.0%      0
```

Results shown in Listing 4.1 on the preceding page were obtained by processing 100 central UrQMD events at the energy 25 AGeV registered in TRD detector. The numbers in the rightmost column indicate the total number of particle trajectories correctly reconstructed. The percentages correspond to particular reconstruction efficiencies. The intrinsic feature of the presented algorithm is suppression of clone tracks and the ghost ratio is kept under 10.0%. The efficiency for primary fast reconstruction is at the level of 92.6% for this particular sample of data. thus the probability of registering a true J/ψ decay is equal in optimal conditions 85.6%.

Reconstructed trajectories are then fitted using Kalman Filter (KF) technique [24] (see also Appendix A on page 79). which is an improved least-square fit method. It performs smoothing of the track. and takes the impact of multiple scattering into account in the calulation of the track parameters. Kalman Filter uses material information and detector geometry to calculate track slopes in the first and the last TRD layers. and also returns the quality parameter (χ^2) value of the fit. KF evaluates the spatial coordinates of 12 hits as an input. taking every hit as an additional measurement of the trajectory slopes. When all hits are processed. the quality value is returned. allowing for separation of the improbable cases. characterized by a high χ^2 value.
Moreover. once the fit is finished. the procedure is able to extrapolate the track further to another detector or even backtrack the trajectory back to the target. assuming the particle is a primary one. The backward fit uses the analytic integral formula designed for the purpose of track finding [50]. For a primary particle. tracing its motion back to the place of origin is sufficient to determine its momentum and charge. which implies that secondary particles are the main source of momentum errors: most secondaries are rejected during momentum and geometrical cuts.
Applying all the above methods and cuts for a pure J/ψ sample accepts 66.0% of events. One must remember that not all created and then decayed charmonia are detectable due to limited detector acceptance. Roughly 1/3 of all e^+e^- pairs from J/ψ can be registered by detection setup. which gives the efficiency of true signature finding at the level of 15.8% (1580 per 10000 events). After the realistic tracking. the number of accepted J/ψ events is 1171 per 10000 (11.7%). The loss is mainly due to J/ψ decay products tracking efficiency. which is at the level of 80-85%. so the probability of registering both daughter particles is reduced to roughly 65-75% for 25 AGeV beam energy.

After processing 1000 background events from Au+Au at 25 AGeV reaction we achieve 95% and 98% background reduction for central and peripheral collisions respectively. This means that the algorithm is passing a background event every 50 desired events. increasing the time available for next level processing by a factor of 50. Tab. 4.9 on the facing page shows the consolidated results for different energy ranges. data types and collisions variants.

The CA algorithm offers good tracking efficiency for the particles with momentum over 1 GeV/c. reaching 90%. With additional tuning for a given detector geometry one can achieve up to 95% of tracking efficiency. The example efficiency in a function of momentum is shown in the Fig. 4.15 on the next page. The detailed information on tracking algorithm are presented in the next chapter.

Energy [AGeV]	Background [rejection/%]	Signal [rejection/%]
15	1000/0.1	
25	500/0.2	8.53/11.7%
35	333/0.3	

Table 4.9. The results of filtering for minimum bias events.

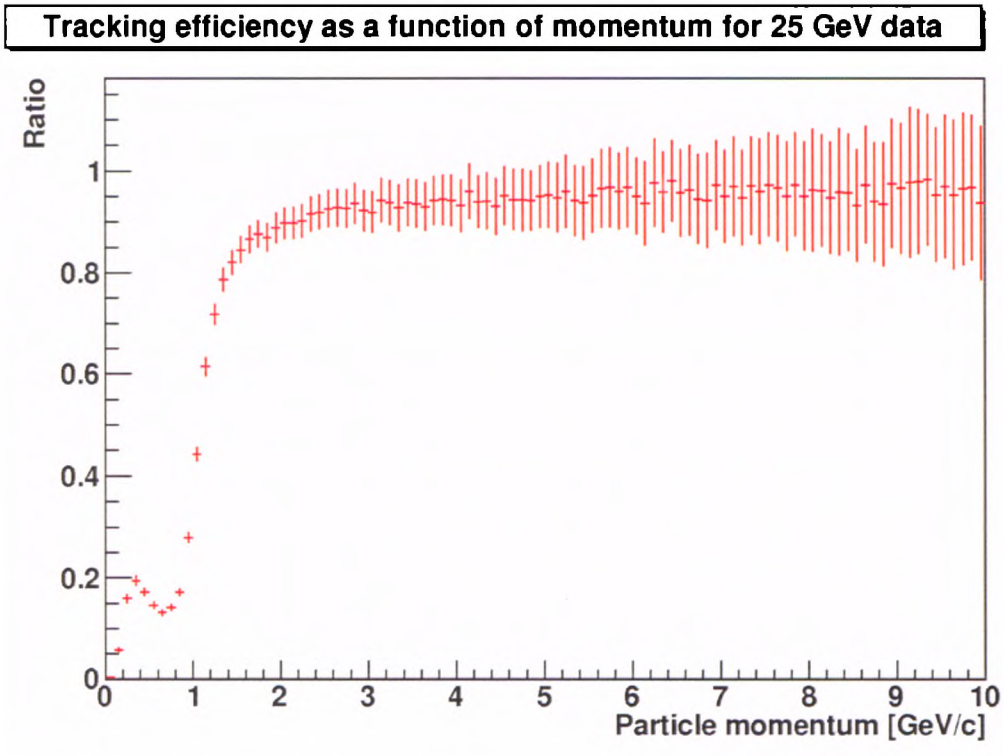

Figure 4.15. Tracking efficiency as a function of momentum. The spectrum was made using 1000 peripheral collisions of Au+Au at the energy 25 AGeV. The algorithm is optimized for high-momentum particles, therefore the tracks with momentum below 1 GeV/c are poorly reconstructed. The errors are the square root of weights.

Along with the tracking algorithm, there is also a momentum determination method implemented. The method uses Kalman Filter and analytic approximation formula with parameterized magnetic field in order to simplify the momentum reconstruction and make it faster. The algorithm traces the particle back to the target, propagating it through the magnetic field. The momentum resolution of the method for three typical energies is shown in Figs. 4.16 to 4.18 on pages 52–53. The data samples used come from peripheral collisions of 15, 25 and 35 AGeV Au+Au respectively. The standard transversal momentum cut at 1 GeV/c was applied, and the Rejection Factor of 99 was used. The invariant mass windows was chosen from 2 to 4 GeV/c^2. For 1000 peripheral collisions, the number of surviving events for 15, 25 and 35 AGeV was 1, 2 and 3 respectively. Thus, the overall background rejection factor was 333-1000, depending on the energy. The mass windows range of 2 to 4 GeV/c^2 is sufficient for the peripheral collisions, and can be narrowed for improved background rejection.

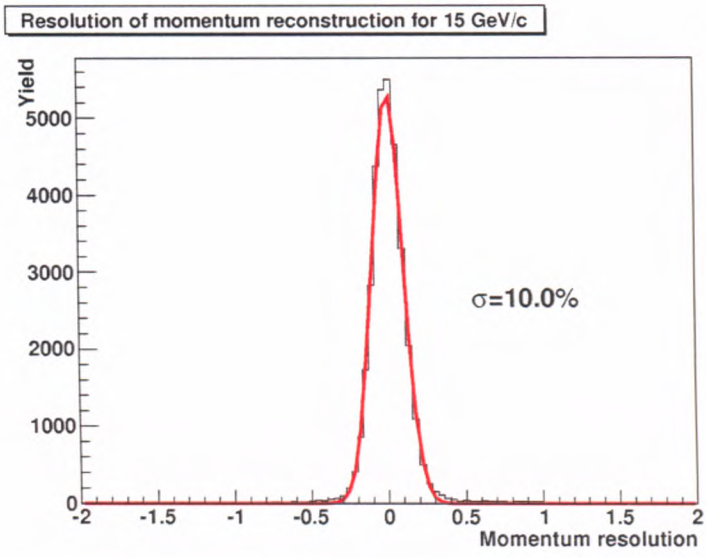

Figure 4.16. Momentum resolution for 1000 minimum bias Au+Au 15 AGeV collisions.

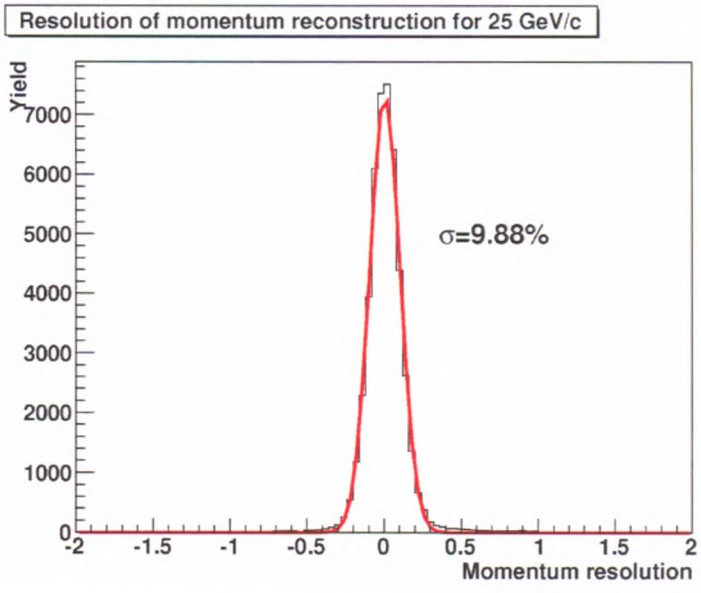

Figure 4.17. Momentum resolution for 1000 minimum bias Au+Au 25 AGeV collisions.

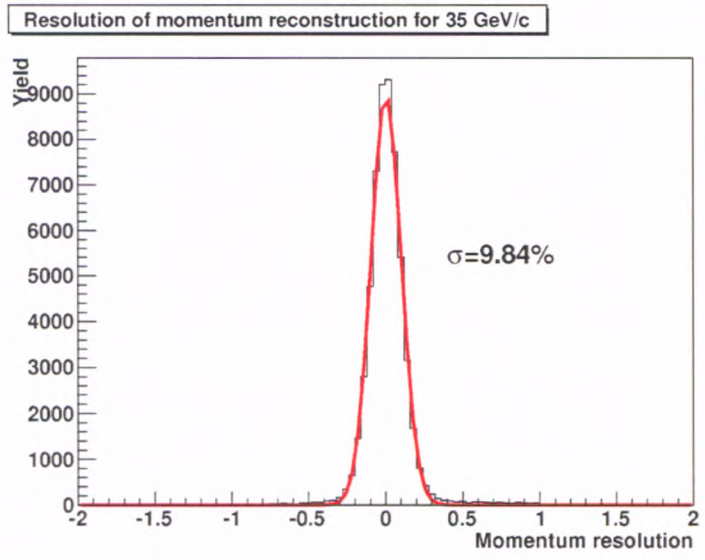

Figure 4.18. Momentum resolution for 1000 minimum bias Au+Au 35 AGeV collisions.

Chapter 5

Cellular Automaton Tracking Algorithm

5.1 Tracking algorithm

The tracking cellular automaton-based algorithm (CA. tracker). developed during my PhD study is described here. The essential feature of a low-level trigger is efficient and fast tracking algorithm. It is a base for pre-analysis of incoming information from detectors. allowing the online event selection system to evaluate the portion of acquired data. The emphasis of the TA is rather put on speed than on overall efficiency or accuracy which easily allow for further optimization. Thus the tracking procedure can be tuned to be used in the online regime. The simplified diagram of the data flow in the running experiment is shown in Fig. 5.1 on the following page.

The tracker requires a part of CBM detectors data - TRD information only. In order to find the paths of the particles TRD tracking system is sufficient and there is no need to employ the global tracking procedures. Such solution reduces the computational time consumption. The initial data flow procedure needed to make low-level decisions is also significantly reduced. As far as the online systems are concerned. time is of the essence. hence the tracker operates on the absolutely minimal data set.

5.1.1 Introduction to Cellular Automaton

Cellular automata were proposed in forties of the 20th century by Stanislaw Ulam[1]. At the same time John von Neumann [2]. who tried to develop hypothetical self-reproduction machine. realized that cellular automata. which reflect the simplified physical model of the real world. is the solution of his search. In the early 1950s cellular automata were studied as a possible model for biological systems. with similarity to bacteria colonies.

[1] "Stanislaw Marcin Ulam (April 13, 1909 - May 13, 1984) was an American mathematician of Polish-Jewish origin, who participated in the Manhattan Project and developed a number of mathematical tools in number theory, set theory, ergodic theory and algebraic topology." [51]

[2] "John von Neumann (December 28, 1903 - February 8, 1957) was a Hungarian-American mathematician who made major contributions to a vast range of fields,[1] including set theory, functional analysis, quantum mechanics, ergodic theory, continuous geometry, economics and game theory, computer science, numerical analysis, hydrodynamics (of explosions), and statistics, as well as many other mathematical fields." [52]

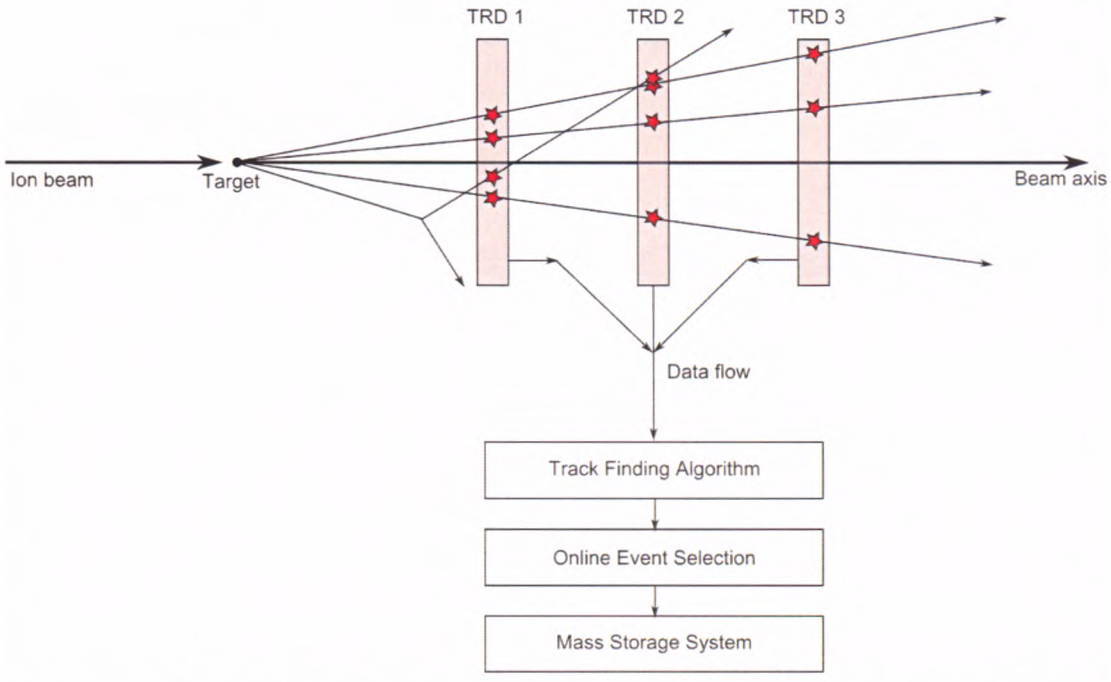

Figure 5.1. The scheme of the event selection in CBM experiment. There are three TRD stations shown on the beam axis, and some example traces of particle created during the collision. The data gathered from detectors are transferred to the tracker (track finding), and then passed to the event selection software and hardware module, where the decision about storing the data is made.

At present they are also numbered among wide and fashionable domains like artificial intelligence. The best-known example and implementation of cellular automata is "The Game of Life" devised by the British mathematician John Horton Conway in 1970. Because of its analogies with the rise. fall and alternations of a society of living organisms. it resembles and simulates real-life processes. It is non-player "game". needing no input from human players. The basic idea is to start with a simple configuration of "organisms" (checkers. counters) spread over a 2-dimensional grid (one in a single cell). Each cell may be empty. or may contain "life". and each cell has 8 neighbors. 4 adjacent orthogonally. 4 adjacent diagonally (Fig. 5.2 on page 58). During the game at each "round". the Conway's "genetic laws" are applied. determining the births. deaths and survivals of the organisms.

The "organisms" are subject to the following general rules:

1. Survivals. Every checker with 2 or 3 neighbors survives to the next round.
2. Deaths. Each checker with 4 or more neighboring counters dies of overcrowd, while every counter having either 1 or none neighbors dies from isolation.
3. Births. Each empty cell adjacent to exactly three neighbors is a "birth cell". It contains a checker in the next round.

Further evolution of the game is only determined by its initial state and conditions that give particular forms of repetitive or other behavior [53]. It is important to understand that all births and deaths occur simultaneously in given time step. One can noticed

that such game based on the cellular automata could be viewed as kind of parallel computers.

An evolution of five examples of the initial sets is shown in Fig. 5.2 on the following page. The leftmost set of cells (forming a square shape) is a static one, i.e. it does not changes in the next generations. Next three sets enter a static phase after a couple of rounds, and the last one finally enters the so called oscillator mode, which continuously switches between two states.

5.1.2 Tracking algorithm overview

In principle, the tracking algorithm can be described as a set of combinatorial operations accompanied by sorting routines, which schematically are presented in the Fig. 5.3 on page 59. The TA procedure takes a set of hits registered in all 12 TRD layers, so the input is a set of points in the 3-dimensional space. The information about the energy loss or pulse shape are not used at the tracking level, so at this point can be discarded. The results of the procedure are the set of data structures known as "reconstructed tracks". Each one has assigned a set of 12 TRD hits and a "χ^2-like" value is calculated (reflecting the linearity of a track) and further denoted as χ^2 value. In other words, for a high-momentum particle track, the χ^2 is a measure of reconstruction quality. Any additional information which are not essential at this stage, like momentum (estimated) or charge (determined), can be obtained later, using some computational effort, but at this point it is not necessary.

The iterative combinatorial parts include the following stages:

- Creation of Space Points (SP, plural SPs) in every even-odd layer pair (6 pairs of layers, 6 parallel processes)
- Creation of segments combining two SPs (3 independent tasks)
- Finding friend segments - 2 processes
- Tagging segments - 2 processes
- Creation of track candidates - one process, but can be implemented on 700-1000 threads using one common data set

The above stages are accompanied by sorting routines. Every newly created set of structures (SPs, segments, track candidates, reconstructed tracks) has to be sorted according to its key feature - geometric coordinates, χ^2 value, tag number or number of friends. Sorting procedure is a part of algorithm optimisation. Using the sorting routine takes some time, but it allows the further parts of the algorithm to execute much faster.

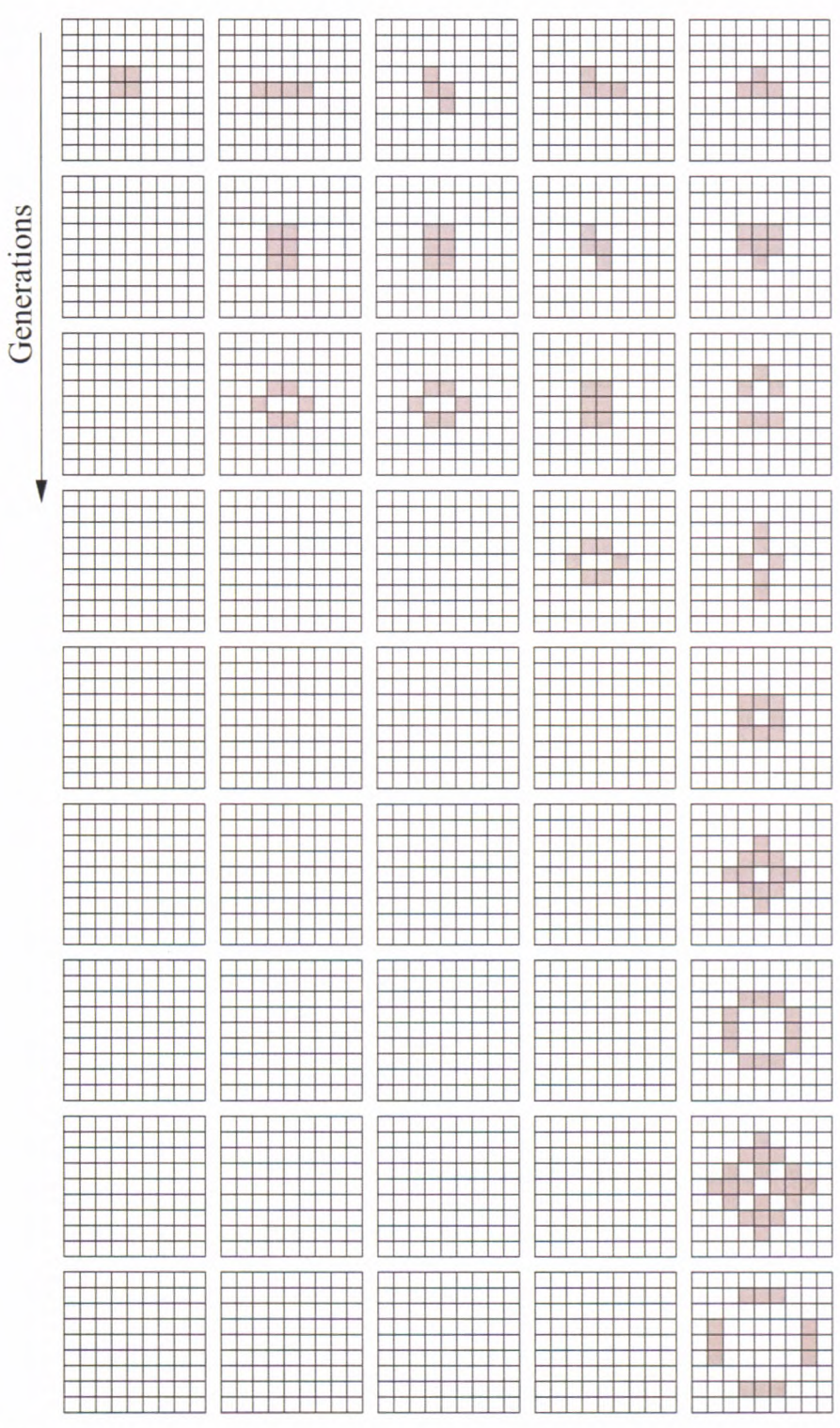

Figure 5.2. The evolution of five simple sets of cells. The columns with empty cells mean that the set remains unchanged in the consecutive steps. Therefore the set entered the static phase.

The sorting parts perform the following operations:

- HITS: Sorting hits according to Y coordinate for every TRD layer inedependently

(12 parallel processes)

- SP: Sorting Space Points according to Y coordinate for every SP plane (6 parallel processes)
- SEGMENTS: Sorting created segments according to Y coordinate (1 process for each TRD station, 3 in total)
- TRACK CANDIDATES: Sorting the track candidates with respect to the χ^2 value (χ^2 value is calculated after creating of each track candidate)

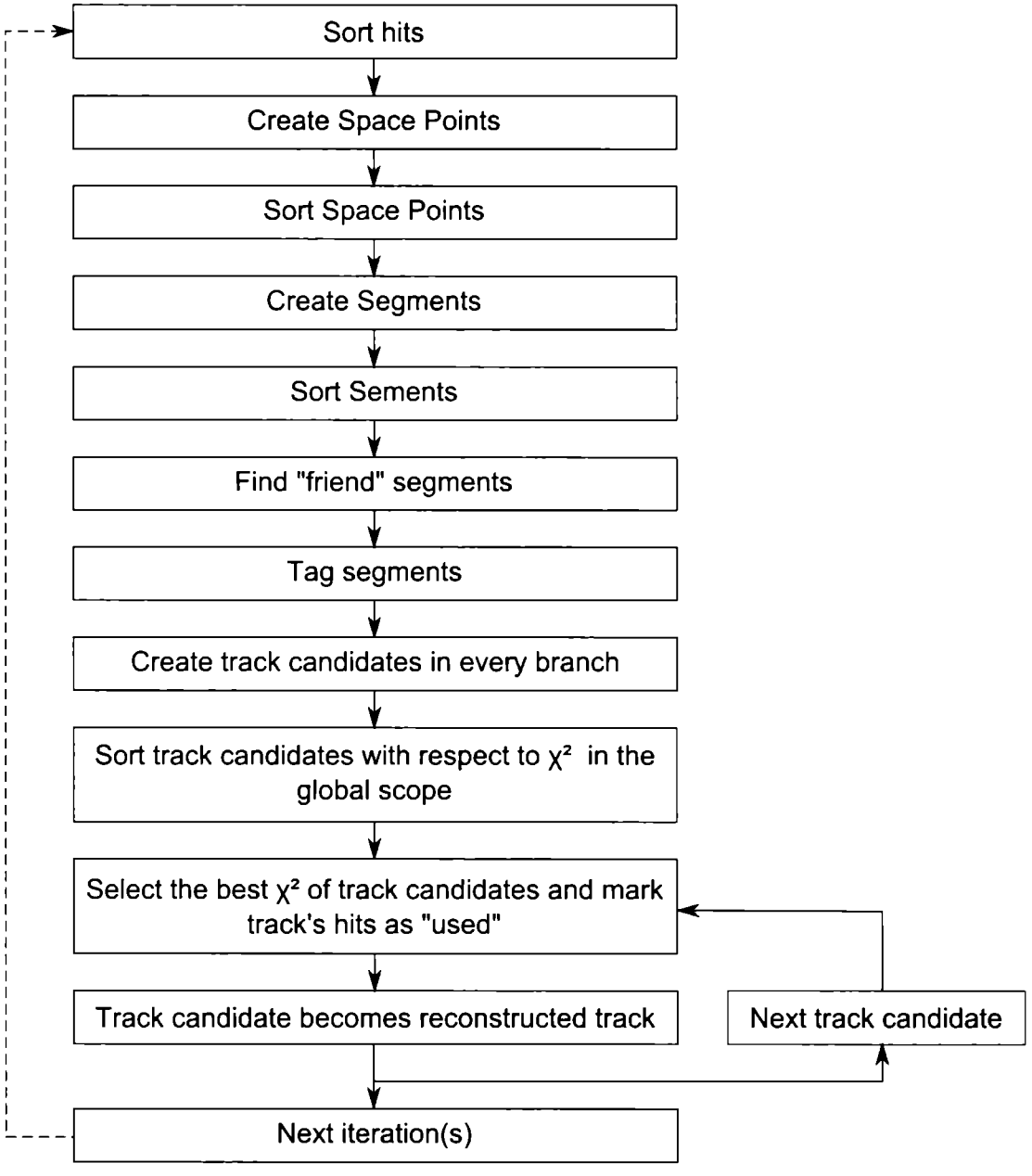

Figure 5.3. Brief sketch of the CA algorithm.

The coordinate, which is the key value to sort, is chosen arbitrary. In the proposed TRD layers set, the first layer offers the acurrate Y coordinate of the hit, thus making it possible to order in accordance to Y. The χ^2 value reflects the linearity of the track, therefore can be used to distinguish real tracks from the fake ones inside the reconstructed tracks pool.

To avoid the confusion, the value of some parameters used in the procedure were ommited, especially the ones in the geometrical restrictions and extrapolations. They can be viewed in the Appendix C on page 87.

5.1.3 Data structure

The data portion which comes out from a single TRD layer has a structure of "hits" and share a common Z-coordinate values. Each hit is a data set, which stores the X, Y and Z coordinates of a place, where the charged particle hit the detector plane. Each has uncertainity due to the detector resolution, but one has to note that the Z position of the detector is known most accurately. It is determined during the construction of the setup. As far as X and Y positions are concerned, one of them is always measured with good precision, while the other has a large spatial uncertainity. This is a direct consequence of the sensitive chamber's shape, and for a given plane all the chambers are oriented unifically. In a globas scope, the next layer contains chambers rotated by 90 degrees in comparison to the previous one. This means that if the first layer has chambers oriented horizontaly (precise Y coordinate in the beamline coordinate set), all odd layers share the same layout, while all even ones are oriented vertically.

An example hit from a single TRD layer is shown in 5.4.

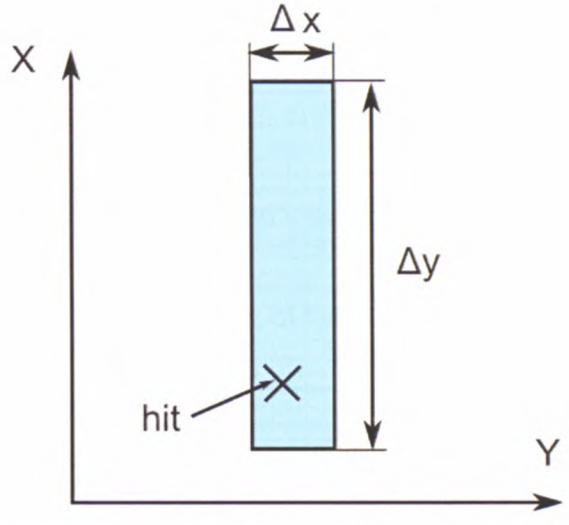

Figure 5.4. An example of a location of the hit and its error value. If a hit is registered, one can obtain information about the chamber position only, so a real particle hit position comes with errors δ_x and δ_y respectively. The draw is not in the scale.

As two neighboring layers contain two precise measurement results, they can be used to construct a structure called Space Point. Each of SPs has an X value, a Y value and an information on the TRD hits of the parents, and the Z coordinate from the hit closer to the target. Any other information is unnecessary and it is discarded to save the

computational effort. SP can be seen as a kind of smeared point in the 3-dimensional environment. The idea of creating a SP can be viewed in Fig. 5.5.

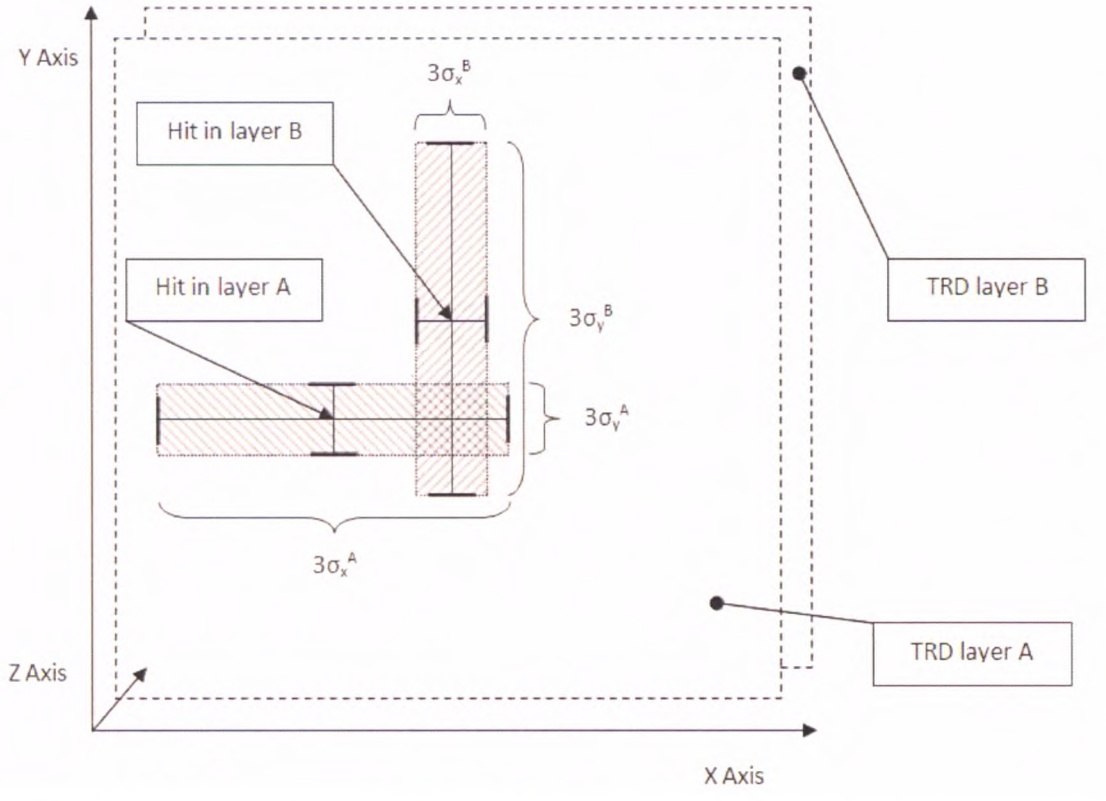

Figure 5.5. The process of creating a SP from hits in two TRD layers designated as A and B. The precision of detector position measurement (σ from the Gaussian distribution) in a given area is known, therefore we construct a Region Of Interest (ROI) around the registered hit using the 3σ value as shown in the figure. Then the ROIs from two layers are projected to the XY plane and if there is an overlap, the SP is created using coordinates from the two hits.

Space Point structures are a base for creation more advanced objects, namely the segments, described below.

5.1.4 Segment creation part

A segment (sometimes called *a tracklet*) is an object created from two Space Points, containing four hits, each from a distinct layer belonging to the same TRD station. In other words, a segment is a part of reconstructed trace, left by a particle crossing the detector sensitive areas. When all SPs are created, the segment creation part starts. In a given TRD station, SPs containing hits from the first and second layers are combined with SPs having hits from third and fourth layers. The geometric restriction must be applied at this point, in order to eliminate unprobable combinations of the SPs. The geometrical constraint is constructed as follows: the line connecting a given SP with a target is prolonged downstream (towards the greater Z values), until the next SP plane is reached. Then, the Space Points are accepted for combination within certain region around the extrapolated point. The others SPs, outside the region, are assumed to be

the unprobable connections and are rejected. The dimension of the region is given as a parameter to the procedure. It differs in each TRD station, and also depends on the iteration number (described further in the text). The schematic idea of segment creation is shown in the Fig. 5.6.

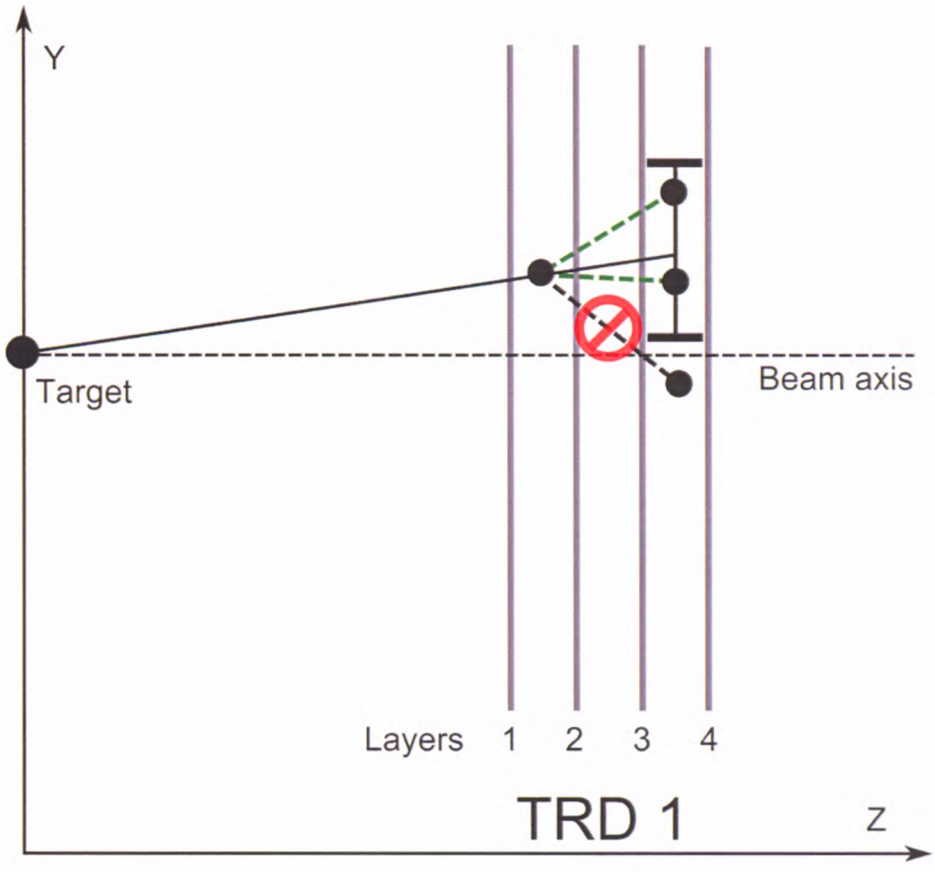

Figure 5.6. The segment creation procedure in a single TRD station. Only segment candidates with the second SP in the area around the extrapolated point are accepted (green dashed lines). The segment with the red sign is not taken into account, because its second SP is too distant from extrapolation (geometrical restriction).

Segments are consistuents of a track. A track is composed of three segments. each from a distinct TRD station. Reconstructed track reflects a probable trace of a particle. traversing all the TRD stations. The first segment in a track (according to the distance to the target) is connected with a segment to the right, the middle segment is connected from both sides to two other segments, and the segment in the last station is attached to the segment from the left.

If segment "a" can be potentially connected to another segment, "b", "a" becomes the *"friend"* of "b" and vice versa. Being a friend means that the geometrical conditions are fulfilled for both segments. The procedure is further described in the next paragraph. In most of cases, one of the "friends" is a part of a real particle track.

5.1.5 Friends finding procedure

Each segment in a given station can be attached to a number of segments in other stations. within certain geometric limitations (similiar to mentioned in 5.1.4 on page 61). To find a friend of a given segment (source segment "a" in the Fig. 5.7). one needs to extrapolate the existing segment upstream to the next station. Then. the procedure looks for segments starting within the region of interest around the point of extrapolation. If any segment is found. all of them are marked as "friends" of the source segment. Each segment may have either many friends. or it may have none.

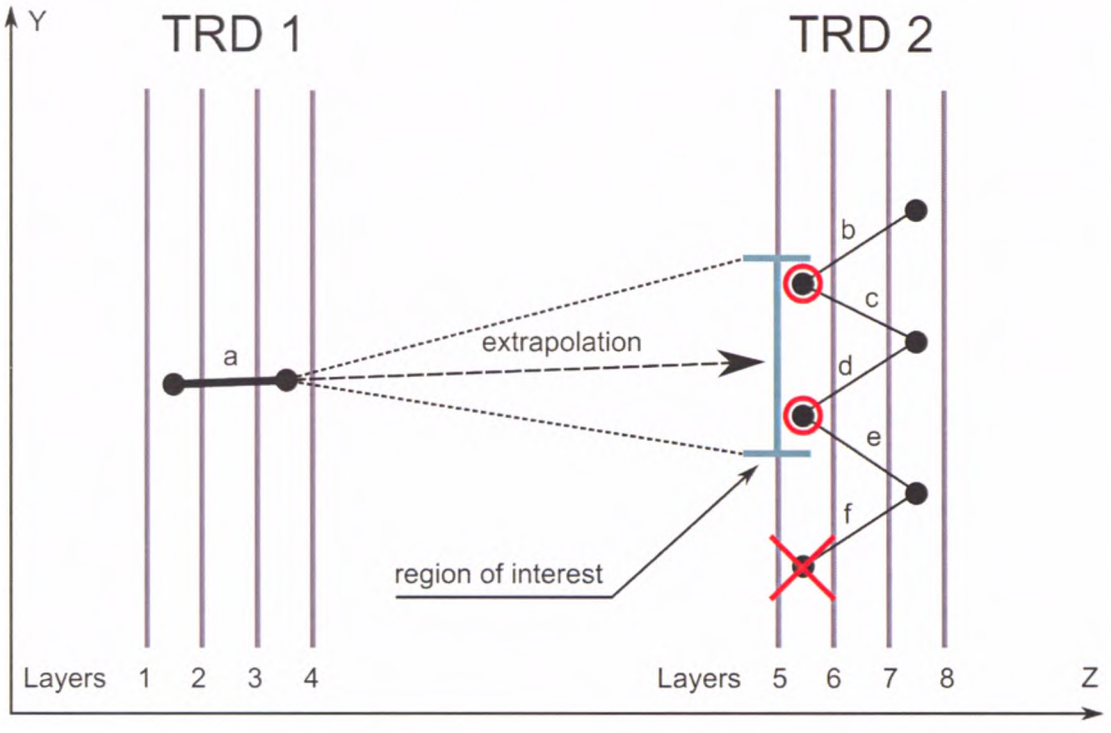

Figure 5.7. Friend finding methods. The segments located within a region of interest around the extrapolated point are considered "friends" of segment "a". At the same time, segment "a" is a friend of segments "b", "c", "d" and "e".

Friend segments can be determined in two independent runs. For every segment in TRD 1. the procedure looks for friends among segments from TRD 2. In analogy. for every segment in TRD 2. the friend segments in TRD 3 are found. As a result. each segment has a list of "friends". If a segment in the middle TRD station (TRD 2) has friends on both sides, it can be a track candidates, because it contains the total number of 12 hits in 3 segments, as shown in Fig. 5.8 on the following page. Two tracks candidates can share a common one or more segments, which is not an issue at this point of track finding method.

Performed benchmarks shown that by employing of the friend finding algorithm the total time consumed by the track finding methods was decreased by a factor 10.

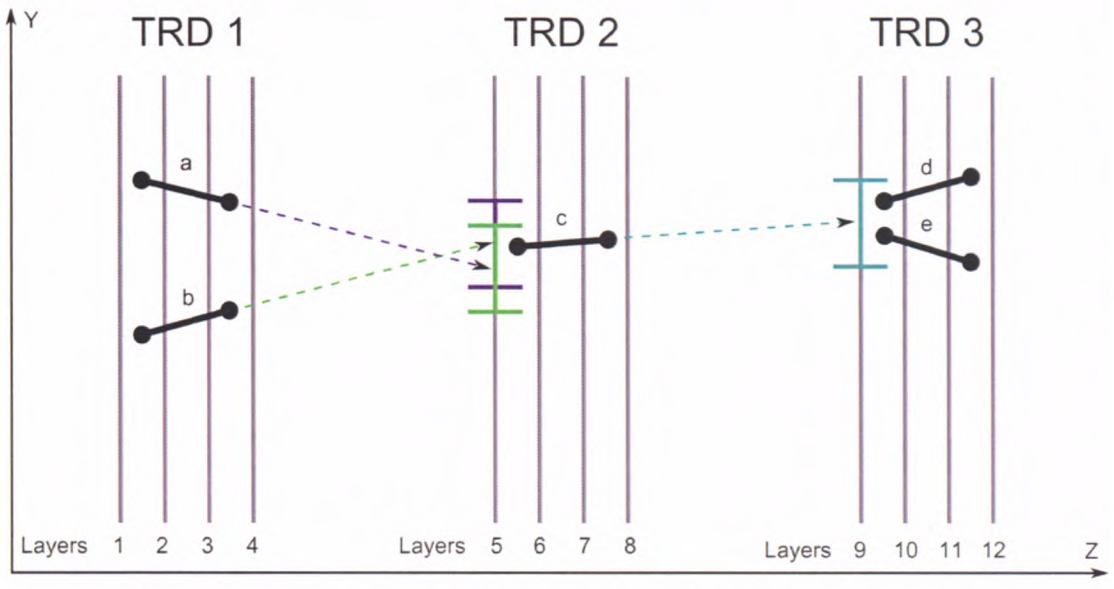

Figure 5.8. An example of "friends" of a segment "c" (from the central station). Segments "a" and "b" are registered as "left-hand" side friends (i.e. friends located closer to the target). Segments "d" and "e" are "right-hand" side friends (more distant from the target). Pointers to the friend segments are stored in two arrays: one for left- and one for right-hand side trackletes each.

5.1.6 Tagging

This stage is one of the most important phases of the algorithm execution: it assigns a so called **tag number** to each segment. The value depends on the number of friends assigned to the particular segment, as well as the tag numbers of the friends. Because each tracklet possesses a list of its friends, exhaustive combinatorial searches are avoided and tagging is very fast. The tagging procedure begins from the third station (TRD 3) and is performed using the followind rules:

- If a segment from any station has no friends, it is "alone" and has always tag number equal 0. Alone segments have empty "friend" arrays.
- If a segment from TRD 2 has at least one friend in TRD 3, its tag number is increased to 2. The tag number of the friend is increased to 1. If these numbers were already increased by previous opearions, no changes are made.
- If a segment in the TRD 2 station has no friend to the right but at least one friend to the left (in TRD 1), its tag number is increased to 1. The tag number of a friend is increased to 2.
- If a segment is a friend of both the segment with number 2 and a segment with a number 1 (both friends are in TRD 3), its tag number also increases. The bigger tag number among the friends is taken, and the segment receives this number increased by one.
- If a segment from TRD 1 has a friend with tag number equal to 2, it receives the tag number 3.

5.1.6.1 Initial state, before the tagging procedure starts

The Fig. 5.9 presents the state just before the tagging procedure begins. The dependencies between tracklets are shown with the arrows. The arrows also denote the points where the extrapolation directs to. The segment "c" is shared by two neighboring branches started by segments "a" and "b".

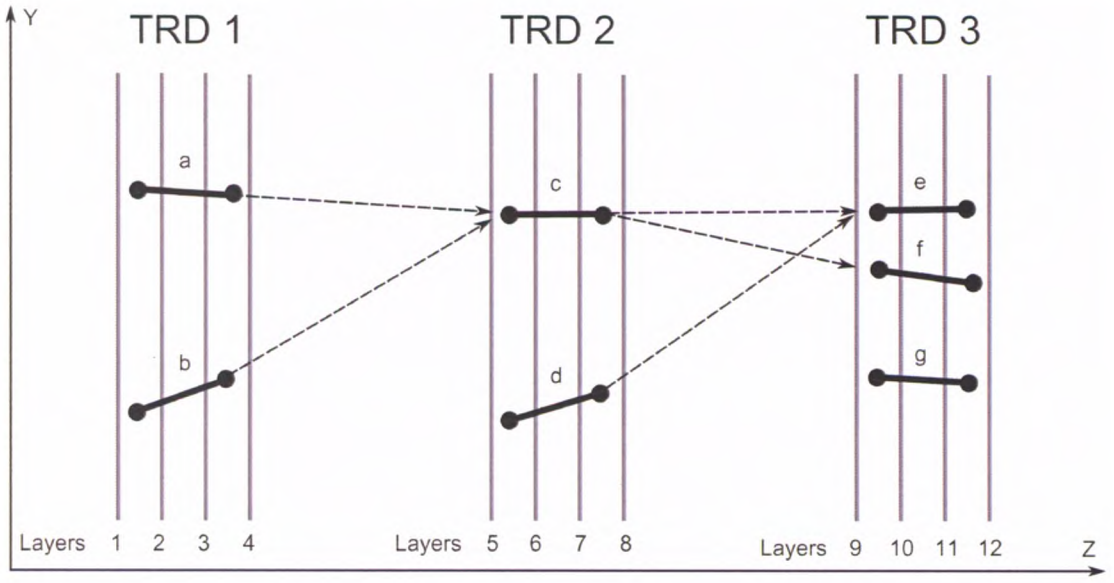

Figure 5.9. State of the track finding algorithm just before applying of the tagging procedure. Segment "c" has 4 friends: "a", "b", "e" and "f". Segment "d" has a friend "e". Segment "g" is alone.

5.1.6.2 Zero-assignment state

In this step the initial value equal to 0 is assigned to every tracklet. At the beginning, we assume all the segments are "alone", unless marked otherwise (See 5.10 on the following page.)

5.1.6.3 Tagging state

The beginning of the tagging procedure for one run is shown in the Fig. 5.11 on the next page. Example procedure starts with segment "c" from the third station. Segment "c" is coupled with segments "a" and "b", therefore it is not alone. Thus, the tag number 1 is assigned to the segment "c". In the same way, the segment "d" is also tagged by 1 ("not alone"). In this example segment "e" has no friends, so its tag number remains 0.

In the similiar way, the further phase of tagging is performed. Each friend of each segment marked with 1 gets the tag number 2.

Segment "c" is a friend of "e", so it acquires the value of its friend increased by one (tracklet "e" has tag value 1, so element "c" gets 2). Segment "c" has another friend, "f", with also a value of 1, but the tag value of "c" has already been increased by one, so it keeps the former value. The value of tracklet "d" is increased, as it is a friend of "e".

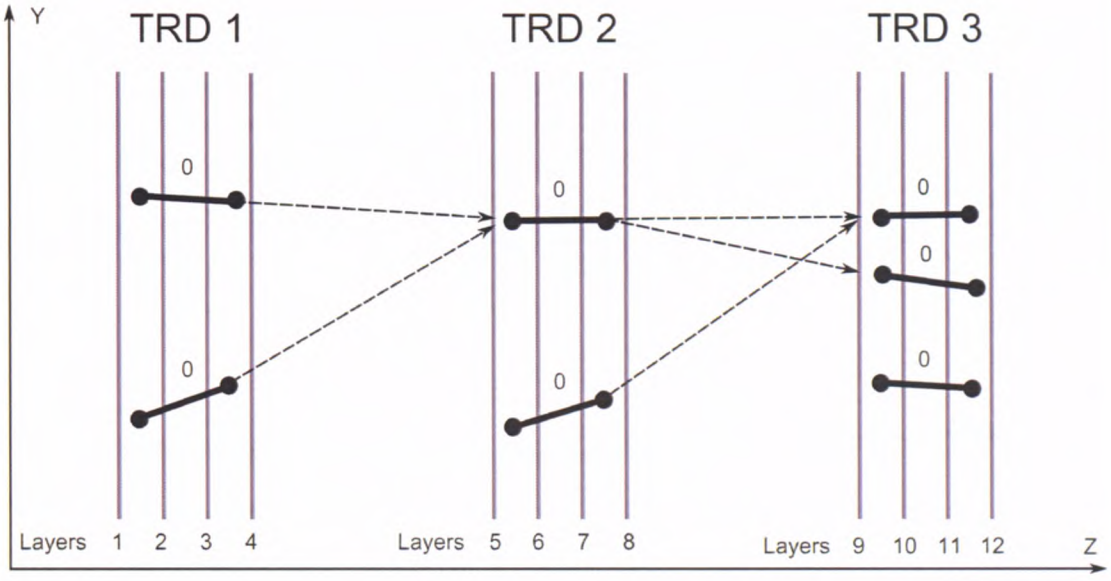

Figure 5.10. Zero-assignment state. Each segment is assigned a tag number 0, which means that initially it is assumed to be alone (i. e. not associated with any other segment).

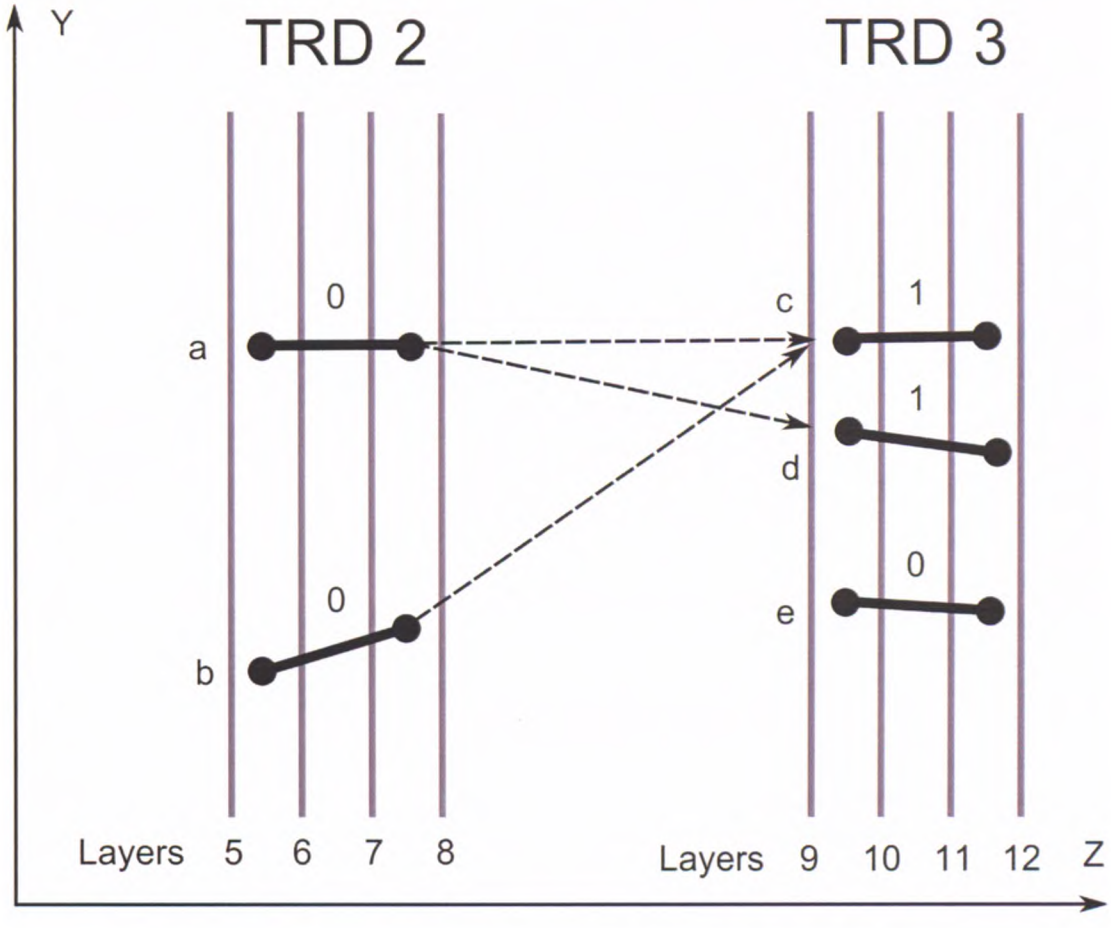

Figure 5.11. Example of tag number assignment (description in text).

Processing first station leads to increasing the tagging values of "a" and "b" to 3, as the neighboring tracklet "c" has its value equal to 2. After tagging, status of all available segments is shown in Fig. 5.12.

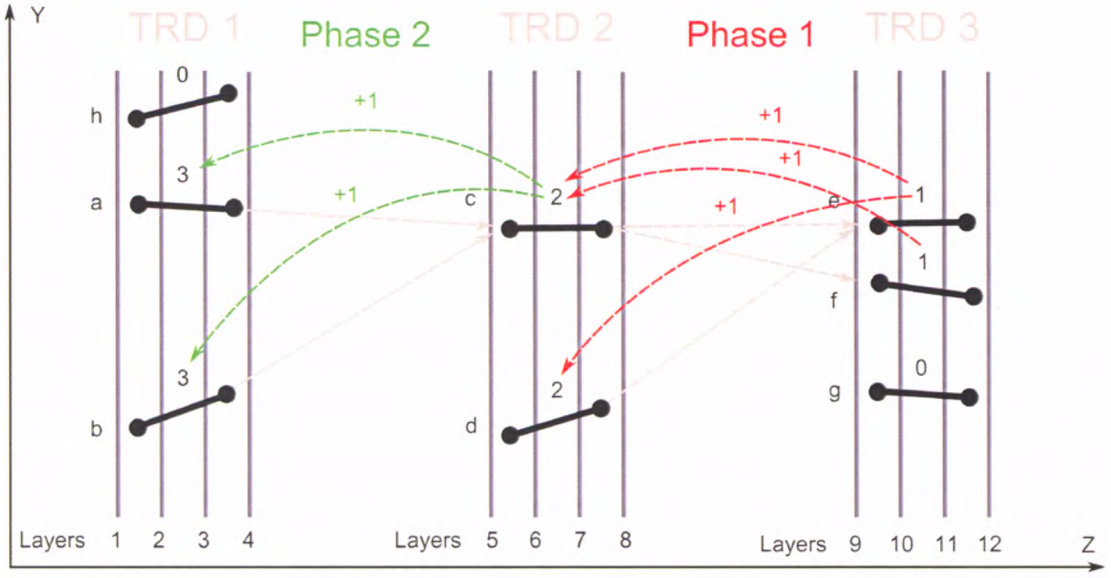

Figure 5.12. The phases of tagging procedure. Segment "e" is known to be connected to the tracklet "c", so it gets a tag value 1 ("not alone"), as does tracklet "f". Segment "g" is alone and not connected to any other one, so it keeps its value of 0.

If a tracklet is connected to two further segments to the right, its number is 3, and a track starting from such segment is considered a candidate to be a real track.

5.1.6.4 Final state

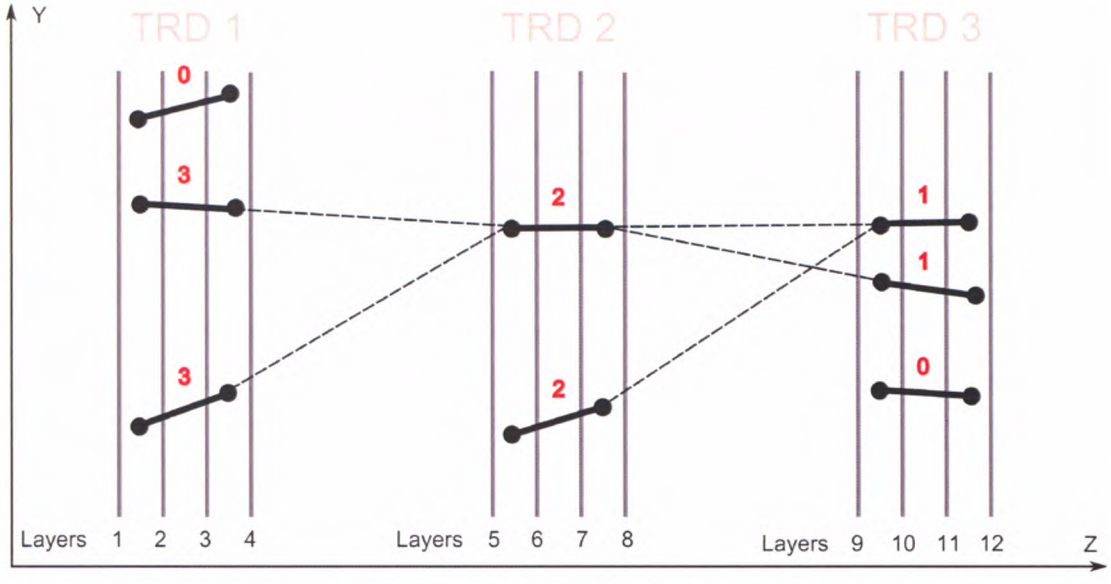

Figure 5.13. The final state, after all the tagging is finished.

When the tagging procedure is finished, the segments in the TRD 1 (with a tag number equal to 3) are the starting points for a so called **branch**. Branch is a set of friend segments, all connected to a common segment from the first station, directly or indirectly. In every branch, there is at least one track candidate. All the segments residing in the first station with tag numbers lesser than 3 are discarded, because they cannot have all 12 hits.

5.1.7 Creating track candidates

A group of segments connected (directly or indirectly) to a segment marked with "3" is called a *branch*. A branch contains at least one segment from each TRD station. All the segments in TRD 2 have tag number 2, and segments in TRD 3 are tagged by 1. There are neither alone segments, nor 2-segment structures in a branch. An example of the branch is shown in Fig. 5.14.

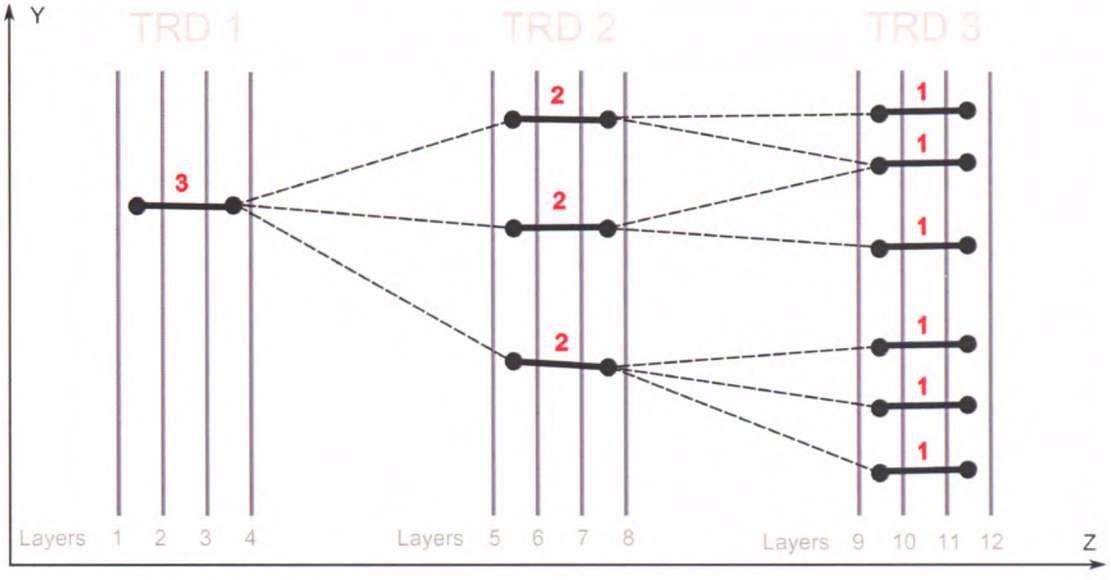

Figure 5.14. The example branch created from a single segment from Station 1.

For every branch created during the previous phases the selection procedure is executed. Within a single branch, every possible track candidate is created, and then for each candidate the χ^2 value is calculated (details below). The χ^2 mentioned here reflects the linearity of a track candidate (the smaller the better). An example branch which is a base for χ^2 values calculated for each track candidate is shown in Fig. 5.14, while the graphic illustration of a χ^2 for a single track is shown in Fig. 5.15 on the next page.

Fig. 5.15 on the facing page shows seven track candidates from a single branch. All of them begin from the same tracklet. The bold green line is used to designate the track with the best (smallest) χ^2 value (the most linear one). The green track is a best candidate to be the trace of a real particle, most probably a high-momentum one. One must notice that there are segments shared among a few track candidates, marked with blue color on the picture. Only one of them can become a reconstructed track, because we assume no hit overlap, but at this stage we create both as track candidates.

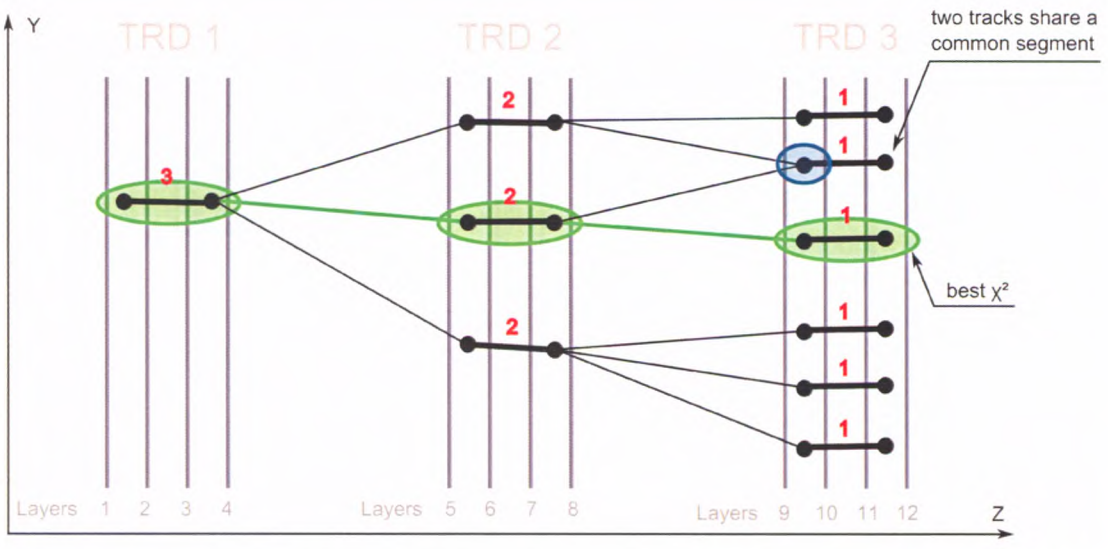

Figure 5.15. The example branch created from a single segment from Station 1 (TRD 1).

5.1.7.1 Calculation of χ^2-like value

The χ^2 parameter (goodness of linear fit) used here is a measure of total distortion of a track from linearity. It is calculated for each track candidate. It is called χ^2-like because it is not a statistical function. The calculation of χ^2-like is simpler and less time-consuming than using more precise Kalman Filter[3], therefore is suitable to be executed multiple times. The precision of the fit has not the highest priority though. In our case the χ^2-like procedure looks as follows. First, the line connecting the first and the last Space Point in a track candidate is created (3-dimensional line equation is created). Then, for each spacepoint, the distance to the line (at Z=const plane) is calculated, on X anf Y axes separately. The output value is a mean hit deviation. The idea of this simple therefore fast and efficient procedure is shown in Fig. 5.16 on the next page. The returned number is a function of a total track deviation from linearity.

5.1.7.2 Collecting the track candidates

When all branches are created, all the track candidates from all the branches are stored in a common array. For each track candidate the χ^2, as a measure of linearity, is calculated. In order to calculate χ^2 (true, statistical value), one can also use Kalman Filter (KF, Appendix A on page 79) technique, which is more precise than the simple procedure described above. It takes multiple scattering and the material budget of detector stations into account. A drawback of this method is that it is iterative, thus very time consuming and therefore it cannot be used for each track candidate. It can be effectively used for up to 1000 track candidates in one event. Above this number, the time of KF χ^2 calculation in typical data event consumes a majority of the total event processing time.

[3]The χ^2-like method treats the first and the last SP in a special way, thus the line connecting there points is not the best fitting line.

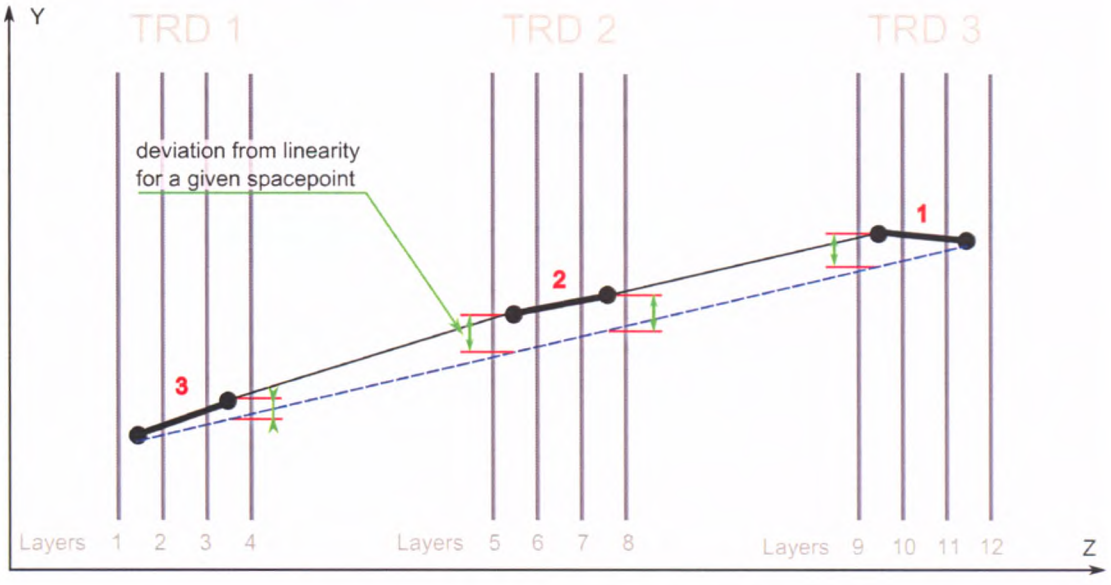

Figure 5.16. The calculation of χ value.

The quality procedure described assignes a reliable χ^2 value for each track. The track candidates are stored in an array and they are sorted with respect to χ^2-value in increasing order. The first track candidate from the array (with the smallest χ^2) is accepted as a true track. All its hits are marked as "used. If the hits marked as "used" are found in the next track in the array. such a track candidate is rejected.

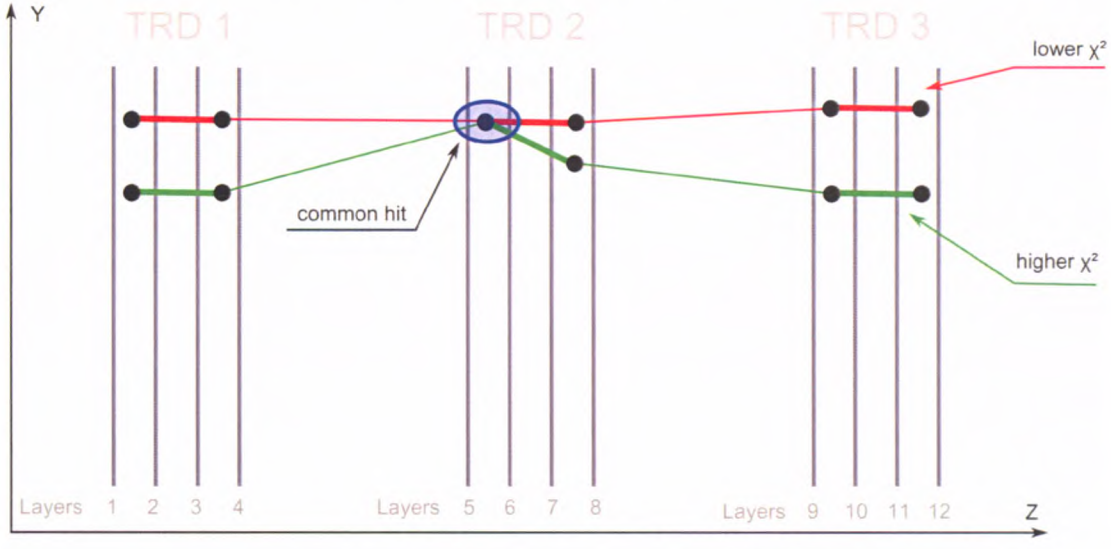

Figure 5.17. The example branch created from a single segment from Station 1 (TRD 1).

The example of such situation is shown in Fig. 5.17. The red track has a lower χ^2, so it appears earlier in the track array than the second track. marked with green line. The mentioned tracks share one common hit. located in the 1^{st} layer of the 2^{nd} station. Red track is processed first, and all its hits are marked as used. Then, when the algorithm analyzes the green track. it founds one of the hits already used. so the whole green

track is rejected. When all the track candidates are processed, reconstructed tracks are chosen and their hits are marked as "used". It is the end of first track finding procedure iteration (loop). Because the geometrical constraints in this iteration are very strict, only the most linear tracks are reconstructed (with the highest momenta). After the first loop, the entire tracking procedure is repeated, but without the hits used in the previous iteration. The geometrical restrictions are looser, thus there is a chance to find traces of particles with lower momentum. Finally, the third loop with very tolerant conditions starts, finding the remaining tracks. The execution has been divided into three phases because one run with less restrictive conditions is simply too slow. There are about 700 hits in the first layer of a first station (Au+Au, 25 AGeV), and up to 900 hits in the last layer of the last station. The number of combinatorics shows asymptotic increase and dividing the execution into smaller parts is a reliable and tested way to overcome it. The exact values of geometrical restrictions can be found in Appendix C on page 87.

5.1.8 Results and performance

The overall track finding (track reconstruction) efficiency is shown in the Tab. 5.1 on the next page. To test the tracking routine, the central collisions as an extreme reaction case were used. Data sample used for this test contained particles generated during 100 Au+Au collisions at the energies of 15, 25 and 35 GeV per nucleon. Because in the reaction Au+Au at these energies the peripheral collisions dominate the total number of reactions, the results with peripheral data sets were also included. The peripheral collisions results are gathered in Tab. 5.2 on page 73. In this section, the following categories of reconstructed tracks were presented:

- **Primary reference all** (Prim. ref. all) - all the primary particles with 12 hits in TRD.
- **Primary reference fast** (Prim. ref. fast) - primary particles with 12 hits in TRD and momentum > 1 GeV/c.
- **Primary reference slow** (Prim. ref. slow) - primary particles with 12 hits in TRD and momentum < 1 GeV/c.
- **Extra reference all** (Extra ref. all) - all the secondary particles with 12 hits in TRD.
- **Extra reference fast** (Extra ref. fast) - secondary particles with 12 hits in TRD and momentum > 1 GeV/c.
- **Extra reference slow** (Extra ref. slow) - secondary particles with 12 hits in TRD and momentum < 1 GeV/c.
- **All reference all** (All ref. all) - all the particles with 12 hits in TRD.
- **All reference fast** (All ref. fast) - particles with 12 hits in TRD and momentum > 1 GeV/c.
- **All reference slow** (All ref. slow) - particles with 12 hits in TRD and momentum < 1 GeV/c.

- **Ghost** - reconstructed track with less than 70% of correct hits.
- **Clone** - the same track reconstructed twice.

The tracking algorithm was optimized in the region of intermediate energies around 25 GeV per nuclen, as can be seen in Tab. 5.3 on the next page. The goal was to find most high-momentum primary tracks (designated "Prim. ref. fast"). The J/ψ decay signal can be found among such kind of particles. The geometrical restriction can be tuned for lower or higher hit densities. Also, the distance from the target to each station has an impact to the track reconstruction efficiency, the closer the better. The results were obtained using standard CBM geometry with TRD 1 at Z = 5 meters.

Reconstruction time of 100 event			
Energy	15 AGeV	25 AGeV	35 AGeV
Tracks per ev.	217	302	362
Stage	**time[s]**		
Do find	15.57	24.29	32.12
Sort Hits	1.05	1.67	1.94
Create SPs	0.56	0.55	0.85
Sort SPs	0.03	0.08	0.11
Create segments	0.07	0.17	0.28
Find friends	0.05	0.30	0.20
Tag Tracklets	0.01	0.06	0.05
Create Tracks	2.10	3.39	5.00
Refit Tracks with KF	2.73	3.36	4.94
Second Loop	6.85	10.90	13.72
Third Loop	4.42	6.10	8.83
Time per ev.	0.16	0.24	0.32

Table 5.1. Time of reconstruction of 100 central Au+Au events at 15, 25 and 35 AGeV.

The time benchmark shows the amount of CPU time needed for reconstruction of one event on a reference PC enviroment with "AMD Opteron 280" processor. There is total time measured as well as the partial times for the key stages of track reconstruction shown in Table 5.1.

The results for central collisions were gathered from 100 events. For the peripheral collisions, 1000 events were reconstructed. The average time consumed for track reconstruction of 1 central event is 0.15 s and the reconstruction of 1 minimum bias takes about 0.03 s for the lowest energies. The lower the energy, the less particles cross the sensitive layers of TRD, therefore the track density is lower. The number of combinatorics decreases, and the processor time consumption is smaller.

The algorithm was designed to work in parallel on multiprocessor machine. When the hits in TRD are sorted, the sorting routine works for each layer independently. This means that there are twelve active threads working on the same sample of data (one event in common memory). Then, there are six threads executing the SP creation routine and next six ones sorting SPs. Three cores are needed to create and sort segments, then two to do the tagging part; two processors are also finding friends at the

Reconstruction time of 1000 event			
Energy	15 AGeV	25 AGeV	35 AGeV
Tracks per ev.	52	69	86
Stage	**time[s]**		
Do find	31.90	46.09	59.74
Sort Hits	2.49	3.10	3.95
Create SPs	0.76	1.09	1.49
Sort SPs	0.07	0.12	0.22
Create segments	0.19	0.29	0.50
Find friends	0.12	0.16	0.28
Tag Tracklets	0.13	0.13	0.10
Create Tracks	4.05	6.55	9.04
Refit Tracks with KF	5.59	7.46	9.21
Second Loop	14.10	20.31	26.02
Third Loop	8.82	12.50	15.78
Time per ev.	0.03	0.05	0.06

Table 5.2. Time of reconstruction of 1000 peripheral Au+Au events at 15, 25 and 35 AGeV

same time. One core is used for one branch, creating the track candidates. Finally, for every track candidate one core can be assigned to calculate the χ^2 value using Kalman Filter method (or simple χ^2-like value). Only the last part, the track competition[4], must be executed by a single core, deciding which track candidates are becoming the reconstructed tracks.

Efficiency of tracking						
	15 AGeV		**25 AGeV**		**35 AGeV**	
Track type.	**[%]**	**tracks**	**[%]**	**tracks**	**[%]**	**tracks**
Prim. ref. all	76.0	16858	83.4	24504	77.3	26811
Prim. ref. fast	89.4	16683	92.6	23299	88.5	26573
Prim. ref. slow	4.9	175	28.5	1205	5.1	238
Extra ref. all	41.8	4853	50.7	8685	44.9	9449
Extra ref. fast	78.6	3589	82.8	6113	77.3	7249
Extra ref. slow	18.0	1264	26.4	2572	18.9	2200
All ref. all	64.3	21711	71.3	33189	65.1	36260
All ref. fast	87.3	20272	90.4	29412	85.8	33822
All ref. slow	13.6	1439	27.0	3777	15.0	2438
Ghost level	6.3	1470	9.4	3495	11.3	4697
Clone level	0.0	0	0.0	0	0.0	0

Table 5.3. Efficiency of tracking for 100 central Au+Au events at 15, 25 and 35 AGeV.

One must notice that the results were obtained using only one computer core. The routines are now working in the loops (iteratively) and can be easily transferred into

[4]Track competition is when all track candidates in a certain branch are found and each of them has a χ^2-like value assigned. The candidates "compete" and only the one with the best χ^2-like value is chosen.

more advanced systems. The multithread environment for CBMROOT is not implemented yet, thus one cannot assess the performance of real multi-core algorithms. At the present shape, one-thread track finding procedure can reconstruct 30 peripheral events each second. Transferring it into multi-core system can increase the speed by a factor 10-100.

Efficiency of tracking						
	15 AGeV		25 AGeV		35 AGeV	
Track type.	[%]	tracks	[%]	tracks	[%]	tracks
Prim. ref. all	76.1	35995	77.3	48347	78.4	58967
Prim. ref. fast	89.4	35654	89.7	47892	90.0	58441
Prim. ref. slow	4.6	341	5.0	455	5.1	526
Extra ref. all	39.1	12335	45.5	16456	44.9	21450
Extra ref. fast	71.9	8994	76.4	12337	76.6	16429
Extra ref. slow	17.6	3341	19.0	4119	19.1	5021
All ref. all	61.3	48330	64.6	64803	65.4	80417
All ref. fast	85.2	44648	86.6	60229	86.7	74870
All ref. slow	13.9	3682	14.8	4574	15.2	5547
Ghost level	4.7	2435	6.4	4532	7.3	6450
Clone level	0.0	0	0.0	0	0.0	0

Table 5.4. Efficiency of tracking for 1000 minimum bias Au+Au events at 15, 25 and 35 AGeV.

5.1.9 Possible improvement using CUDA

One of possible ways of improving the speed of the algorithm is to transfer the code into multi-core architecture, namely CUDA (Compute Unified Device Architecture)[5]. This allows the program flow to be divided into many smaller parts that can be executed in parallel. For instance, at the beginning the hits in each layer must be sorted according to the geometric coordinates. As there are 12 layers in the entire detector, there can be 12 active threads, one for each layer. Next, when SPs are being created, 6 threads running in parallel can do this task. Finally, when the array of track candidates is created, each can be fitted with Kalman Filter using a separate processor core, improving the speed even more.

The execution time of each stage of the algorithm is presented in Tab. 5.6 on page 76 along with the possible speed gain due to multi-core environment.

The total processing time increase is expected to be greater, as the platform-specific code optimization will take place. Also, the present simulation framework for PC was designed to be flexible and easily-extendable, therefore it is not optimized for speed. The modern CUDA-compatibile processor (for instance nVidia TESLA series) contains hundreds of cores, which allows for calculation of multiple events in the same unit. With the above assumptions, one TESLA processor is able to process 10 events at the same time. The expected number of processors in a computer farm is one thousand.

[5]Developed by nVidia Corporation.

Estimated speed gain due to optimizations		
Feature	**Speed gain factor**	**Total efficiency [events/s]**
Track reconstruction speed	1	30
Magnetic field parametrization	5	$1.5 \cdot 10^2$
Transfering to CUDA (multi-core model)	12	$1.8 \cdot 10^3$
CUDA code optimization	10	$1.8 \cdot 10^4$

Table 5.5. The expected improvement of track reconstruction time after the particular optimization. The track reconstruction speed is taken from the current PC-based version. The factor 12 gain after transfering to CUDA architecture is discussed below.

5.1.10 Tracking Algorithm Summary

As the algorithm was designed to find and reconstruct the J/ψ decay signals, so the main interest lays in high-energy particles (of momentum above 1 GeV/c). Tracks, which belong to high-momentum particles, are not as much affected by multiple scattering process, in comparison to low-energy particles. This implies the main emphasis in algorithm design to be put on almost straight tracks at the acute angle along the beam axis, which is roughly 90% reconstructable. This is enough for an event filtering to be performed, as the previous section concluded.

The algorithm is ready to be implemented on nVidia CUDA environment in multi-core environment, as there is a C/C++ support in CUDA. The computational farm dedicated for the CBM experiment is most likely to be multi-core parallel processing cluster.

The tracking algorithm combined with 1000 processor parallel CUDA-like environment offers enough computation power for online TRD track reconstruction. The maximum throughoutput is at the level of 10^7 events/s (10 MHz for A-A collisions [22]), as there is 1000 processors and one bunch processes 10^4 events per second on a modern hardware. Therefore, assuming 1% target interaction rate, the maximum beam intensity used for J/ψ measurement is 10^9 ions per second, which is coherent with CBM scientific goals.

Estimated time gain of separate tracking parts due to porting to CUDA			
Tracking stage name	Time per 1000 events [s]	Time per 1000 events with CUDA [s]	Cores used
Total reconstruction time	25.84		
Sort hits	1.67	0.14	12
Create SPs	0.55	0.09	6
Sort SPs	0.08	0.01	6
Create segments	0.17	0.06	3
Find friends	0.30	0.10	3
Tag tracklets	0.06	0.03	2
Create tracks	5.09	0.16	32
Fit tracks	3.36	0.34	10
Second loop	10.90	0.89	$\leq$32
Third loop	6.10	0.50	$\leq$32
		Total gain	**$\sim$ 12x**

Table 5.6. The estimated time improvement of track reconstruction time of the various stages of tracking algorithm. As the CUDA assumes running threads in bunches, up to 32 cores are used to process one portion of data, i.e. one event. The sorting/combinatorial tasks were splitted into small parts. The Kalman Filter track fit, which is also time consuming, can be calculated by all 32 cores from a bunch, as well as the track creation part, which involves similiar calculations. The total time needed for one event is expected to be decreased by at least factor 12.

Chapter 6

Summary and conclusions

In this thesis the J/ψ filtering algorithm for the CBM experiment was presented. The assumption was to use the TRD detector information only. which can be used to reconstruct particle trajectories. momenta. charge and finally the invariant mass of particle pairs. The essential part is tracking algorithm. which was developed basing on the Cellular Automaton idea. The requirements were to create a fast and precise track finding procedure. suitable for parallel execution. The event filtering part was to be low time-consuming and offering background rejection of the order of 1000. preserving the major part of J/ψ signal.

The obtained results show that track finding routine. using Cellular Automaton algorithm. works with the effeciency of 90%. Optimization for further improvement can be done by tuning the tracker to a specific TRD geometry. The time benchmark was performed on a standard PC computer and the time per central event is 0.16 s for 15 AGeV energy. The peripheral event at the same energy takes factor 5 less computing time (0.03 s). The term "standard PC computer" refers to PC with a modern 2.5-3 GHz processor and at least 1 GB of RAM memory. Porting the code to parallel processing environment can increase the number of simultaneously processed events. Since the algorithm supports multitasking. the time per event can be reduced at least by a factor of 10. because the sorting. combinatorial and track fitting parts can be executed simultanously.

The example of similiar application of CA tracker for other detector (STS [54]) shows. that using modern hardware properties (for instance incorporating **S**ingle **I**nstruction **M**ultiple **D**ata (SIMD) instructions [24]) or software techniques (like magnetic field polynominal parametrisation instead of memory-consuming and slow mapping). the time needed for processing one event (~700 reconstructed tracks) can be decreased to tens of miliseconds on a standard PC. Moreover. taking the multi-core CUDA architecture into consideration. one processor with 240 internal cores can handle up to 10^4 events per second. Such efficiency is sufficient for the event selection to be performed in the on-line basis.

Appendix A

Overview of the Kalman Filter method

The Kalman Filter [55] is a technique that allows to estimate the signal using repeated measurements in noisy environment. It is an efficient recursive method that determines the state of a dynamic system from a series of incomplete and distorted readings. It processes all available information, regardless of its precision, to estimate the current value of variables of interest.

More specificaly, the Kalman filter is essentially a set of mathematical equations that implement a predictor-corrector type estimator that is optimal in the sense that it minimizes the estimated error covariance.

The Kalman Filter has two distinct phases:

1. Predict
2. Update

The predict phase uses the state estimate from the previous timestep to produce an estimate of the state at the current timestep.

During the update phase, the measurement information at the current timestep is used to refine this prediction to come to a new, more accurate state estimate, again for the current timestep.

For example, to determine the velocity of an aircraft one can use the following devices: Doppler radar, velocity indications coming from the plane onboard navigation system or the pitot[1] and static pressure and relative wind information in the air data system. Kalman filter can be used to combine all of these data and knowledge of the various systems' dynamics to generate an overall best estimate of velocity. The "recursive" means that the filter does not need all the previous measurements to be kept in a storage and reprocessed every time a new measurement is taken. It needs the current estimate and one new measurement to execute the next predict-update cycle. One have to notice that in computational appliances this has the major impact on the idea of data processing system. Thus the amount of memory needed for system operations is reduced, and the key requirement is the arithmetic unit.

Another example of KF appliance is shown in Fig. A on the following page. There is an object that is subject to random bursts of acceleration which have a standard

[1] A pitot tube is a pressure measurement instrument used to measure the fluid or gas flow velocity.

deviation of 0.5 feet/s^2 [56]. The position was measured with an error of 10 feet (one standard deviation). The figure shows how the KF was able to estimate the position, in spite of the large measurement noise.

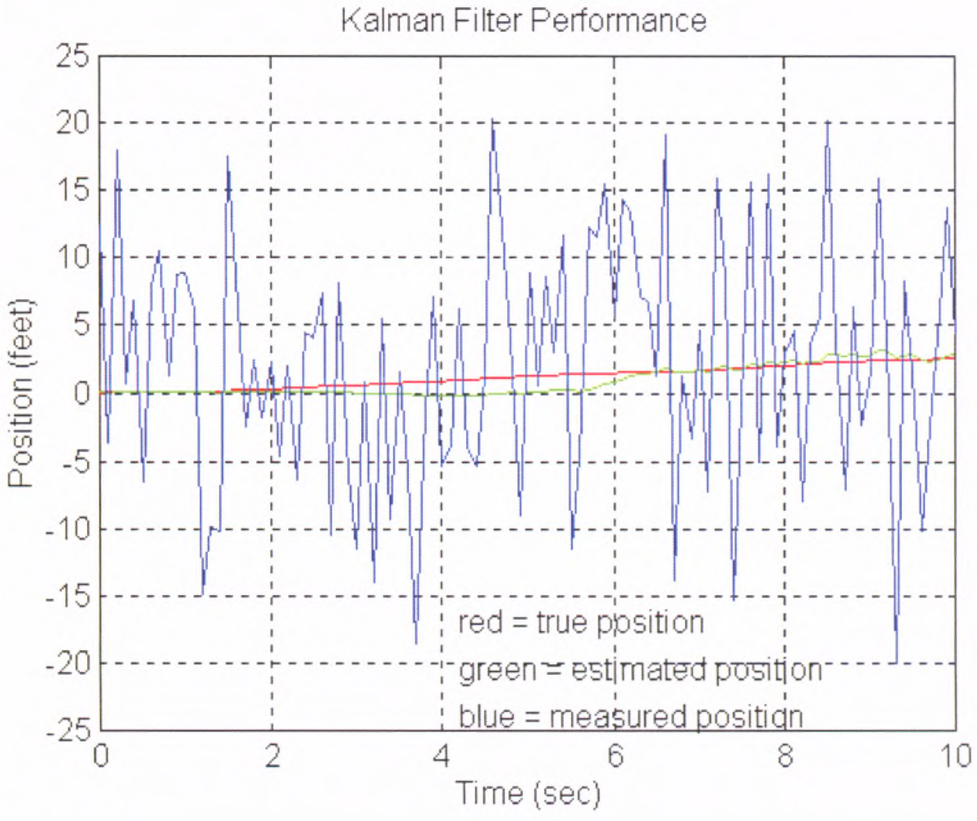

Figure A.1. The Kalman Filter example. The red line denotes the real value, the blue line with visible peaks reflects the measurement values, the green line is estimated value. The measurement is taken a few times per second. Image taken from [56].

Among the numerous applications of the filter are GPS positioning systems, robotics and automation.

In the case of CBM experiment, Kalman Filter is used to estimate the parameters of the reconstructed track, containing a set of points registered by the detector system. Each detector hit is considered as a next measurement of the key track parameters: position (x, y, z), track slopes (t_x, t_y) at the position, and q/p fraction of the particle which left the trace in the detector. The material used to build the detector is also taken into account, as well as the detector geometric properties. Moreover, after processing all hits belonging to one track, the track can be refitted over and over again, leading to even more precise results. The fitting can start from the first point and go to the last one. Next, the refitting can be done in the opposite direction. This has a fundamental role in momentum determination, where the slope of the reconstructed track is a key feature in backtracking the trajectory to the target. The first TRD station is at the distance of 5 m from the target with the RICH detector just before it. RICH contains of a big radiator, having the considerable impact on the traversing particle trajectory. For each

reconstructed track. the target is treated as an additional point of measurement, and an assumption is made that the track is a primary. With the magnetic field parametrized and the RICH material known. this method allows for momentum determination with an relative accuracy $\Delta p/p$ of 14%.
The technique is also used in CBM for fitting the tracks which bend in the magnetic field. The tracks are composed of hits registered in the Silicon Tracking Stations (STS) and Micro-Vertex Detectors (MVD) and their curvature is calculated with the use of the Kalman Filter and the analytic formula for track propagation.

Kalman Filter incorporated in CBM has its implementations for standard PC. vector SIMD. cell and graphic processors. which offer fitting speed of the order of microseconds per track.

Appendix B

Transition radiation effect

Tradition detection is one of the fundamental aspects of nuclear and high energy physics. The radiation. either electromagnetic or particle-based. can only be registered through its interaction with matter using different processes. depending on the measurement technique.
Charged particles leave characteristic trails as they travel through detector material. The material can be gaseous. liquid or solid. depending on the detector type. Charged particles lose their energy mainly in collision with atomic electrons of the material (excitation and ionisation). The other relevant process is emission of bremsstrahlung. which occurs during scattering on nuclei. Hadrons can transfer their energy through interactions like inelastic nuclear collisions or nuclear excitations. For photons. the energy loss may occur by Compton scattering on atomic electrons. photoelectric effect or pair production. which is dominant at energies far over 1 MeV. The resulting electrons and positrons can be detected through their energy loss from excitation of medium and ionisation. The process of energy loss of a charged particle is crucial for most particle detectors. especially to gaseous detectors.

B.1 Additional mechanisms for energy loss of charged particles

Ionisation and excitation are the main reasons of energy loss. Besides that. charged particles may also lose their energy by radiation like *Cherenkov radiation* and *transition radiation.* For our case. the most interesting process is transition radiation as it is essential for particle identification in TRD detector. TR is produced when a relativistic particle traverses an inhomogeneous medium. especially the boundary between materials with different dielectric constants ϵ. The Cherenkov radiation is emited when a charged particle. moving in a medium. has a velocity exceeding the velocity of light in that medium. If the particle is moving with a uniform constant velocity. its electric field will interact with the medium and this interaction can cause the emission of real photons. In a material with the dielectric constant $\epsilon > 1$. the threshold velocity for Cherenkov emission is smaller than c. If $e < 1$. the threshold velocity is larger than c and no real photon is possible in an infinitelu long radiator. Under certain conditions a real photon is emmited instead of ionizing an atom or exciting the matter. These conditions are influenced by the radiator size and alignment. The conditions can also be influenced

by finite length radiators. This phenomenon is called the sub-threshold emmision of Cherenkov light. This sub-threshold emission of photons when particle traverse a thin segment of material is called transition radiation (TR). It is caused by a transition in the index of refraction between the vacuum and the material (or two materials). TR already occurs when being below the β threshold for Cherenkov radiation but in a finite length medium.

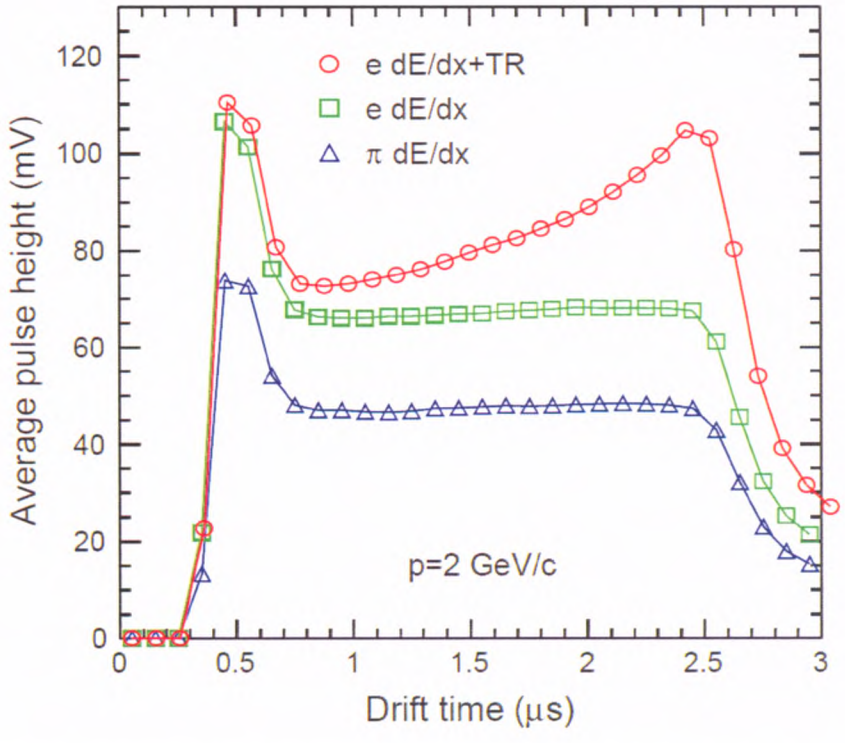

Figure B.1. Average pulse height as a function of drift time for pions and electrons (with and without radiator) [57].

While Cherenkov light is typically emitted in the optical region and near UV, the TR is emitted in the X-ray region. The angular distribution of transition radiation is peaked forward with a sharp maximum at $\Theta=1/\gamma$, hence strongly collimated along the direction for relativistic electrons [58]. In a simple picture, TR is emited due to changing the dipole moment formed by charge and its mirror charge on the opposite of the medium boundary. The induced mirror charge is equivalent in effect to the to the induced charge density at the interface needed to match the boundary conditions. The charge and image charge pair creates a dipole which changes with time and changes direction at the point of crossing the interface thus causing radiation. The interface is the point where the pointing of the dipole vector flips direction indicative of maximum acceleration. TR is suitable for particle discrimination, especially in the momentum range when Cherenkov radiation becames useless. The proportionality of the energy of emmited TR to the Lorentz factor makes it possible to use for particle identification, when β approaches unity.

B.2 Energy loss of a particle in a TRD detector

The CBM project considers the usage of ALICE-like TRDs [57]. The detector pulse height for incoming particle of a momentum 2 GeV/c is shown in the Fig. B.1 on the preceding page. The peak at small drift times originates form the amplification region, while the plateau is from the drift region. For electrons when using the radiator there is additional peak at longer drift times, which comes from the contribution of TR absorbed at the entrance of the detector.

The energy deposited during the passage of a particle through the material of the detector is shown in Fig. B.2. The momentum of particles was 2 GeV/c. In the figure one can see the difference of energy deposited, which is a base for e/π identification.

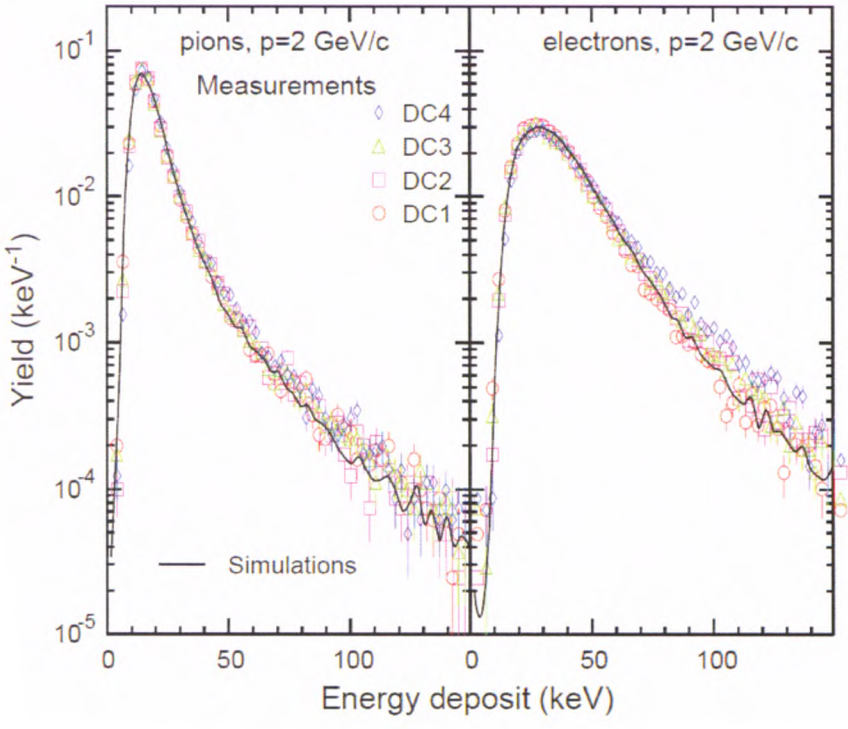

Figure B.2. Comparison of spectra of energy deposit of electrons and pions of a momentum 2 GeV/c. The symbols represent the measurement, the lines are calculations. [57].

Appendix C

The parameters used in the Track Finding procedure

During the execution of the track finding procedure, the geometrical restriction must be applied. It allows to eliminate the less probable connections between the certain structures (like hits, Space Points and Segments).

The FL, SL and TL suffixes stand for First Loop, Second Loop and Third Loop, denoting the distinct iterations of track finding procedure. There are three main parts where the parameters were used: Space Point creation part, segment creation part and find neighbour part.

Listing C.1. The geometric parameters tuned for the energy 25 AGeV and for high-momentum particle trajectories. Different energies may require additional corrections to achieve better efficiency and/or speed.

```
//--- Function: CreateSpacePoint ----
//A denotes the first hit in TRD. B denotes the second one
Double_t
  sigmaA_FL = 2. //multiplier for SP creation in First Loop (FL)
  sigmaB_FL = 2. //multiplier for SP creation in FL
  sigmaA_SL = 3. //multiplier for SP creation in Second Loop (SL)
  sigmaB_SL = 3. //multiplier for SP creation in SL
  sigmaA_TL = 4. //multiplier for SP creation in Third Loop (TL)
  sigmaB_TL = 4; //multiplier for SP creation in TL
//--- Function: CreateSegments; ----
//Y denotes one coordinate in the detector plane, Y denotes another
//values in centimeters
Double_t
  dY_FL = 0.3. //distance for tracklet creation in FL
  dX_FL = 0.3. //distance for tracklet creation in FL
  dY_SL = 0.5. //distance for tracklet creation in SL
  dX_SL = 0.5. //distance for tracklet creation in SL
  dY_TL = 0.7. //distance for tracklet creation in TL
  dX_TL = 0.7; //distance for tracklet creation in TL

//--- Function: FindNeighbour ----
```

```
//distance from Y-propagated point. around which we look for neighbou
//values in centimeters
Double_t
  distPropLongY_FL = 2.5. //parameter used in FL
  distPropLongX_FL = 2.5. //parameter used in FL
  distPropLongY_SL = 3.   //parameter used in SL
  distPropLongX_SL = 3.   //parameter used in SL
  distPropLongY_TL = 4.   //parameter used in TL
  distPropLongX_TL = 4;   //parameter used in TL
```

The initial values of these parameters were chosen using Monte-Carlo simulations. where the optimal cuts values could be calculated. Next. the parameters were optimized manually.

There are always two concurrent goals to pursuit in algorithm development: speed and efficiency. Trying to come to a compromise between these two goals. the parameters were further tuned manually to the values stated below.

For Space Point creation part. the numbers sigmaA_FL and sigmaB_FL correspond to the multiplier of the position error of a hit. The position error σ differs from station to station. it also depends on the area of the TRD layer. the further from the center. the less precise. Therefore. in the first loop. the region of interest around the first hit has a size of $2\sigma_x \times 2\sigma_y$. where the suitable hits in the next layer are sought. The second loop takes 3σ values. and finally 4σ for the third loop.

Considering the segment creation part. the numbers are a measure of distance around the line propagated to the layer 3 of TRD station. The line is made by connecting the target point with the first SP in layers 1 and 2. Then. the line is prolonged into layer 3 and all the SPs found in the square region of 2σ in each dimension (namely 2·dY_FL×2·dX_FL. see Listing C.1 on the previous page part 2) are taken into consideration. As the emphasis is put on high-energy linear tracks. the values in the first loop are strict (0.3 cm). The next loops bring the restrictions loosen to 0.5 and 0.7 cm.

In the Find Neighbour phase. the variables like distPropLongY_FL and distPropLongX_FL (see Listing C.1 on the preceding page part 3) are used. The "Prop" part of the name comes from "Propagation". The reconstructed segment of a track is propagated to the next TRD station. first layer. The region of interest is formed using 2·distPropLongY_FL×2·distPropLongX_FL and all segments with the first SP inside the region are selected. These segments are marked as "friends" or "neighbours" of the base segment.

Appendix D

Multicore Processors

The nVidia Corporation have been developing the series of parallel processing units. for instance the Tesla series. These are highly-effective and programmable general-purpose units. capable of multi-thread calculations (a couple of hundreds of independent cores integrated in a single chip).

At the beginning. the purpose of the chips was to provide the PC computer with enough power to process detailed 3D graphics in the real time. The chips located on graphics cards were single-core. gradually evolving into more complicated systems. A graphic processor is dedicated to manipulate computer graphics using sophisticated algorithms. The modern graphics processing units (GPUs) have highly parallel structure which makes them more efficient than a general-purpose CPU (Central Processing Unit - an "ordinary" computer processor) in performing calculations of geometry. complex vector transformations or multi-object rendering in the real time.

At some point. when the powerful graphics accelerator cards were manufactured for the PC market. there came the idea to use a graphic card as a specialized set of processors. The tool developed to help in this task is CUDA - Compute Unified Device Architecture. developed by nVidia. CUDA is the computing engine for nVidia GPUs that is accessible to software developers through variants of industry standard programming languages. Programmers use C language with nVidia extensions to code algorithms for executions on GPUs. The origin of CUDA dates back to February 2007.

The schematic view on the CUDA architecture is showed in Fig. D on the next page.

Unlike general-purpose CPUs. which executes a single thread (or a couple of them) very fast. GPUs have a parallel throughput architecture that emphasizes slowly executing many concurrent threads. This feature can be used for the purpose of data processing in modern physics for the online analysis. During the experiment. a portion of data from the detectors is transferred to GPU's memory and a group of cores is assigned to process the data. As there are data buffers in use. it is effective to calculate many events at the same time. even if a time need for a single event is longer. The total number of events processed over a longer period of time is bigger comparing to a traditional. single-core approach though.

The Tesla line of processors is a serie of General Purpose GPU (GPGPU) intended for the high performance computing market. Tesla units posess far superior computational power compared to recent microprocessors. They are based on recent nVidia GPU cores (G80. Quadro) which lack the ability to display output images. The main

purpose of these units is large scale calculations, especially floating-point, used for image generations for scientific of professional fields.

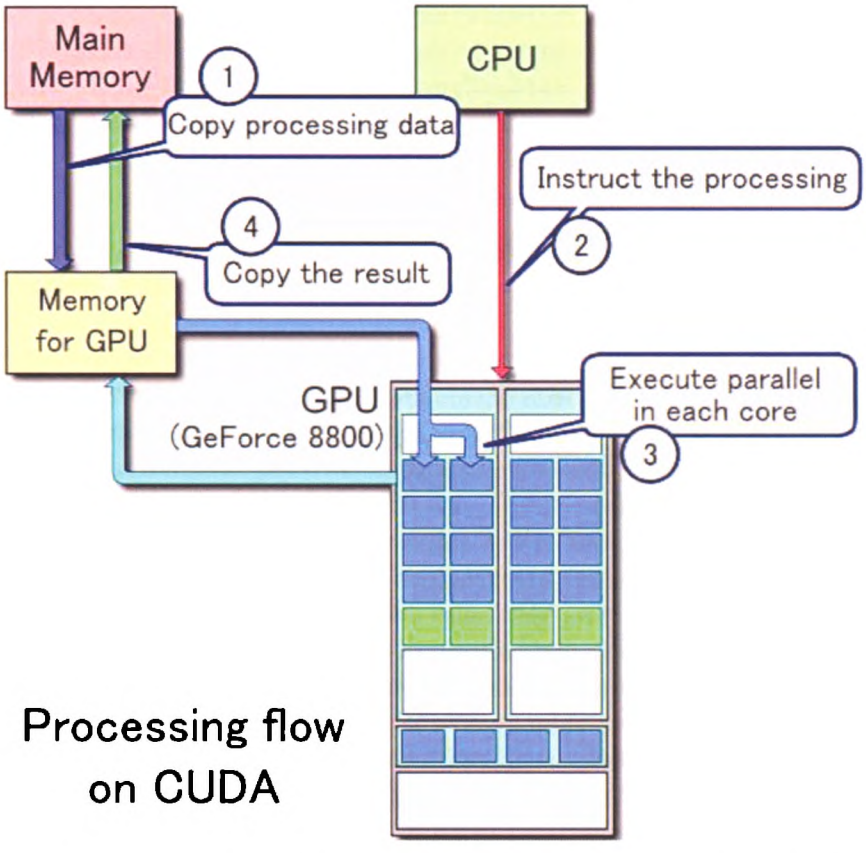

Figure D.1. Example of CUDA processing flow 1. Copy data from main mem to GPU mem 2. CPU instructs the process to GPU 3. GPU execute parallel in each core 4. Copy the result from GPU mem to main mem. Figure from [59].

nVidia provides Tesla as a graphic card-like computer module, a standalone workstation, a server module or complete rack system. The number of units in a single module varies from 1 to 4. The total number of thread processors can be 128 (1 core) up to 1792(4 cores $\times$ 448). There is also a special edition of systems equipped with 8 GPUs. Tesla line is fully compatibile with CUDA, making it feasible to use for CBM experiment.

The next generation (in January 2011) CUDA architecture has a codename Fermi. It delivers computational power of a supercomputer at $1/10^{th}$ the cost and $1/20^{th}$ the power of traditional CPU-only servers, offering further improvement of the parallel thread execution.

Appendix E

Generation of events with UrQMD and Pluto

The Ultra-relativistic Quantum Molecular Dynamics (UrQMD [20]) model is used to simulate ultrarelativistic heavy ion collisons in the energy range of modern (2011) accelerators. It includes various physical phenomena (like creation of dense hadronic matter, creation and transport of rare particles, strangeness, emission of electromagnetic probes) in one transport engine. The model needs the initial parameters stored in files. The input files used to create the hadron production data are presented below.

E.1 UrQMD central collisions

In Listing E.1 is shown the input for UrQMD software to perform central Au+Au collision at the laboratory energy 25 AGeV (impact parameter = 0). For other energies the only difference is the beam momentum parameter *plb*. The impact parameter *tim* determines the total time span to calculate (in fm/c) and the time interval after which the output is written to files.

Listing E.1. Input parameters for UrQMD model for central collisions.

```
# Projectile Gold
pro 197 79
# Target Gold
tar 197 79
# Number of events
nev 100
# Beam momentum
plb 25
# Impact parameter
imp 0.0
# Calculation time
tim 100 100
# Suppress outputs
f13
f15
f16
```

```
f19
f20
# End of input file
xxx
```

E.2 UrQMD minimum bias collisions

In Listing E.2 is shown the input for UrQMD software to perform minimum bias Au+Au collision at the laboratory energy 25 AGeV (impact parameter varies from 0 to 100 fm). For other energies the only difference is the *plb* parameter. The impact parameter is weighted quadratically (cto parameter).

Listing E.2. Input parameters for UrQMD model for minimum bias collisions.

```
# Projectile Gold
pro 197 79
# Target Gold
tar 197 79
# Number of events
nev 100
# Beam momentum
plb 25
# Impact parameter
IMP 0 100
cto 5 1
# Calculation time
tim 100 100
# Suppress outputs
f13
f15
f16
f19
f20
# End of input file
xxx
```

E.3 Pluto source

An example ROOT C macro used to generate the J/ψ signal is listed below. The important parameters are the temperature of a fireball (T1 = 170 MeV) and the beam energy (Eb = 15 GeV). The beam energy and temperature may vary.

Listing E.3. Pluto macro for J/ψ decay generation.

```
void gen_pluto(Int_t index = 10)
{
  gROOT->Reset();
```

```
  gROOT->LoadMacro("$VMCWORKDIR/gconfig/basiclibs.C");
  basiclibs();

  Float_t Eb   = 15;
  Float_t T1    = 0.170;    // temperature in GeV
  Float_t T2    = 0.;       // temperature in GeV
  Float_t blast = 0.;       // radial expansion velocity
  Int_t const num_of_react=10000;
  Int_t ran=12345;
  gRandom->SetSeed(ran);
  Char_t filename[80];
  sprintf(filename,"jpsi_pluto15GeV");

  PFireball *source_JPsi
    =new PFireball("J/Psi",Eb,T1,T2,1.,blast,0.,0.,0.,0.);
  source_JPsi->setSigma(0.8);

  source_JPsi->Print();

  PParticle *JPsi = new PParticle("J/Psi");
  PParticle *mumJPsi = new PParticle("e-");
  PParticle *mupJPsi = new PParticle("e+");

  PParticle* s_JPsi[]     = {source_JPsi,JPsi};
  PChannel* c_sJPsi    = new PChannel(s_JPsi,1,1);

  PParticle *s_JPsidimu[]  ={JPsi,mumJPsi,mupJPsi};
  PChannel  *c_JPsidimu  = new PChannel(s_JPsidimu,2,1);
  PChannel  *cc_JPsi[]    = {c_sJPsi,c_JPsidimu};

  PReaction *r_JPsi
    = new PReaction(cc_JPsi,filename,
        sizeof(cc_JPsi)/sizeof(cc_JPsi[0]),0,0,0,0);

  r_JPsi->Print();
  r_JPsi->setHGeant(0);
  r_JPsi->loop(num_of_react);
}
```

Acknowledgments

Numerous people have been supporting me during the preparations of this thesis.

First of all I would like to thank my supervisor Prof. Dr. Hab. Wiktor Zipper for his support, suggestions and ideas during the course of this study. He was the one who gave me the opportunity to work in the CBM Collaboration. His knowledge, continuous interest and remarks greatly helped me to make this thesis complete.

I owe great debt to Dr. Arkadiusz Bubak who was like an elder brother helping me when I was making my first steps in physics, computing, programming and presentations. He spent his most precious time to read through my drafts and made many, many remarks and invaluable comments and suggestions.

I wish to express my sincere gratitude to Dr. Walter Müller for discussions, advice and tasks during the meetings in the GSI.

I am indebted to Prof. Dr. Peter Senger for inviting me to work with many great specialists in physics at the GSI, Darmstadt and KIP, Heidelberg.

I would also like to thank Dr. Ivan Kisel for his patience and guidance in the field of track finding in modern particle detectors and his great influence on my work.

I am deeply grateful to Sergei Gorbunov for helping me to resolve many technical issues in my code during the stay in Heidelberg.

My family: Ola, Agnieszka, Krzysiek and my mother Renia who supported me and always believed in me and all I was doing. Thank you.

At the end of my thesis I would like to thank all my professors and colleagues from Department of Nuclear Physics and its Applications.

Bibliography

[1] P. Senger et al.. CBM Progress Report. 1st ed. (GSI Collaboration. 2009).

[2] K. Rajagopal and F. Wilczek. *The condensed matter physics of QCD.* (2000). hep-ph/0011333.

[3] Z. Fodor and S.D. Katz. *Critical point of QCD at finite T and mu, lattice results for physical quark masses.* Journal of High Energy Physics **2004** (2004) 050.

[4] . R. and . Bellwied. *The measurement of transverse polarization of Lambda hyperons in relativistic heavy ion collisions.* Nuclear Physics A **698** (2002) 499 . ¡ce:title¿15th Int. Conf. on Ultra-Relativistic Nucleus-Nucleus Collisions (Quark Matter 2001)¡/ce:title¿.

[5] F. Weber. *Strangeness in neutron stars.* Journal of Physics G: Nuclear and Particle Physics **27** 465.

[6] F. Wilczek. *QCD Made Simple.* **53** (2000) 22.

[7] A. Milov. *Light Vector Mesons.* Eur.Phys.J. **C61** (2009) 721. 0809.3880.

[8] B. Mueller and J. Rafelski. *Temperature dependence of the bag constant and the effective Lagrangian for gauge fields at finite temperatures.* Phys. Lett. B **101** (1980) 111.

[9] S. Frixione et al.. *Heavy quark production.* Adv.Ser.Direct.High Energy Phys. **15** (1998) 609. hep-ph/9702287. To be published in Heavy Flavours II. ed. by A.J. Buras and M. Lindner. World Scientific.

[10] W. Reisdorf and H.G. Ritter. *COLLECTIVE FLOW IN HEAVY-ION COLLISIONS.* Annual Review of Nuclear and Particle Science **47** (1997) 663. http://www.annualreviews.org/doi/pdf/10.1146/annurev.nucl.47.1.663.

[11] M. Bleicher. S. Jeon and V. Koch. *Event-by-event fluctuations of the charged particle ratio from non-equilibrium transport theory.* PHYS.REV.C **62** (2000) 061902.

[12] K. Chung et al.. *Nuclear matter properties in the relativistic mean field model with sigma omega coupling.* Eur.Phys.J. **A11** (2001) 137. nucl-th/0011025.

[13] K. Sumiyoshi. K. Oyamatsu and H. Toki. *Neutron star profiles in the relativistic Brueckner-Hartree-Fock theory.* Nuclear Physics A **595** (1995) 327 .

[14] F. Weber. R. Negreiros and P. Rosenfield. *Neutron Star Interiors and the Equation of State of Superdense Matter*. Neutron Stars and Pulsars. Springer. 2009.

[15] *Guide to the Nuclear Wall Chart*. BNL webpage (2011).

[16] P. Senger. *Introduction to CBM Experiment*. GSI Report **1** (2006) 20.

[17] C.Y. Wong. *Signatures of quark gluon plasma phase transition in high-energy nuclear collisions*. Nucl.Phys. **A681** (2001) 22. nucl-th/0007046.

[18] A.V. Olinto. "Neutron Star" Macmillan Encyclopedia of Physics. (New York: Macmillan. 1996) pp. 1037–1038.

[19] S.A. Bass et al., *Microscopic models for ultrarelativistic heavy ion collisions*. Progress in Particle and Nuclear Physics **41** (1998) 255 .

[20] M. Bleicher et al.. *Relativistic Hadron-Hadron Collisions in the Ultra-Relativistic Quantum Molecular Dynamics Model (UrQMD)*. J.PHYS.G **25** (1999) 1859.

[21] B. Friman et al.. The CBM Physics Book (Springer. 2010).

[22] P. Senger et al.. Technical Status Report CBM Experiment. 1st ed. (GSI Collaboration. 2005).

[23] J.M. Heuser. *"Development of a silicon tracking and vertex detection systems for CBM experiment at FAIR"*. Nuclear Instruments and Methods in Physics Research **A 582** (2007) 910.

[24] S. Gorbunov et al.. *Fast SIMDized Kalman Filter Based Track Fit*. 2007. https://www.gsi.de/documents/DOC-2007-Mar-127.html.

[25] I. Kisel. *Presentation on CBM Collaboration Meeting*. Darmstadt. 2008.

[26] *Cherenkov radiation — Wikipedia, The Free Encyclopedia*. Wikipedia (2010).

[27] J.D. Lebedev. Semen [LIT. Algorithms and software for cherenkov ring reconstruction and electron identification in the CBM experiment. PhD thesis. 2011. PhD Thesis.

[28] S. Gorbunov and I. Kisel. *Elastic net for stand-alone RICH ring finding*. Nuclear Instruments and Methods in Physics Research **A 559** (2006) 139.

[29] *CBM Workshop*. 2009.

[30] R.C. R. Santonico. *"Development of resistive plate counters"*. Nuclear Instruments and Methods in Physics Research **A 187** (1981) 377.

[31] P. Fonte. *"A new high-resolution TOF technology"*. Nuclear Instruments and Methods in Physics Research **A 443** (2000) 201.

[32] P. Cortese et al., *"Time of flight system"*. ALICE TDR 8 **CERN/LHCC/200216**.

[33] A. Schuttauf. *"Timing RPCs in FOPI"*. Nuclear Instruments and Methods in Physics Research **A 533** (2004) 65.

[34] H. Alvarez-Pol et al.. *A large area timing RPC prototype for ion collisions in the HADES spectrometer*. HADES. Nucl. Instrum. Meth. **A535** (2004) 277.

[35] M. Bogomilov et al.. *"The HARP RPC time-of-flight system"*. Nuclear Instruments and Methods in Physics Research **A 508** (2003) 152.

[36] B. Bonner et al.. *"A single Time-of-Flight tray based on multigap resistive plate chambers for the STAR experiment at RHIC"*. Nuclear Instruments and Methods in Physics Research **A 508** (2003) 181.

[37] A. Kiseleva. P. Senger and I. Vassiliev. *Vector meson study for the CBM experiment at FAIR/GSI*. Physics of Particles and Nuclei **39** (2008) 1090. 10.1134/S1063779608070204.

[38] E.l. Tarkovsky. *The HERA-B electromagnetic calorimeter*. Nucl. Instrum. Meth. **A379** (1996) 515.

[39] L. Aphecetche et al.. *PHENIX calorimeter*. Nuclear Instruments and Methods in Physics Research Section A: Accelerators. Spectrometers. Detectors and Associated Equipment **499** (2003) 521 . ¡ce:title¿The Relativistic Heavy Ion Collider Project: RHIC and its Detectors¡/ce:title¿.

[40] S. Barsuk et al.. CERN preprint LHCb-2000-043 (2000).

[41] *Review of Particle Physics*. Particle Data Group (2000).

[42] I. Fröhlich et al.. *Pluto: A Monte Carlo Simulation Tool for Hadronic Physics*. PoS **ACAT2007** (2007) 076. 0708.2382.

[43] A. Andronic. ALICE TRD Group. private communication.

[44] GEANT. Detector Description and Simulation Tool - User Manual (CERN. 1994).

[45] *OPERA-3D*. Internet web page: http://www.cobham.com/about-cobham/aerospace-and-security/about-us/antenna-systems/aurora/products/opera-3d/statics.aspx. Cobham Technical Services.

[46] *CBMROOT Framework*. Internet web page: http://cbmroot.gsi.de. CBM Collaboration.

[47] *ROOT*. Internet web page: http://root.cern.ch. CERN.

[48] J. Heuser. *Development of the CBM Silicon Detector*. 2009. GSI Darmstadt. https://www.gsi.de/documents/DOC-2009-Dec-95.html.

[49] *Monte Carlo method — Wikipedia, The Free Encyclopedia*. 2010. [Online; accessed 22-Aug-2010].

[50] Z. Gorbunov. Sergey [DESY. *An Analytic Formula for Track Extrapolation in an Inhomogeneous Magnetic Field* , 2005. https://www.gsi.de/documents/DOC-2005-Mar-212.html.

[51] *Stanislaw Marcin Ulam — Wikipedia, The Free Encyclopedia*. 2010. [Online; accessed 12-Aug-2010].

[52] *John von Neumann — Wikipedia, The Free Encyclopedia*. 2010. [Online; accessed 12-Aug-2010].

[53] M. Gardner, *Mathematical games. The fantastic combinations of John Conway's new solitaire game "life"*. Scientific American **223** (1970) 120.

[54] I. Kisel, *Event reconstruction in the CBM experiment*. Nucl. Instrum. Meth. **A566** (2006) 85.

[55] R.E. Kalman, *A New Approach to Linear Filtering and Prediction Problems*. Transactions of the ASME–Journal of Basic Engineering **82** (1960) 35.

[56] *Kalman Filtering, Dan Simon*. Internet web page: http://www.innovatia.com/software/papers/kalman.htm. Innovatia Software.

[57] A. Andronic. *Electron identification performance with ALICE TRD prototypes*. Nuclear Instruments and Methods in Physics Research Section A: Accelerators. Spectrometers. Detectors and Associated Equipment **522** (2004) 40 . TRDs for the Third Millenium. Proceedings of the 2nd Workshop on Advanced Transition Radiation Detectors for Accelerator and Space Applications.

[58] D. Green, The physics of particle detectorsCambridge monographs on particle physics, nuclear physics, and cosmology (Cambridge University Press. 2000).

[59] *CUDA — Wikipedia, The Free Encyclopedia*. 2010. [Online; accessed 14-Sep-2010].